Development and application of dynamic light scattering methods for characterizing reaction kinetics

Elaine Marie Wells-Gray
B.S. University of Iowa, 2003

January 2011

Department of Science and Engineering
Division of Biomedical Engineering
School of Medicine
Oregon Health & Science University

_____

CERTIFICATE OF APPROVAL
_____

This is to certify that the Ph.D. dissertation of

Elaine M. Wells-Gray

has been approved

_____
Sean J. Kirkpatrick, Ph.D., Advisor
Professor, Dept. of Biomedical Engineering
Michigan Technological University

_____
Donald D. Duncan, Ph.D.
Research Professor, Dept. of Electrical and Computer Engineering
Portland State University

_____
Monica T. Hinds, Ph.D.
Assistant Professor

_____
Scott A. Prahl, Ph.D.
Assistant Professor

_____
Ronald L. Sakaguchi, D.D.S., Ph.D.
Professor, Dept. of Restorative Dentistry

_____
Ruikang K. Wang, Ph.D.
Professor

ii

Dedicated to my parents, Tim and Betty.

Acknowledgements

Many people were instrumental in the completion of this dissertation.

I would first like to thank my advisor Sean Kirkpatrick for teaching me about optics, lasers, and, most importantly, speckle. I am grateful for his encouragement, mentoring, and patience during this long process. I would not have been able to complete this dissertation without his help.

Also I would also like to thank all the members of my advisory committee. I am grateful to Don Duncan for teaching me Fourier and statistical optics, which are fundamental to this work. I am also grateful for his guidance and the many meetings in which he helped clarify difficult concepts. Scott Prahl has given me valuable suggestions and feedback about my research at the group seminars. I also appreciate his detailed critique of my dissertation, from which I've been able to make many improvements. I'm grateful to Ron Sakaguchi for introducing me to the world of restorative dentistry, and for providing the dental composite and curing lamp that were instrumental in most of the experiments in my dissertation. His practical advice and encouragement to find clinical applications for my research have been greatly appreciated. Ricky Wang has offered useful suggestions and advice. I'm also grateful to him for allowing me to use his OCT systems for several experiments over the last 5

Table of Contents

List of Figures

List of Tables

List of abbreviations

ACF	Autocorrelation function
CCD	Charge coupled device
DC	Degree of conversion
DLS	Dynamic light scattering
DSC	Differential scanning calorimetry
DWS	Diffusing-wave spectroscopy
FFT	Fast Fourier transform
GRV	Gaussian random variable
IR	Infrared
LSCA	Laser speckle contrast analysis
LSCI	Laser speckle contrast imaging
PCS	Photon correlation spectroscopy
PSD	Power spectral density
QLS	Quasi-elastic light scattering
ROI	Region of interest
SSC	Sequential speckle correlation

Abstract

The aim of dynamic light scattering (DLS) is to characterize dynamic processes through the measurement of correlations in temporally varying scattered light. This dissertation deals with the development and application of DLS techniques for monitoring processes that undergo rapid changes in dynamic behavior. Theoretical and technical concepts are examined through the experimental investigation of dental composite polymerization, which is of clinical importance in the field of restorative dentistry. This reaction exhibits changes in dynamic behavior that occur faster than can be resolved with established DLS techniques.

A basic overview of DLS is presented through the theory and application of quasi-elastic light scattering (QLS). Due to the stochastic nature of the scattered light signal, thousands of intensity fluctuations must be averaged in order to obtain a statistically reliable measure of the temporal autocorrelation function (ACF). QLS relies on single-detector measurement of dynamically scattered light, and the necessary temporal averaging is time consuming, taking tens of seconds to minutes for a single measurement. Accordingly, QLS is not well suited for studying reactions that vary on the order of seconds or faster.

The remainder of this work deals with the development and application of dynamic-speckle-based DLS methods that utilize CCD camera detection. Multi-pixel detection allows for ensemble (spatial) averaging, which enables these methods to achieve faster measurements of dynamic behavior compared to QLS. A sequential speckle correlation (SSC) method was developed and implemented that uses the correlation coefficient between pairs of dynamic speckle patterns to describe reaction dynamics. The temporal resolution of this method compared to QLS is improved by a factor roughly equal to the number of independent speckles included in the region of interest (ROI). For the study of dental composite polymerization, a 64 x 64 pixel ROI was used with a minimum speckle dimension of two pixels, achieving a ~1000 fold increase in temporal resolution (~50 ms).

Another multi-pixel DLS method, laser speckle contrast analysis (LSCA), was also implemented. With LSCA, temporal averaging of intensity fluctuations causes a reduction in contrast of the speckle pattern which can be used to characterize the motion of the scattering medium. This method is able to measure spatial variations in reaction dynamics as well as the temporal behavior. LSCA has previously been used to study blood flow velocity, but this work marks its first successful application for studying dental composite polymerization.

The reaction kinetics of the photo-activated polymerization of dental resin composite were explored with these DLS methods, for a variety of sample dimensions

and curing protocols. Results are presented for samples 0.1-17 mm thick and for curing irradiances between 20 - 320 mW/cm^2. Reaction profiles obtained with SSC and LSCA are qualitatively similar to results in the literature obtained using other techniques. Results for polymerization rate as a function of curing irradiance for thin samples using LSCA demonstrate a square root dependence that agrees well with established polymerization theory, as well as with previous results in the literature. Our findings suggest that the multi-pixel DLS methods presented here can be advantageously applied to the study of dental composite polymerization, as well as to other highly scattering dynamic systems.

Chapter 1: Introduction

1.1 Dynamic processes and dynamic light scattering (DLS)

Dynamic processes are of great interest in many areas of biomedical research. Particle motion can be used to characterize material properties such as viscosity [1], conformational changes and aggregation behavior of proteins [2], and flow velocity of blood [3], to name a few examples. Finding ways to measure dynamic processes, for which motion may be highly stochastic and on a microscopic (or smaller) scale, can present a challenge. Many biological structures—including a wide range of molecules, proteins, and larger bio-structures—scatter light. When illuminated, their motion results in temporal variations, or fluctuations, in scattered light. Dynamic light scattering methods (DLS), which measure and analyze scattered light signals, are the focus of this dissertation.

The common aim of all DLS techniques is the statistical analysis, often in terms of autocorrelation, of the temporal variations in scattered light, for the purpose of characterizing the motion of a dynamic system. DLS has been applied in many areas of science and industry [1][4]. Examples specific to the biological sciences include studies of membranes [5][6], vesicles [7][8], blood cells [9], proteins [10-12], bacteria [12][13], and viruses [14].

The first fully implemented DLS method was quasi-elastic light scattering (QLS), which is sometimes referred to as photon correlation spectroscopy [15]. Its origins as a quantitative technique date back to the 1960s, when the advent of the laser and improvements in photo-detector technology made possible the measurement of light scattered from dilute suspensions [16]. This technique, discussed in Chapter 2, is capable of determining particle size and media viscosity based on the temporal autocorrelation function of scattered light, and using the well-known Stokes-Einstein relationship that describes diffusive motion [17][18]. The development of QLS was also important in paving the way for a number of other DLS techniques, such as diffusing wave spectroscopy (DWS) [19] and laser speckle contrast analysis (LSCA) [20].

QLS is used to characterize scattering processes that are statistically stationary, such as Brownian motion [1]. It can also be usefully applied to non-stationary systems whose dynamic characteristics change only slowly with time [21]. Due to the stochastic nature of the light scattered from a dynamic system, a large number of fluctuations (>1000) must be averaged in order to obtain a statistically reliable measure of dynamic behavior. Therefore QLS is only suited to study systems exhibiting changes in dynamics that occur more than three orders of magnitude slower than the time-scale of an average signal fluctuation [22].

One way to reduce the temporal sampling requirements is by ensemble (i.e. spatial) averaging. This can be achieved using multiple detectors, usually in the form of a charge-coupled device (CCD) camera. A CCD-based version of QLS has been

developed [23], but this method can only be used to study processes exhibiting temporal fluctuations that are slower than the sampling rate of the camera (~200 Hz, compared to MHz for a typical point detector). However, for applications where measurement of the temporal autocorrelation function is not needed (or can be assumed), a CCD-based approach can be used to effectively monitor relative changes in dynamic behavior. Laser speckle contrast analysis (LSCA) is one such technique [3]. With this method, ensemble averaging over >25 pixels allows the dynamic behavior to be characterized faster than with QLS. LSCA and another CCD-based technique, referred to as sequential speckle correlation (SSC), were implemented for this work and are discussed in this dissertation in Chapters 4-6. The temporal resolutions of these methods are increased, compared to QLS, by a factor equal to the number of spatial coherence areas (speckles) included within the ensemble averaging region of interest (ROI). Experimental studies using these methods were conducted to study the polymerization kinetics of dental resin composite, an often studied dynamic process in the field of restorative dentistry.

1.2 Dental resin composite

Dental resin composites have been widely used in the field of restorative dentistry since their introduction over 40 years ago [24].Their popularity has grown in part due to appealing aesthetic and mechanical properties, and also because of the declining use of another common restorative material, dental amalgam. More than half of the anterior and posterior restorations placed today in the United States are made

from resin composite materials [25][26]. Many of the problems associated with their early use such as insufficient mechanical strength and poor bonding to the surrounding tooth, have been solved or minimized [24]. However several issues still remain. In particular, the volumetric shrinkage that occurs during the polymerization reaction is a persistent problem that drives further research into these materials [27][28].

While there is variation among different formulations of dental composites, they all consist of an organic polymer resin matrix and inorganic filler particles. Dimethacrylates comprise the most common type of resin matrix, which includes bisphenol-A-glycidyldimethacrylate (BisGMA), triethylene glycol dimethacrylate (TEGDMA), and urethane dimethacrylate (UEDMA). The inorganic filler particles, which can account for 30-70% of the volume of the composite, are added to improve mechanical properties of the finished restoration, as well as to reduce wear and polymerization shrinkage. These particles are commonly small pieces of quartz or glass that are coated with an organo-silane coupling agent to improve bonding between the matrix and the filler. They range in size from tens of nanometers to tens of micrometers [24]. Smaller filler particles are often combined with larger particles to increase the total volume of filler in the composite. Several other components are also added in small amounts, including pigmentation, inhibitor, and, in the case of photo-activated composite, photo-initiator and co-initiator.

In practice, the composite starts as a soft, paste-like material. After it is applied to a cavity preparation, it must undergo a chemical hardening process referred to as

curing. In many composites, the curing process is a free-radical polymerization that is made possible by the addition of a photo-sensitive chemical species, which is known as a photo-initiator, and the use a curing lamp with light emission targeted to match the absorption spectrum of the photo-initiator. This polymerization reaction is typically designed to occur quite rapidly, on the order of seconds. This is appealing for both the patient and the clinician.

A major problem arising from the curing of these composites, which tends to be exacerbated at higher rates of polymerization [29], is volumetric shrinkage that accompanies the reaction, and the corresponding stress that ensues. This can lead to a number of undesirable outcomes, including pain, damage to the tooth, marginal failure (gap formation) between the restoration and tooth, as well as failure of the restoration itself [30]. This issue is one of the main motivations for research and development into new composite materials and new curing protocols.

Researchers have sought a better understanding of the kinetics of the polymerization reaction, including the rate of polymerization, how the rate changes with time, and how it relates to the development of the physical properties of the final composite restoration. It is commonly believed that a better understanding of these complex relationships will lead to the development of composites that exhibit less shrinkage stress during curing.

Numerous studies have investigated how the polymerization kinetics affect shrinkage stress and the development of mechanical properties [29][31-34]. This topic will be discussed in Chapters 4 and 6. In general it can be said that many of the current experimental methods for measuring polymerization rate are less than ideally suited to the task. Mechanical testing apparati tend to have compliance issues that make measuring small deformations and high stresses difficult [28][35], particularly early in the reaction when polymerization undergoes rapid acceleration [36]. Other methods, such as infrared spectroscopy [37][38] and calorimetry [39], require complex and potentially unrealistic testing conditions and sample configurations. Alternatively, DLS techniques have the potential of elucidating the polymerization kinetics without any of the aforementioned limitations. They can be applied to composite samples in a variety of configurations, they do not suffer from compliance issues, and they require no calibration. Further, DLS techniques offer the potential for a temporal resolution superior to many other methods.

1.3 Dissertation overview

The aim of this dissertation is to extend the use of DLS for reactions and processes that cannot be monitored with traditional single detector methods. A overview of DLS in the single scattering regime, quasi-elastic light scattering (QLS), is presented in Chapter 2. Included in this chapter are a mathematical description of the dynamic scattering process, an overview of QLS instrumentation and experimental procedure, as

well as results from a microsphere study. Instrumentation for QLS uses a point detector, which serves as a comparison for the multi-pixel CCD methods presented later.

Chapter 3 examines the role of laser speckle in DLS, and considers the optimal spatial sampling requirements for multi-pixel CCD detection. The results and theory of this chapter influence the experimental design of the methods described in the following chapters.

Chapter 4 introduces a method referred to as sequential speckle correlation (SSC) that uses an ensemble averaged correlation between pairs of dynamic speckle images to characterize the polymerization reaction of dental composite. One of the main benefits of this technique is the increase in temporal resolution that is achieved through ensemble averaging. Another method that uses ensemble averaging to improve temporal resolution is laser speckle contrast analysis (LSCA), which is explored in Chapter 5. LSCA has previously been used to monitor blood flow, but this study is the first time it has been used to study dental composite polymerization. Unlike the SSC method, LSCA is able to measure spatial variations in dynamic behavior, the results of which are shown in Chapter 5. In Chapter 6 LSCA is used to quantitatively characterize composite polymerization as a function of curing irradiance. The results agree well with polymerization theory and prior experimental studies, which serves as a validation of the method. Conclusions, further discussion, and directions of future work are presented in Chapter 7.

Chapter 2

Quasi-elastic light scattering (QLS): Implementation of dynamic light scattering in the single scattering regime and implications for the study of dental composite

2.1 Introduction

One of the simplest methods for studying dynamic light scattering is the technique known as quasi-elastic light scattering (QLS). This versatile optical technique has a variety of useful applications, including particle sizing, micro-rheology, and the monitoring of thermodynamic transitions and slowly occurring chemical reactions. The theory behind QLS is applicable for systems exhibiting single-scattering, and is most useful for the case of small, statistically independent particles. In this chapter the theory behind QLS, which is in many ways applicable to a range of other dynamic light scattering (DLS) techniques, will be presented. Specific attention will be given to the correlation analysis used to quantify signal fluctuations and the manner in which it can be used to characterize the dynamics of a medium. The advantages and limitations of QLS as a method for describing dynamic processes will be discussed, along with implications that apply to other DLS techniques.

The study of dynamically scattered light had a breakthrough with the development of the optical technique known as quasi-elastic light scattering (QLS)

[1][40]. Also commonly known as photon correlation spectroscopy (PCS), or sometimes simply referred to as dynamic light scattering (DLS), this method has been thoroughly developed from both a theoretical and technical point of view. The experiments of Forrester, Gudmunson, and Johnson [41] on the temporal correlation of light, and of Hanbury-Brown and Twiss [42] on spatial correlations are considered to be the pioneering works on the statistical analysis of optical fields, which paved the way toward the correlation analysis of dynamically scattered light[16][18]. With the development of the laser in the 1960s, as well as the development of increasingly higher sensitivity photo-multiplier tubes in the years that followed, the technical necessities were in place to advance the study of scattered light, which had previously been difficult, if impossible, due to low signal levels.

The QLS method saw a considerable development over the next 20 years, with the design of various optical configurations for detecting and analyzing temporal variations in scattered light. QLS became a reliable method for conducting particles sizing and rheology experiments, and has been applied to study systems ranging from simple colloidal suspensions [43], to more complicated systems containing proteins [10], polymers [44], and biomolecules [45].

The theory behind QLS is based on a number of key assumptions about the dynamic medium in question. The basis for the "quasi-elastic" assumption is that the wavelength (and frequency) of the scattered photons are essentially the same before and after scattering. Scatterer velocities in a QLS experiment are typically low enough for

this assumption to be valid. Other important assumptions are that scattering occurs in the single-scattering regime; scattering particles are smaller than the probing wavelength; the behavior of individual scattering particles are statistically independent of one another; and the number of scatterers is sufficiently large so as to invoke the central limit theorem. When these assumptions are met, the temporal autocorrelation function (ACF) of the scattered light can be directly related to the diffusive motion of the scattering particles, which is known to be a function of particle size, viscosity and temperature of the medium. In this manner the dynamically scattered signal can be used to investigate material properties of a sample, or to monitor changes in particle diffusivity.

The purpose of this chapter is to provide an overview of QLS and to serve as an introduction to the principles of dynamic light scattering. A theoretical description of the scattering process and how it can be used to study the diffusive properties of a scattering medium is described. The optical design of a QLS apparatus and the digital autocorrelation processing algorithm are also presented, along with experimental results from ideal scattering systems consisting of microsphere suspensions. Finally we relate the use of QLS to the overall theme of monitoring transitions in kinetic behavior.

2.2 QLS Theory

In describing the theoretical framework behind QLS, there are two main facets of the problem to consider. The first is a mathematical model of the scattering process as it relates to the dynamic properties of the scattering medium. The second is the quantitative assessment of the experimentally measured intensity signal based on its statistical properties.

2.2.1 Correlation

Statistical measures of correlation, and specifically that of autocorrelation, are central to the study of QLS and to DLS as a whole. These concepts form the basis of analysis of the scattered intensity signal, in which the aim is to relate the temporal variations to the underlying dynamic process of interest. Generally speaking, correlation can be described as a measure of similarity. For two random variables, X and Y, correlation can be expressed most simply as the average value of their product:

$$\Gamma_{XY} = E\{XY\} \tag{2.1}$$

where $E\{-\}$ indicates the expected value

$$E\{XY\} = \int_{-\infty}^{\infty} xy\, p(x,y)\, dx\, dy \tag{2.2}$$

and $p(x,y)$ is the joint probability distribution of *X* and *Y*. The larger this expected

value, the greater the degree of similarity of the two variables.

Additionally, correlation may be defined in a number of various ways, which mainly

differ in the manner of normalization. For example, the commonly used Pearson's

correlation coefficient (also referred to as the Pearson product-moment correlation

coefficient) [46] is defined as the expected value of the product of the two variables,

after subtracting off their respective means, normalized by the product of their standard

deviations:

$$\rho_{XY} = \frac{E\{(X - \mu_x)(Y - \mu_y)\}}{\sigma_x \sigma_y} \tag{2.3}.$$

This common method of standardization (subtracting the mean and normalizing by

standard deviation) yields a correlation measurement that varies from (-1,1), with 1

representing complete linear correlation, -1 representing anti-correlation, and 0

indicating no correlation.

When the random variables vary with time (i.e. a random *process*) a temporal

cross correlation function can be defined that describes the correlation between them as

a function of two points in time

$$\Gamma_{XY}(t_1,t_2) = E\left\{X(t_1)Y^*(t_2)\right\} \tag{2.4}$$

where the asterisk denotes the complex conjugate.

Of particular interest for studying dynamically scattered light is the case in which X and Y are the same process, which is known as autocorrelation:

$$\Gamma_{XX}(\tau) = E\left\{X^*(t)X(t+\tau)\right\}. \tag{2.5}$$

Eq (2.5) assumes that the process is wide-sense stationary and hence the autocorrelation can be represented as a function of the time difference between the two realization of X: $\tau = t_2 - t_1$.

Autocorrelation describes the self-similarity of a signal, providing a measure of the time-scale of signal fluctuations. A useful measure in this case is the decorrelation time τ_{dc} which is defined as the time delay it takes for a delayed signal to become uncorrelated with the un-delayed signal. This is the time at which Γ_{XX} reaches a value of $1/e$ of the zero-time-delay correlation.

One can define a standardized autocorrelation (similar to the Pearson's correlation coefficient),

$$\gamma_{XX}(\tau) = \frac{E\left\{[X^*(t) - \mu_x][X(t+\tau) - \mu_x]\right\}}{\sigma_x^2}, \qquad (2.6)$$

which varies in the range [-1,1] and is the normalized auto-covariance.

Ergodicity and dynamic heterogeneity

In the definitions of autocorrelation motioned above, the expected values represent averaging in the ensemble sense. The general approach in QLS, however, is to treat these quantities as temporal averages, with the implicit assumption that the process may be considered ergodic. This assumption is generally not valid for media that display any solid-like behavior, or experience dynamic heterogeneity [47-49].

Frequency domain

Autocorrelation describes the behavior of a dynamic signal in the *time domain*; the power spectral density (PSD) is an analogous measure that can be used to describe the dynamic behavior of the signal in the *frequency domain*. The relationship between these two descriptions is the well-known Wiener-Khinchin theorem, which states that the autocorrelation of a signal forms a Fourier transform pair with its PSD.

$$S(f) = \left| \frac{1}{\sqrt{2\pi}} \int_{-\infty}^{\infty} x(t) e^{i2\pi ft} dt \right|^2 \tag{2.7}$$

$$\Gamma_{XX}(\tau) = \int_{-\infty}^{\infty} S(f) e^{-i2\pi\tau f} df \tag{2.8}$$

Therefore either representation (autocorrelation or PSD) of the signal provides equivalent information regarding the dynamic behavior of a system. In this work emphasis will be given to the autocorrelation approach, with occasional reference to the frequency domain description.

Field and intensity autocorrelation

Two autocorrelations may be used to describe dynamically scattered light: the electric field autocorrelation and the intensity autocorrelation. Both are typically represented in the literature by the letter G, with a subscript 1 denoting field autocorrelation and a subscript 2 denoting intensity. Use of upper case G is usually reserved for an un-normalized autocorrelation function, whereas lowercase g is used when the function has been normalized. These are the conventions we use. The intensity autocorrelation is obtained experimentally through the use of a square-law detector, while the field autocorrelation may be derived as shown in Section 2.2.2. Intensity is the squared modulus of the field, however relating the two autocorrelation functions requires use of the Seigert Relation, discussed in the following section.

The field autocorrelation is defined as:

$$G_1(\tau) = \left\langle E(t)E^*(t+\tau) \right\rangle, \tag{2.9}$$

where $E(t)$ is the electric field, and the bracket notation represents a temporal average, such that

$$\left\langle E(t)E^*(t+\tau) \right\rangle = \frac{1}{T-\tau} \int_0^{T-\tau} E(t)E^*(t+\tau)dt, \tag{2.10}$$

where T is the temporal duration of the signal. Equation (2.9) is normalized by the autocorrelation at zero time delay (which is equivalent to the expected value of the intensity),

$$g_1(\tau) = \frac{\left\langle E(t)E^*(t+\tau) \right\rangle}{\left\langle E(t)E^*(t) \right\rangle} \tag{2.11}$$

such that $g_1(0)$ is by definition equal to unity, and is less that unity at all other times.

Similarly, the intensity autocorrelation function is defined as:

$$G_2(\tau) = \left\langle I(t)I(t+\tau) \right\rangle. \tag{2.12}$$

where $I(t)$ is the intensity. There are several methods of normalizing the intensity autocorrelation. The most common, and the method used herein, is normalization by the square of the expected (mean) intensity:

$$g_2(\tau) = \frac{\langle I(t)I(t+\tau)\rangle}{\langle I(t)\rangle^2}. \qquad (2.13)$$

It is worth pointing out that, while the normalized *field* autocorrelation has a zero time-delay intercept of unity and decays towards zero, the normalized *intensity* autocorrelation, as defined here, has an intercept between 1 and 2, and decays towards unity.

Siegert relation

When the scattered field is a Gaussian random variable (GRV), the field autocorrelation can be directly determined from the experimentally obtained intensity autocorrelation function through the Siegert relationship [50]:

$$g_2(\tau) = 1 + \beta|g_1(\tau)|^2. \qquad (2.14)$$

The derivation of this formula relies on the Gaussian moment theory, which states that, for zero mean GRVs, all higher order moments can be determined from second order moments [51]. The scattered field can be assumed to be a GRV when a large number of

independent scatters are contained within the scattering volume and when scattering

occurs in the single scattering regime [52].

The factor β in Eq (2.14) takes into account the variability in the $\tau = 0$ intercept

of g_2. This factor is affected by the degree of polarization of the scattered light, as well

as by the size of the spatial coherence area at the detector [53]. A single spatial

coherence area is commonly referred to as a speckle (see Chapter 3), the size of which

is determined by the characteristics of the optical detection system and is on the order of

$$\square \; \frac{2.4(1+M)\lambda f}{d} \; , \tag{2.15}$$

where λ is wavelength, f is focal length, M is the system magnification, and d is the

diameter of the pupil. If the detector size is large in comparison to S_{min}, then multiple

statistically independent speckles will be averaged together, which acts to reduce the

variance of the observed fluctuations and causes a decrease in the value of g_2 at $\tau = 0$.

β typically has a value between 0 and 1, with low values observed for a detector that is

much larger that the speckle size, and values near 1 occurring when the speckle size is

larger or matched to the detector size. See Goodman [52] for a detailed derivation and

discussion of β, which is the inverse of his M parameter. It is also worth pointing out

that if un-polarized light is detected, the upper limit on β is reduced to $1/\sqrt{2}$ due to the

averaging of orthogonal polarization states. Fig. 2.1 illustrates the relationship

between g_1, g_2, and β.
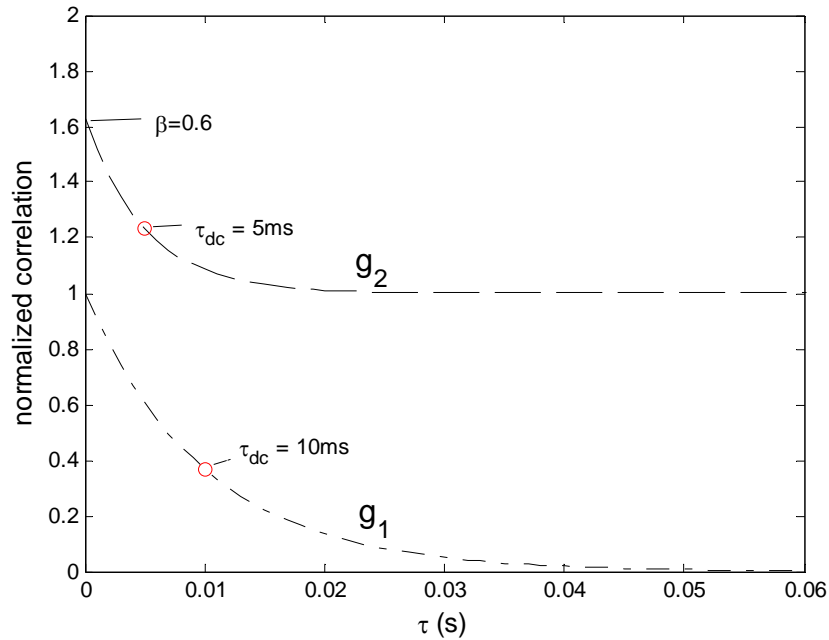
Fig. 2.1 The relationship between the normalized field autocorrelation g_1, intensity autocorrelation g_2, and the coherence factor β. Example is for a field decorrelation time τ_{dc} of 10 ms, which correspond to an intensity τ_{dc} =5 ms. β =0.6 is arbitrary.

Calculating autocorrelation from experimental data

With QLS the scattered intensity is measured via a square-law detector. There

are a number of ways to determine the autocorrelation from the intensity signal. The

brute-force approach is to use the definition of $G_2(\tau)$ in Eq (2.12) and compute the

expected value for each finite time delay τ by taking the arithmetic mean of all pairs of

data separated by that time delay:

$$\left\langle I(t)I(t+\tau)\right\rangle = \frac{1}{N_\tau}\sum_{i=1}^{N_\tau}I_iI_{i+\tau}. \tag{2.16}$$

However this is not a particularly efficient method.

A better approach (in terms of coding and computational efficiency) is to make

use of the Wiener-Khinchin theorem, which involves performing two FFT

transformations [54][55]. The first FFT is taken over the entire intensity signal. To

avoid aliasing, the number of points N in the FFT (achieved through zero-padding) must

be at least $2L$, where L is the number of data points in the sequence. A second FFT is

then performed on the *squared modulus* of the result of the first FFT (which has a

length N). Again, the FFT length should be $N \geq 2L$. The result is the raw

autocorrelation:

$$G'(\tau) = FFT^{-1}\left\{\left|FFT\left\{I(t)\right\}\right|^2\right\} \tag{2.17}$$

which is a biased estimator of the autocorrelation as defined in Eq (2.12). Normalization

to remove the bias is achieved by dividing the autocorrelation at each time delay τ by

$N/2 - \tau r$, where $N/2$ is the length of the one-sided autocorrelation, and r is the sample

rate of the autocorrelation function. The sample rate is dependent on the time duration T

of the original data signal, and N, the padding length of the FFT:

$$r = \frac{N}{2T} \tag{2.18}$$

Note that when $N=2L$, r is simply the initial data acquisition rate, L/T. The resulting

autocorrelation

$$G(\tau) = \frac{2}{N(1 - \tau/T)} G'(\tau) \tag{2.19}$$

has been corrected for the number of samples that contribute to the calculation for each

delay time.

2.2.2 Physical description of scattering

In this section the theoretical framework used to derive of the autocorrelation

from the point of view of the scattering process is presented. A dynamic light scattering

experiment, at its most basic, can be broken down into 1) the probing light, typically a

laser beam, 2) the scattering medium, and 3) a detection scheme. This is illustrated in

Fig. 2.2. A narrow beam of light is propagated through the scattering medium. The

detection optics gather scattered light from a small area of this beam. The region where

the laser beam and the detection field of view (detector angle) coincide within the

medium is specified as the *scattering volume*, and all scattering particles within this

region at any giving time contribute to the measured signal.
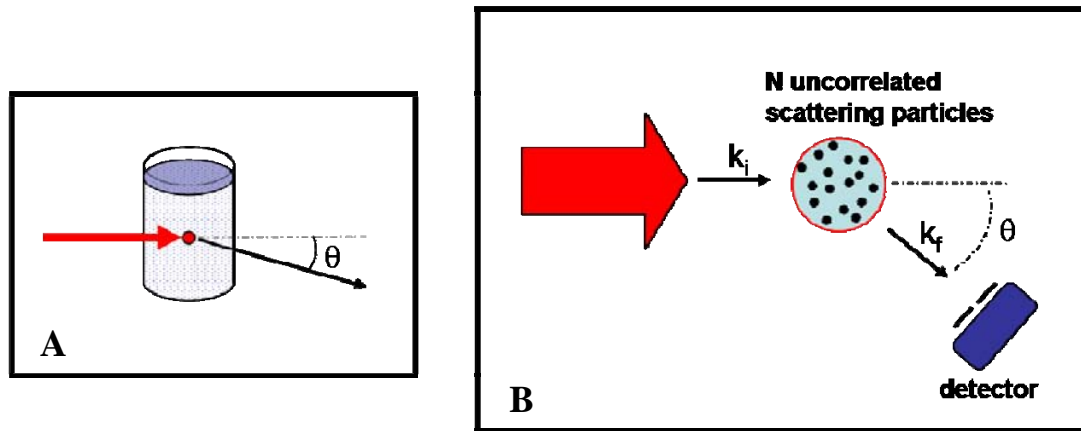
Fig. 2.2. Basic principles of a QLS experiment. A. General overview. B. View of the
plane containing the laser beam, scattering volume, and detector.

Consider the case of a single, small (on the order of the wavelength), spherical

particle within the scattering volume. The particle is described in terms of a position

vector **r**, with an origin located within the scattering volume. The incident laser beam

can be described by wave vector $\mathbf{k_i}$, which for convenience may be considered to be

oriented at an angle which defines 0 degrees, and the direction of detection can be

defined by wave vector $\mathbf{k_f}$. The magnitudes of both vectors are equal and defined by

$$\left|\mathbf{k_f}\right| = \left|\mathbf{k_i}\right| = \frac{2\pi}{\lambda}. \tag{2.20}$$

The field scattered by a hypothetical reference particle located at the origin is defined as

$$E(t) = a_0(t) e^{i\phi_0} , \tag{2.21}$$

where $a_0(t)$ is the amplitude of the scattered light and ϕ_0 is an arbitrary phase defined by the scattering path. Using ϕ_0 as a reference, the change in phase of the light scattered by the particle located at **r** can be defined based upon the change in total pathlength (i.e. the sum of the pathlengths from source to scatterer, and scatterer to detector) relative to the phase of light scattered the hypothetical particle at the origin. A key assumption in this approach is that the incident and detection wave vectors remain essentially unchanged for scattering occurring at any location within the scattering volume. This assumption holds when the source and detector distances are much greater than the dimension of the scattering volume. In this case the phase difference between a scattering particle at **r**, compared to the hypothetical scattering event occurring at the origin, is given by

$$\Delta\phi = \mathbf{q} \cdot \mathbf{r} , \tag{2.22}$$

where

$$\mathbf{q} = \mathbf{k_f} - \mathbf{k_i} \tag{2.23a}$$

$$|\mathbf{q}| = \frac{4\pi n \sin(\theta/2)}{\lambda} . \tag{2.23b}$$

is known as the scattering vector and n is the index of refraction.

The field at the detector is therefore:

$$E(t) = a(t)e^{i\phi_0 + i\mathbf{q}\cdot\mathbf{r}}. \tag{2.24}$$

For the case of N uncorrelated particles within the scattering volume and photons are only scattered once (the single scattering regime), then the total field at the detector is the superposition of the fields scattered by the individual particles:

$$E(t) = \sum_{k=1}^{N} a_k(t)e^{i\phi_0 + i\mathbf{q}\cdot\mathbf{r}_k(t)} \tag{2.25}$$

where $\mathbf{r}_k$ is the position of the kth particle.

The field at the detector is stochastic due to the indeterminate position of the scatterers. To study the dynamics of the system, it is useful to examine the field autocorrelation as defined in Eq (2.9). Without loss of generality time may be fixed at $t = 0$, in which case

$$G_1(\tau) = \left\langle E(0)E^*(\tau) \right\rangle = \left\langle \sum_{j=1}^{N}\sum_{k=1}^{N} a_j(0)a_k(\tau)\exp\left(i\mathbf{q}\cdot\mathbf{r}_j(0) - i\mathbf{q}\cdot\mathbf{r}_k(\tau)\right) \right\rangle. \tag{2.26}$$

Note that the reference phase term ϕ_o has cancelled. Because the phase and amplitude are statistically independent these terms may be averaged separately [56]:

$$G_1(\tau) = N\left\langle |a|^2 \right\rangle \left\langle \sum_{j=1}^{N} \sum_{k=1}^{N} \exp\left(i\mathbf{q}\Box\mathbf{r}_j(0) - i\mathbf{q}\Box\mathbf{r}_k(\tau) \right) \right\rangle. \qquad (2.27)$$

For the case of identical, independent, scatterers, the cross terms $j \neq k$ vanish:

$$G_1(\tau) = N\left\langle |a|^2 \right\rangle \left\langle \sum_{j=1}^{N} \exp\left(i\mathbf{q}\Box\mathbf{r}_j(0) - i\mathbf{q}\Box\mathbf{r}_j(\tau) \right) \right\rangle \qquad (2.28)$$

$$= N\left\langle |a|^2 \right\rangle \left\langle \exp\left(-i\mathbf{q}\Box\Delta\mathbf{r}(\tau) \right) \right\rangle \qquad (2.29)$$

where $\Delta\mathbf{r}(\tau) = \mathbf{r}(\tau) - \mathbf{r}(0)$.

The normalized field autocorrelation becomes:

$$g_1(\tau) = \frac{G_1(\tau)}{G_1(0)} = \frac{\left\langle E(0)E^*(\tau) \right\rangle}{\left\langle E(0)E^*(0) \right\rangle},$$

$$g_1(\tau) = \left\langle \exp\left(-i\mathbf{q}\Box\Delta\mathbf{r}(\tau) \right) \right\rangle \qquad (2.30)$$

and it can be shown [57] that if $\Delta \mathbf{r}(\tau)$ is a GRV then

$$g_1(\tau) = \exp\left(-\frac{q}{2}\left\langle \Delta r^2(\tau) \right\rangle\right). \tag{2.31}$$

For uncorrelated scatterers undergoing Brownian motion, from diffusion theory we have [58]:

$$\left\langle \Delta r^2(\tau) \right\rangle = 2D\tau, \tag{2.32}$$

where D is the diffusion coefficient of the particle motion. For spheres, D can be related to the properties of the system by the Stokes-Einstein equation:

$$D = \frac{kT}{6\pi\eta a}, \tag{2.33}$$

where k is Boltzmann's constant, T is temperature in degrees Kelvin, η is viscosity of the medium, and a is the particle radius. This leads to a working form of the field autocorrelation that relates the particle diffusion coefficient to the scattered signal:

$$g_1(\tau) = \exp(-q^2 D\tau). \tag{2.34}$$

From the Siegert relationship it follows that the normalized intensity autocorrelation is given by

$$g_2(\tau) = 1 + \beta \exp(-2q^2 D\tau) .$$ (2.35)

This is the equation used to relate the experimental intensity autocorrelation function, determined from the scattered intensity signal via Eq (2.19), to the properties of the scattering medium, in particularly viscosity, temperature, or scatter size.

To reiterate, in arriving at Eqs (2.34) and (2.35) the following assumptions were used: the field at the detector is the superposition of a the fields from large number of scattering events; the movement of individual scattering particles is statistically independent of each other; the scatterers are small and monodisperse; and scatter motion is diffusive (although up to Eq (2.30) is valid without this assumption).

2.3 Experimental design and methods

A number of different optical systems have been developed over the years for studying QLS [40]. The one implemented for this work utilizes a homodyne detection scheme, and is described in this section. The key features of this system include a goniometric detection arm for angle resolved measurement, confocal detection optics, and a digital post-processing autocorrelation scheme for analysis of the measured light.

2.3.1 Experimental design
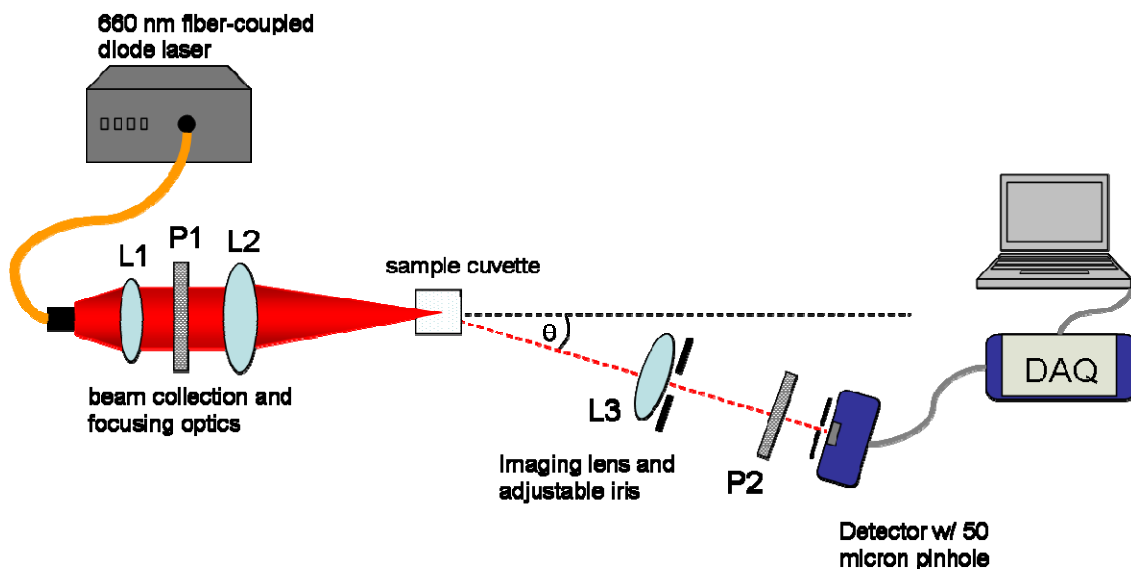
Fig. 2.3. Experimental design of the goniometric QLS system. L1-L3 are lenses, P1 and P2 are polarizers.

Fig. 2.3 shows the schematic diagram of the QLS system designed and implemented for this work. The source is a fiber-coupled diode laser (B&W Tek Inc.) which operates at a wavelength of 660 nm with a nominal output of 60 mW. The first lens (L1, $f = 6\,\text{cm}$) is used to capture the diverging beam exiting the fiber, after which the second lens (L2, $f = 7.5\,\text{cm}$) focuses the beam onto the center of scattering sample, contained within a 1 cm cuvette. The location of this focal spot coincides with the center of rotation of the detector arm and partially defines the scattering volume. The detector arm consists of an imaging lens (L3, $f = 7.5\,\text{cm}$), also focused on the center of the sample, which images the scattered light onto the detector, and further defines the scattering volume. An adjustable iris adjacent to the imaging lens allows the spatial

coherence dimension—i.e. speckle size—to be varied at the detector. The detector is a silicon photo-receiver with a 200 kHz bandwidth (New Focus, 2001-FS) and a 1mm^2 detector size. In front of the detector is a $50\,\mu m$ pinhole, which is roughly conjugate to the beam diameter at the center of rotation (taking into account magnification). The pinhole helps reject the detection of multiply scattered photons and avoid detector saturation. Polarizer P1 is oriented to allow only linearly polarized light through the system. Polarizer P2 is aligned parallel to P1, and is used to help reject stray scattering and multiple scattering.

Coherence issues

To maximize the dynamic range in the intensity autocorrelation function, the detector should measure as few speckles as possible. The signals from uncorrelated coherence areas will add together at the detector, reducing the observed fluctuations. This effect lowers the value of the coherence factor β. For a fixed focal length, magnification, and wavelength, the coherence area at the detector can be varied by changing the aperture size. In order to avoid averaging over multiple coherence areas, the expression in Eq (2.15) can be matched to the detector size, or in this case to the size of the detector pinhole, which is $50\,\mu m$ for this system. The system magnification $M = 2.9$, the focal length $f = 7.5$ cm, and wavelength $\lambda = 660$ nm. For these parameters, a $50\,\mu m$ coherence size (to match the pinhole size) can be achieved by setting the lens aperture to ~9 mm. A smaller aperture could also be used, but reduces the intensity without improving the range of the autocorrelation function.

For a single coherence area and a single polarization state being detected, the theoretical zero-time-lag intercept of g_2 function is two ($\beta = 1$). The highest values of β obtained with this system have been on the order of 0.9, and were often considerably lower.

2.3.2 Data acquisition and processing

Data acquisition for this system was controlled by a custom-written LabView routine using an NI 6221 DAQ board. Sampling rate and experiment duration could be adjusted at the time of the experiment. The scattered intensity signal was saved to a file for post-processing. A Matlab routine was written for performing numerical analysis of the recorded data and is included in the Appendix. This routine calculates the normalized autocorrelation function $g_2(\tau)$ using the Wiener-Khinchin theorem, as described in section 2.2.1.

The presence of 60 and 120 Hz noise was often problematic, particularly when scattering signal levels were low. An optional filtering subroutine was designed that can be called during autocorrelation processing (after the PSD was calculated, but prior to the second FFT), which acts as a notch-filter, removing all frequency components within a two Hz bandwidth centered around 60 Hz and 120 Hz.

The normalized intensity autocorrelation was least-squares fit to a three parameter negative exponential model of the form

$$y = a\,e^{-\tau/b} + c \,. \tag{2.36}$$

From the b parameter, the experimental decorrelation time τ_{dc} of the data can be determined, which may be compared with theory or used to characterize the medium if one of the variables in Eq (2.33) is unknown. The a parameter accounts for the coherence factor β, and c accounts for the possibility of long time-scale correlations that prevent $g_2(\tau)$ from decaying to unity. Fitting was performed over the range $\tau = 0$ - $5\tau_{dc}$, where τ_{dc} was estimated at the time of fitting as the time at which the value of g_2 first drops below 0.38. The cutoff for the fitting ($5\tau_{dc}$) was chosen to be long enough for g_2 to fully decay (within 0.5% of the baseline value c).

2.3.3 QLS experimental procedures

Experiments on dilute microsphere suspensions were used to validate the QLS system. The majority of the experiments used 100 nm or 200 nm spheres (Duke Scientific) because they satisfy the requirement that the scatterers be smaller than the probing wavelength ($\lambda = 660$ nm). Dilute suspension were made by adding several drops (~1-4) of stock 10% (by weight) microspheres to ~10 mL filtered de-ionized water. The water had previously been passed through a 100 nm filter (Whatman) to

remove large impurities. The microsphere suspensions were diluted to an extent that ensured single scattering. Based on Mie theory [59], it was determined that a concentration of ~ 0.05 spheres/μm^3 for 200 nm spheres (two drops stock solution in 10 mL water) or ~ 2 spheres/μm^3 for 100 nm spheres (8 drops in 10 mL) achieved a scattering mean free path of ~ 1 cm, the length of the sample cuvette. In other words, each photon is scattered only once (on average) upon propagation across the entire sample. This condition is more than sufficient to ensure detection in the single scattering regime.

The sample cuvette was placed on a stage at the center of rotation of the goniometer. In general the scattering angle could be chosen between $0° - 120°$. The beginning of the experiment was initiated by running the Labview routine and was terminated automatically after the duration specified prior to the experiment. Sampling rate and experimental duration varied depending on sphere size and scattering angle. Sampling rate was generally between 1-10 kHz, and experimental duration varied from ~30 seconds to ~30 minutes.

2.4 Experimental results

Fig. 2.4 shows an example of an intensity signal from a QLS experiment. This particular data set was obtained from a suspension of 100 nm spheres, at a scattering angle of 32 degrees, and at room temperature, $21\,^{\circ}C$. (The corresponding viscosity of

water at this temperature is 10^{-3} kg$\cdot$s$^{-1}\cdot$m^{-1}). From Eq (2.33) the theoretical diffusion

coefficient was found to be $D = 4.3\cdot10^{-3}$ mm^{3}s^{-1} and using this value in Eq (2.35), along

with $q = 7\cdot10^6$ m^{-1} (from Eq (2.23b)), the expected 1/e decay time is 2.4 ms.

Fig. 2.5 shows the computed normalized intensity autocorrelation

function $g_2(\tau)$ along with the results of the negative exponential fitting. These results

demonstrate that the fluctuations seen in Fig. 2.4 occur with a characteristic 1/e

decorrelation time of 2.1 ms, while theory predicted 2.4 ms. The exponential time

constants from a series of experiments on 100 nm and 200 nm microsphere over a range

of scattering angles are shown in Figs. 1.6 and 1.7.
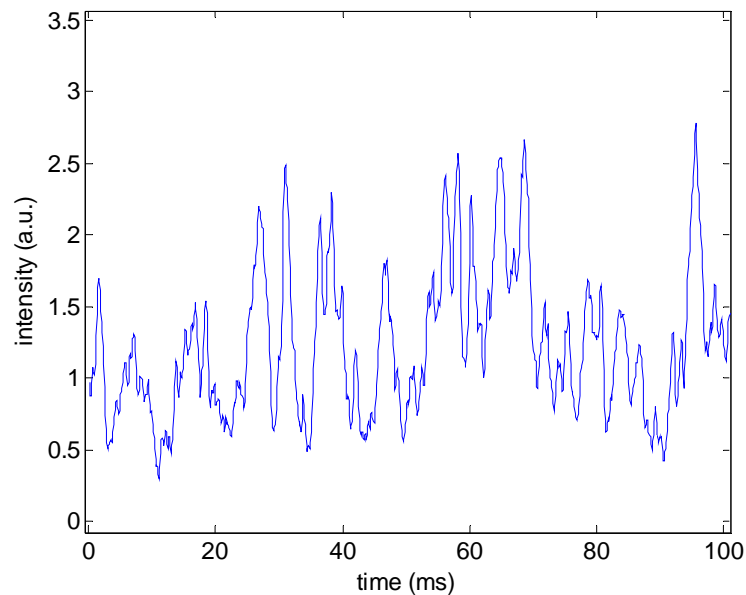
Fig. 2.4. A portion of the intensity signal from a QLS experiment. The suspension
consisted of 100 nm microspheres in water at a concentration of ~1.2 μm^{-3} . Scattering
angle was $32\,^\circ$.
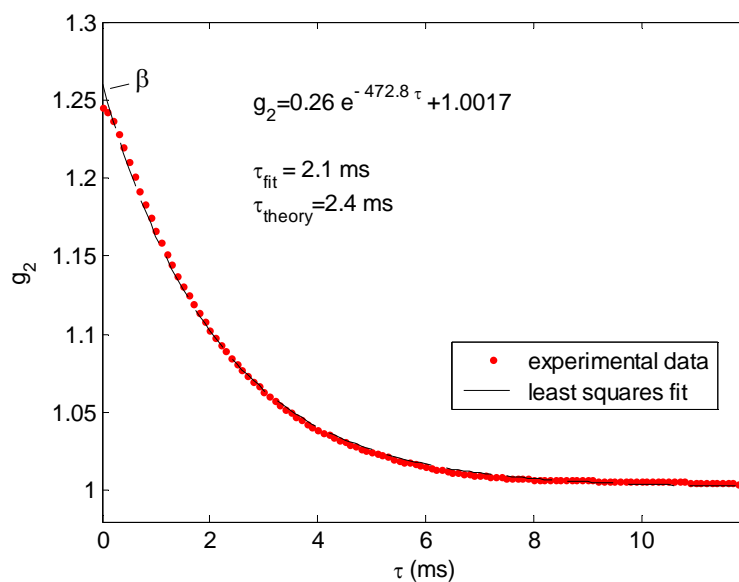
Fig. 2.5. Normalized intensity autocorrelation g_2 for the QLS data shown in Fig. 2.4. The dashed line represents the least squares fit to the data for the exponential function given in Eq. 2.36. The field of view of the figure delineates the data included in the fit.
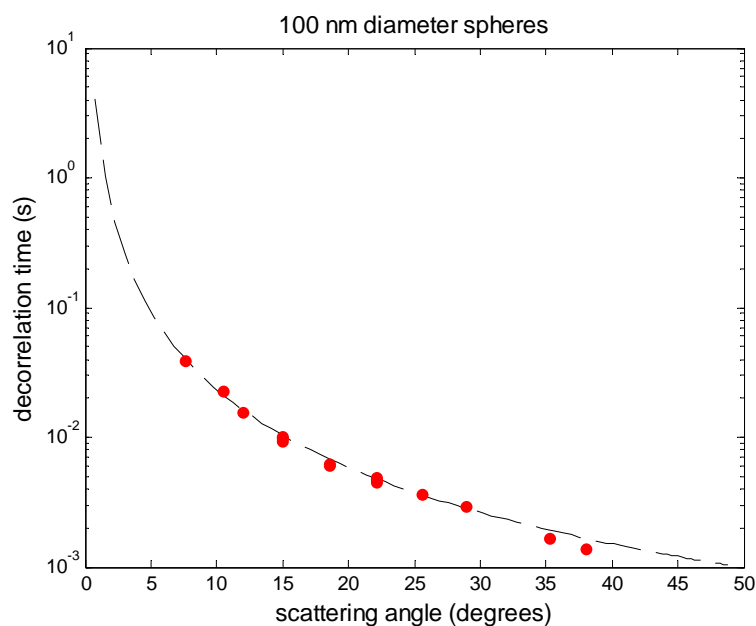
Fig. 2.6 QLS experimental result for 100 nm diameter microsphere suspensions measured at a range of scattering angles.
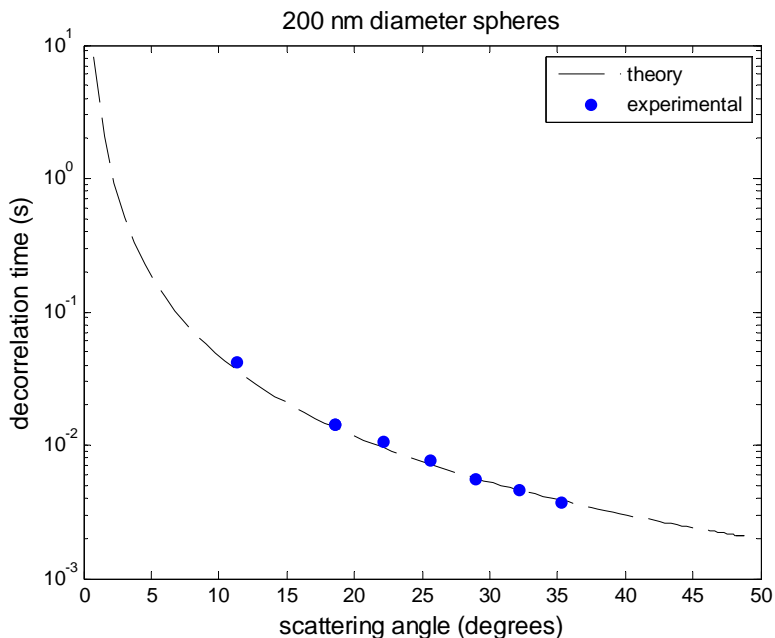
Fig. 2.7. QLS experimental result for 200 nm diameter microsphere suspensions measured at a range of scattering angles

2.5 Statistical considerations

2.5.1 Sampling rate

It is important to acquire the scattered intensity data from the detector at a sufficiently high sampling rate. Ten times faster that the decay rate of the autocorrelation function is a good rule of thumb for a minimum sampling rate if the expected decay rate is known *a priori*, although lower rates can be tolerated if a rough estimate of the autocorrelation profile is sufficient. Under-sampling will lead to loss of

measurement of the highest frequency fluctuations, causing a roll-off in the ACF near

$\tau = 0$. If hardware memory is not an issue, it is generally a good practice to sample at a

rate more that 10 times faster than expected decay rate.

2.5.2 Experiment duration

To achieve accurate results with QLS, it is necessary to acquire data for a

duration several orders of magnitude longer than the decorrelation time of the temporal

fluctuations. The autocorrelation for a given time delay, τ, is the mean correlation of all

pairs of data in the sequence separated by τ seconds;

$$G_2(\tau)_N = \left\langle I(t)I(t+\tau) \right\rangle_N ; \qquad (2.37)$$

the longer the duration of the experiment, the more pairs of data, N, contribute to this

mean. For experimental data recorded for T seconds at a rate of r samples per second,

the sample size from which the expected correlation is measured is

$$N(\tau) = (T - \tau)r . \qquad (2.38)$$

As the number of independent samples N_I contributing to a mean (such as the

one in Eq (2.37)) increases, the expected variation about the sample mean decreases

with $1/\sqrt{N_I}$ [58]. However, when calculating an autocorrelation, each pair of data

separated by τ is *not* statistically independent. Pairs of data become roughly

decorrelated every $t = \tau_{dc}$ seconds and thus the number of statistically independent

samples contributing to the autocorrelation is approximately $N(\tau)/\tau_{dc}\,r$. For $T > 20\tau$

and $\tau \approx \tau_{dc}$,

$$N_I \approx T / \tau_{dc}. \qquad (2.39)$$

Let Γ be the random variable defined by the product of two intensity values

separated by $\tau = \tau_{dc}$:

$$\Gamma = I(\tau)I(\tau + \tau_{dc}). \qquad (2.40)$$

For a sequence of N randomly drawn Γ values (i.e. N intensity pairs) the sample mean

is given by

$$\overline{\Gamma}_N = \frac{1}{N}\sum_{i=1}^{N} I(\tau_i)I(\tau_i + \tau_{dc}), \qquad (2.41)$$

which is equivalent to the value of the un-normalized ACF G_2 (Eqs. 2.12 and 2.19)

measured at $\tau = \tau_{dc}$. Based on the Central Limit Theorem, $\overline{\Gamma}_N$ exhibits a normal

probability distribution. The number of samples N needed to achieve a desired level of

confidence in $\overline{\Gamma}_N$ can be determined from a standard normal table (using the Z statistic), if the population standard deviation σ_Γ and mean μ_Γ are known

$$N = \left(\frac{Z\sigma_\Gamma}{c\,\mu_\Gamma}\right)^2, \tag{2.42}$$

where c defines the confidence interval centered around μ_Γ ($\mu_\Gamma \pm c\mu_\Gamma$) [58]. For a 95% confidence level, i.e. the probability $P(\mu_\Gamma - c\mu_\Gamma \leq \overline{\Gamma}_N \leq \mu_\Gamma + c\mu_\Gamma) = .95$, Z=1.96.

The population statistics μ_Γ and σ_Γ can be determined for experimental data by selecting a large sample size (i.e. N=100,000) and calculating the sample mean and standard deviation according to

$$\mu_\Gamma = \frac{1}{N}\sum_{i=1}^{N}\Gamma_i \tag{2.43}$$

$$\sigma_\Gamma = \left(\frac{1}{n-1}\sum_{i=1}^{N}(\mu_\Gamma - \Gamma_i)^2\right)^{1/2}. \tag{2.44}$$

For the experimental data shown in figure 2.5, σ_Γ and μ_Γ were found to be 1.82 and 1.89, respectively. Therefore, to ensure that $\overline{\Gamma}_N$ is within 5% (c=0.05) of μ_Γ, with a probability of 0.95, the number of independent samples N should be ~1430. For a 10% confidence interval (c=0.1) the number of sample is $N \approx 360$. This was verified by

randomly drawing a sequence of N pairs of intensity data, calculating $\bar{\Gamma}_N$, and repeating 10,000 times. The histogram of $\bar{\Gamma}_N$ for $N=1430$, shown below (Fig 2.8), demonstrates that $\bar{\Gamma}_N$ was within 5 % of μ_Γ with a probability of ~0.95.
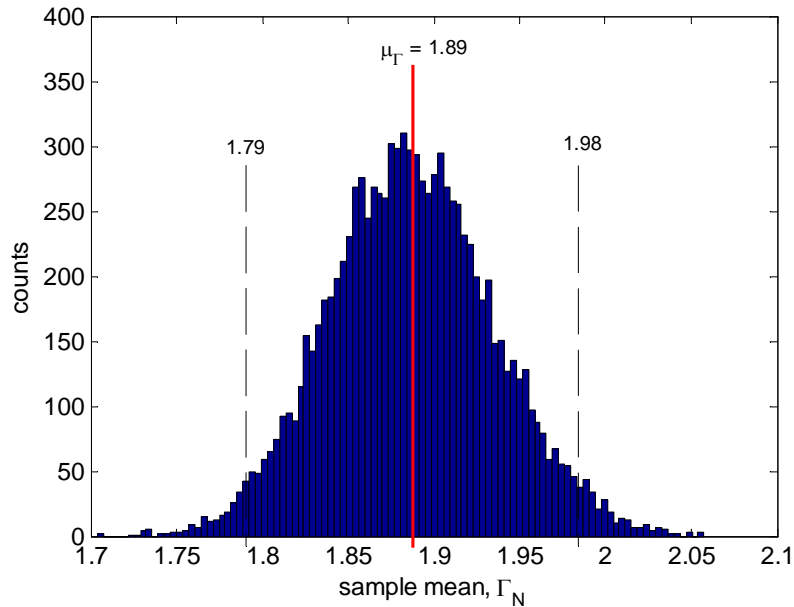
Fig. 2.8. Histogram of the correlation calculated from *N=1430* statistically independent pairs of intensity data separated by τ_{dc}, repeated 10,000 times. 9486 of the 10,000 trials (~ 94.9% confidence level) yielded $\bar{\Gamma}_N$ that were within ± 5 % of the expected value of $\mu_\Gamma = 1.89$.

Based on this analysis it can be concluded that, for this specific data set, to measure τ_{dc} with less than 5% error requires averaging over ~1400 independent intensity fluctuations. The decorrelation time was determined to be $\tau_{dc} = 2.4$ ms, therefore an experimental duration of $T > 3.4$ s would be needed.

The previous analysis utilized randomly drawn data in order to ensure statistical independence. In practice, a contiguous intensity signal is used. Fig. 2.9 shows the standard deviation of the calculated correlation $g_2(\tau_{dc})$, over n=15 repeated trials, as a function of the experimental duration normalized by the decorrelation time τ_{dc}. The abscissa in this figure is indicative of the number of independent fluctuations N_I (Eq.2.39) averaged in the correlation calculation. For each scattering angle, the observed behavior was the same. Standard deviation decreases with increasing T/τ_{dc}, approaching a plateau at approximately $T/\tau_{dc} = 1000$. The β values for each data set were in the range 0.20-0.23, determined by inspection of g_2 calculated from the entire experiment (>20,000 τ_{dc}).
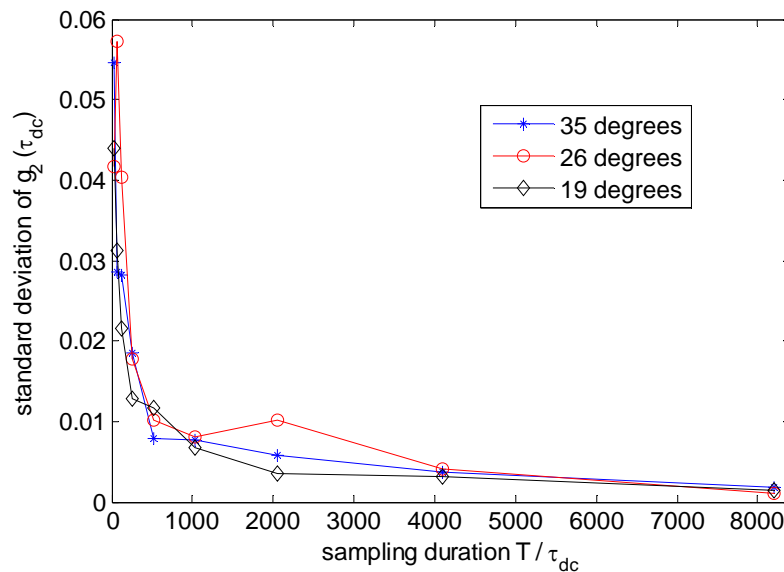
Fig. 2.9. Standard deviation of g_2, measured at τ_{dc}, as a function of the sampling duration normalized by the characteristic decorrelation time, for three scattering angles. Each calculation was repeated n=15 times. Microspheres had a diameter of 200nm. Decorrelation times were 4 ms, 7.4 ms, and 14 ms, for angles 35 degrees, 26 degrees, and 19 degrees, respectively. β values were in the range 0.20-0.23.

Figure 2.10 examines the effect of the coherence factor β for three sets of data measured at the same scattering angle (18.5 degrees). These results demonstrate a slower convergence to the expected correlation for larger values of β. The effect of β on experimental duration was further explored by calculating the hypothetical number of independent samples N needed to achieve a c=0.05 confidence interval, using (Eq. 4.42), for a range of β. The results, shown in Fig. 2.11, indicate that fewer independent samples are needed as β decreases, which may be attributed to ensemble averaging at the detector (over multiple independent speckles) which acts to reduce the temporal sampling requirements.
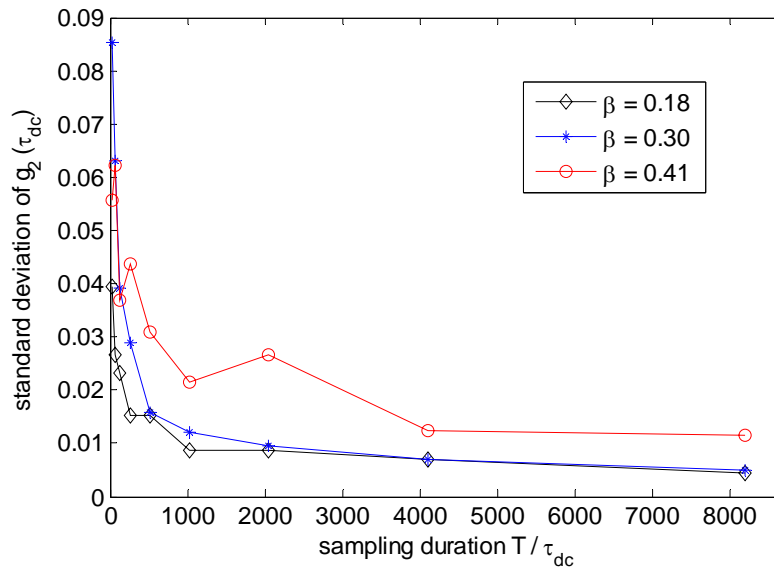
Fig. 2.10. Standard deviation of g_2, measured at τ_{dc}, as a function of the sampling duration normalized by the characteristic decorrelation time, for three β values. Calculation was repeated n=15 times. Microspheres had a diameter 100nm. Scattering angle was 18.5 degrees and τ_{dc} = 7 ms for each data set.
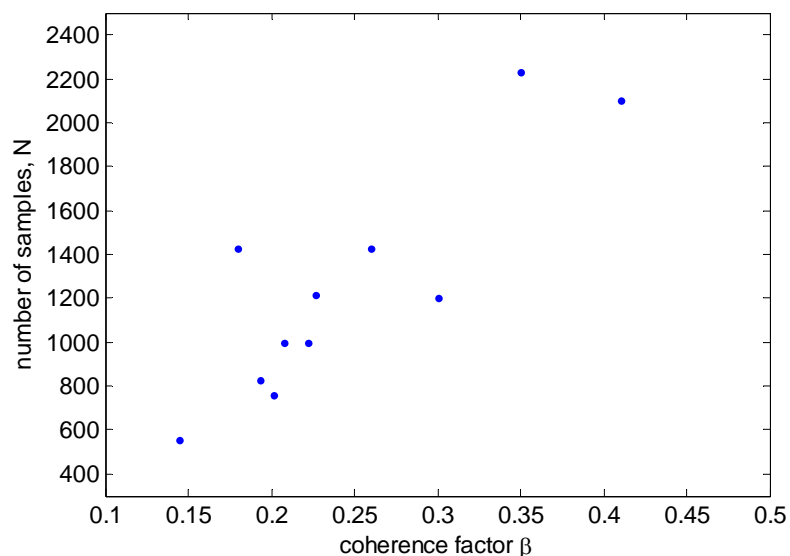
Fig. 2.11. Number of independent samples _N_ needed to achieve a 5 % confidence interval, as a function of coherence factor _β_. _N_ was calculated using Eq. 4.42 for _Z_=1.96 (95 % confidence level) Data includes experiments with 100 nm and 200 nm microspheres and a variety of scattering angles.

2.6 Discussion and conclusions

In this chapter the theory behind the experimental use of the QLS method was described. In addition to its usefulness in measuring the diffusive dynamics of scattering systems, QLS also describes the physical framework of dynamic light scattering. Many of the statistical concepts relating to the analysis of temporal variations of signals are fundamental to other DLS methods. The DLS techniques described in the subsequent chapters can be considered extensions of the QLS technique which simply utilize different detection or processing schemes.

A statistically reliable representation of the decay time of a system requires an experimental duration that can be quite long, often on the order of minutes. This is not an issue for systems in equilibrium, such as microspheres suspended in aqueous solution. For systems with dynamics that evolve relatively slowly, QLS can also be usefully applied, and many studies have been carried out using this technique to quantitatively characterize such systems [8][2][21]. Such experiments can be designed to ensure that the dynamics of the process under investigation changes at a slow enough rate, for example by reducing the concentration of a chemical reactant [21]. Yet for a great number of dynamic processes and reactions involving scattering media, the rate of change in kinetic behavior occurs rapidly, and cannot be practically slowed to an extent that QLS is feasible [22].

Chapter 3

Spatial sampling issues in dynamic light scattering: the effect of speckle size.

3.1 Introduction

The laser speckle phenomenon is ubiquitous in the study of coherent light scattering, and dynamic light scattering (DLS) is no exception. The results of a DLS experiment using a multi-pixel detector, such as a CCD camera, are affected by the statistical properties of the dynamic speckle patterns. Even when a speckle pattern is not explicitly observed, the properties of the speckle can impact interpretation of the temporal correlation analysis. This was seen in Chapter 2 when the detector pinhole size was matched to the dimension of the speckle to improve the signal to noise ratio in the measured autocorrelation function. Even though temporal variations in scattered intensity are the main focus of DLS, the spatial variations relating to speckle play an important role for proper interpretation.

3.2 Theoretical description of laser speckle

3.2.1 Physical description

Laser speckle is an interference phenomenon that is characterized by a spatial intensity pattern exhibiting a granular, or speckled, appearance. Speckle arises when a coherent light source, usually a laser beam, is scattered from a rough surface or object. The field at any observation point is the sum of the contributions from each individual scattering source within the area of laser illumination[52],

$$A(r) = \frac{1}{\sqrt{N}} \sum_{k=1}^{N} |a_k| e^{i\phi_k} \, , \tag{2.1}$$

where a_k and ϕ_k are the individual amplitude and phase at the detection point, and N is the total number contributing scattered fields. If the differences in scatterer-to-detector pathlength vary by more than a wavelength for the contributing fields, then ϕ_k can be assumed to be uniformly distributed on $(-\pi, \pi)$. It also may be assumed that the phase and amplitude of each scattering contribution are statistically independent of each other, and also independent of the phase and amplitude of all other scattering contributions. [52].

3.2.2 Statistics of the field

Furthermore, in the limit of a large number of scatterers the real (A_r) and imaginary (A_i) parts of the scattered field are uncorrelated, have identical variances (σ^2) and are zero mean (see Goodman [52] for a more detailed approach). The assumption of a large number of scattering sources, N, allows the central limit theorem to be invoked, which implies that both the real and imaginary components of the field are Gaussian random variables (GRV). The joint probability density function of the real and imaginary components is therefore [60]:

$$p(A_r, A_i) = \frac{1}{2\pi\sigma^2} e^{-\frac{A_r^2 + A_r^2}{2\sigma^2}} \qquad (3.1)$$

where the variance is defined as

$$\sigma^2 = \lim_{N \to \infty} \frac{1}{N} \sum_{k=1}^{N} \frac{\langle |a_k|^2 \rangle}{2} . \qquad (3.2)$$

3.2.3 First order statistics of intensity

The intensity probability distribution for a field consisting of real and imaginary components that are identically distributed, zero-mean GRVs, corresponds to a negative exponential [52]:

$$p(I) = \begin{cases} \dfrac{1}{\langle I \rangle} e^{-I/\langle I \rangle}, & I \geq 0 \\ \\ 0 & \text{otherwise} \end{cases}, \qquad (3.3)$$

where $\langle I \rangle$ is the ensemble average intensity. A fully-formed speckle pattern, for which only a single polarization state is observed, will exhibit such a distribution. A key property of this distribution is that its variance is identically equal to the square its mean,

$$\sigma_I^2 = \langle I^2 \rangle - \langle I \rangle^2 = \langle I \rangle^2. \qquad (3.4)$$

This important relationship demonstrates that the expected contrast of an ideal, fully-formed, speckle pattern is unity (when contrast is defined as the quotient of intensity variance to the square of the mean intensity).

3.2.4 Second order statistics of intensity: speckle size

The previous section presented the intensity probability distribution for a single point in space. Often the speckle size, a second order statistic, is of interest. Goodman [56] has shown that for the case of objective (non-imaged speckle) the characteristic minimum speckle dimension is on the order of

$$x = \frac{\lambda z}{d},$$ (3.6)

where λ is the wavelength, z is the propagation distance between object and observation

plane, and d is the dimension of the illuminated spot on the object. For DLS the

scattered light is collected in an imaging configuration. The size of subjective (imaged)

speckle is related to the imaging configuration by

$$x = \frac{2.44\,(1+M)\lambda f}{d}$$ (3.7)

where M is the system magnification, f is the focal length, and d is the diameter of the

imaging pupil[56]. It should be emphasized that Eqs. (3.6) and (3.7) describe the

minimum, not the mean, speckle size.

3.2.5 Polarization

Orthogonal polarization states produce statistically independent speckle patterns.

Therefore when multiple polarization states are present, as with unpolarized light, the

independent speckle patterns add together resulting in a deviation from the statistics

described in the previous section. Instead of the negative exponential intensity

probability seen for the case of polarized speckle, for unpolarized speckle the intensity

distribution is given by [26]:

$$p_I(I) = \begin{cases} \left(\dfrac{2}{\langle I \rangle}\right)^2 I e^{-2I/\langle I \rangle}, & I \geq 0 \\ 0 & \text{otherwise} \end{cases}.$$ (3.8)

This has the effect of increasing the probability of observing higher intensity values

(compared to polarized speckle), reducing the contrast to an expected value of 0.7.

Figure 3.1 shows the probability distributions of normalized intensity for polarized and

un-polarized speckle patterns.
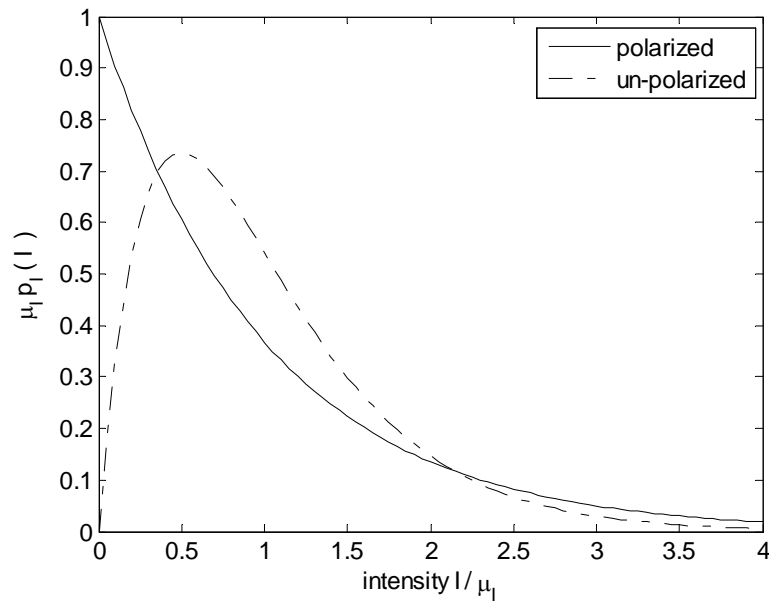
Fig. 3.1 PDFs of polarized and un-polarized speckle patterns. Intensity is
normalized by mean intensity μ_I

3.3 Experimental considerations

3.3.1 Manipulating speckle size

In scattering experiments using coherent light, including those involving DLS, it is often desirable to be able to adjust the speckle size in order to ensure that it is adequately sampled. This requires checking that the spatial sampling frequency, which is the inverse of the pixel size, is equal to, or greater than, twice the maximum spatial frequency in the image. This requirement is the spatial Nyquist criterion [61]. The maximum spatial frequency in a speckle pattern is the inverse of the minimum speckle size.

For the case of imaged speckle, the size can be manipulated by changing any of the parameters in Eq (3.7). However it is not often practical to vary the wavelength, and the focal length and system magnification are also usually restricted. The simplest way of changing the speckle size is thus by varying the pupil dimension, d, of the imaging lens. Opening the aperture stop produces smaller speckle and closing the aperture stop produces larger speckle.

3.3.2 Measuring speckle size

To determine the speckle size quantitatively requires obtaining an image of the pattern. For a digital speckle image, one of the easiest approaches is to use the power

spectral density (PSD), obtained from the squared modulus of a 2-dimensional spatial

FFT operation. From the PSD it can be determined if high spatial frequencies are cut-

off, which is an indication of under sampling. When this is the case, the imaging

aperture diameter can be reduced, and the process repeated, until an appropriate speckle

size is reached. Figure 3.2 shows the PSDs for various speckle sizes.
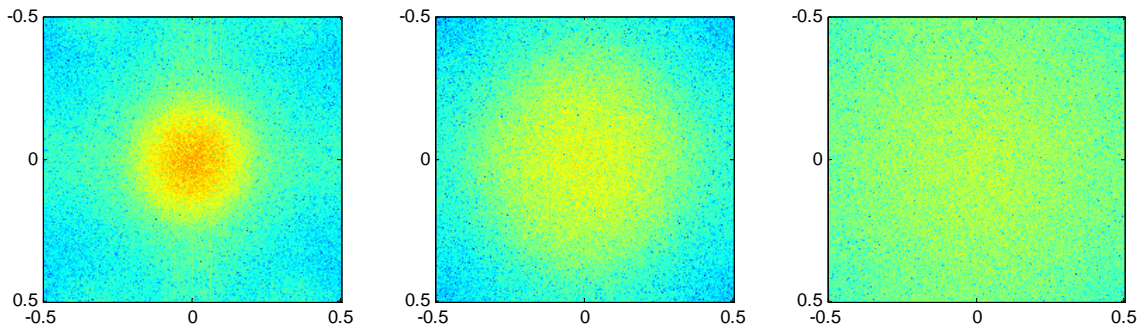
Fig. 3.2 PSD for different speckle sizes. A. Minimum speckle size ~4 pixels. B. Minimum speckle size ~2 pixels. C. Speckle size too small (< 2pixels) to be determined from the PDS. The axes markings represent spatial frequency in inverse pixels.

3.4 Phantom experiment

When the minimum speckle size does not meet the Nyquist criterion, the speckle

pattern will be under-sampled. In this case each pixel averages the intensity of more

than one independent speckle. This has the effect of shifting the measured intensity

distribution to slightly higher values in such a way that the speckle contrast is reduced

[52]. We investigated this sampling behavior by conducting speckle experiments on

static scattering phantoms.

Rough single scattering samples were created by application of silver spray paint to a paper note card. This card was illuminated normal to its surface with a linearly polarized, 3 cm diameter beam expanded from a 543 nm HeNe laser. The backscattered speckle pattern was imaged onto a CCD camera (Dragonfly Express, Point Grey) with pixel size ~ 7 μm, using a 75 mm focal length lens and a system magnification of $M = 0.4$. A polarizer oriented parallel to the incident beam was placed before the camera to ensure detection of only a single polarization state. Speckle patterns of varying speckle size were achieved by adjusting the diameter of the aperture stop on the imaging lens. Minimum speckle size was determined from Eq. (3.7) and checked against the $1/e$ full-width half-max of the PSD (in the case that speckle size was greater than two pixels). Speckle contrast was calculated as the intensity standard deviation divided by the mean:

$$C = \frac{\sigma_I}{\mu_I} \tag{3.9}$$

and the results are shown in Fig 3.3.

The process was then repeated for non-imaged (objective) speckle. In this case the speckle size was controlled by expanding or condensing the incident beam to change the illuminating spot size *d,* which varied between 3 mm to 5 cm. The distance *z* between the not card and the camera was ~30 cm. The minimum speckle size was determined via Eq. (3.6) and the results are shown in Fig 3.4.
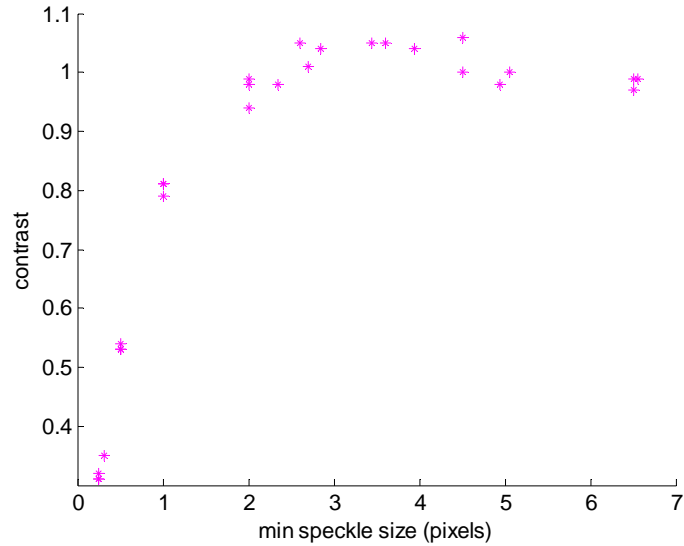
Fig. 3.3. Contrast as a function of minimum speckle size for fully-formed imaged (subjective) speckle. The physical pixel size in the image plane was ~17 μm.
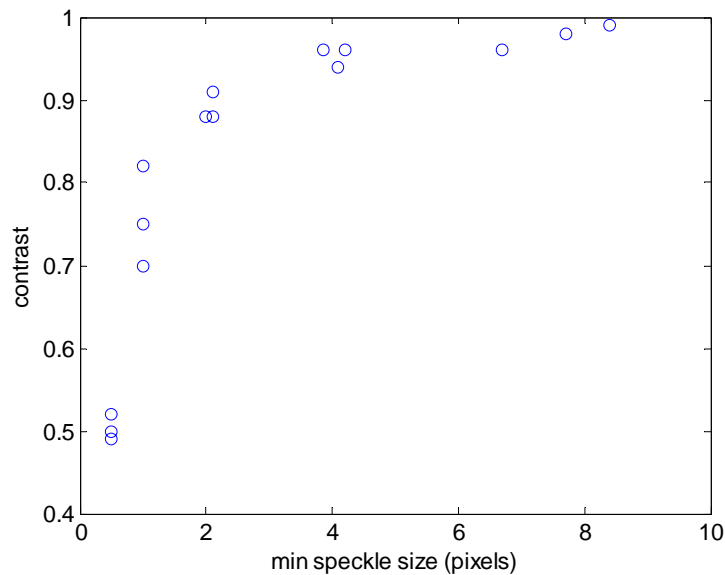
Fig. 3.4 Contrast as a function of minimum speckle size for fully-formed objective speckle. The pixel size was ~7 μm and the distance between the card and the camera was ~30 cm.

3.5 Discussion

Speckle size can have a significant effect on the measured intensity in a DLS experiment. As was described in Chapter 2, if the detector pinhole size is larger than the speckle size at the detector, then multiple independent speckles will be averaged together, which reduces the signal-to-noise ratio in the scattered fluctuations. This leads to a reduction in the zero-time delay value of the resulting autocorrelation function. It is generally agreed that the best approach for QLS [3][53] is to match the detector size to the speckle size to avoid unnecessary spatial averaging, while maintaining high intensity levels at the detector.

However, this practice of matching detector size to speckle size is not appropriate for the CCD-based DLS technique known as laser speckle contrast analysis (LSCA). As the name implies, this method relies on the calculation of speckle contrast to characterize the dynamic process being studied (see Chapter 5 for details). For appropriate interpretation of the contrast results of this method, the speckle pattern must be fully resolved. If the speckles are under-sampled, then the resulting reduction in contrast can be misinterpreted as artificially high levels of scatter motion.

Chapter 4

Sequential speckle correlation (SSC): computational methodology for analyzing dynamic light scattering and its application to dental composite polymerization

This chapter was co-authored by Sean Kirkpatrick and Ron Sakaguchi, and was published in Dental Materials [62]. *It is included here, with permission, in its original format.*

Abstract

The purpose of this study was to develop and evaluate a dynamic light scattering-based method for monitoring the polymerization reaction of a light activated dental composite. Laser light back-scattered from thin disk-shaped composite samples was used to study the curing reaction kinetics. Samples were irradiated simultaneously on opposite surfaces with a 633 nm laser beam and a halogen curing lamp (320, 160, or 100 mW/cm^2). Dynamic laser speckle patterns were imaged onto a CCD camera at a rate of 32 frames per second for 2 minutes. The intensity decorrelation rate calculated from sequential speckle patterns was used to assess the rate of motion within the samples during the reaction. Motion within the composite increased immediately upon the onset of light exposure for all trials. This was followed by a brief period

characterized by a relatively constant high rate of motion. Finally the rate of motion

decreased exponentially. The reaction acceleration, deceleration, and maximum rate

were dependent upon the irradiance of the curing light source. This method monitors

reaction rate and the change in reaction rate at high temporal resolution without contact.

Reaction kinetics were shown to begin immediately after light exposure suggesting

limited opportunity for viscous flow and stress relief.

4.1 Introduction

The curing kinetics of dental resin composites have been the subject of substantial research since the introduction of these materials over 40 years ago. One of the main issues driving continued research in this area is the clinically significant volumetric shrinkage that occurs in all such composites as they cure. The resulting stress that accumulates within the composite and the surrounding tooth structure can lead to a number of unwanted outcomes including pain, damage to the tooth, marginal failure between the restoration and tooth, as well as failure of the restoration itself [63]. Many studies have focused on reducing this stress, both through the development of new composite materials as well as through the use of novel curing protocols [64]. However, minimizing the shrinkage stress has proven difficult due to the many interrelated variables that play a role in the curing reaction [28], particularly when considering the necessary balance between reducing shrinkage stress while at the same time maintaining adequate mechanical and physical properties of the final restoration [27].

There have been numerous studies investigating how the polymerization kinetics affect shrinkage stress and the development of mechanical properties [20][22-25]. The rate of polymerization of dimethacrylate monomers, which are commonly used in dental composite, has been shown to exhibit a rapid increase early in the reaction due to the auto-acceleration effect associated with free-radical termination becoming diffusion

controlled. Soon thereafter, due to the increasing size and complexity of the polymer network, propagation also becomes diffusion controlled, causing a rapid decrease in polymerization rate, known as auto-deceleration [36][65]. It has been shown that increasing rates of polymerization are associated with higher levels of shrinkage stress [20][66] and the reaction rate also has an effect on final conversion of the composite [67]. For the purpose of developing ways to reduce shrinkage stress, it is therefore important to have a means of monitoring polymerization kinetics, particularly early in the reaction when conversion rate is highest and changes rapidly with time. However there is currently no well-established technique, which can be used under clinically relevant curing and sample configurations, that is capable of measuring composite polymerization with the temporal resolution necessary to assess early reaction kinetics.

Degree of conversion (DC), the fraction of the initial monomer double bonds converted into polymer double bonds, is typically used to describe rate and extent of cure. A common means of measuring DC is by spectroscopy, specifically in the mid-[22][68][69] or near-IR bands [38][70]. With this method, IR spectra are typically obtained before and after completion of curing, and based on the change in magnitude of absorption peaks specific to unreacted monomer, the overall DC can be determined. Time resolved conversion is occasionally measured with IR techniques [22][57], however due to the scanning time needed to obtain a single spectra and the fact that several spectra are usually averaged to reduce noise in the measurement, the sampling rate has generally been limited to less than 1 Hz. Coupled with the fact that, to obtain conversion rate information from DC, the data must be differentiated, thereby

accentuating any noise, IR techniques are not well-suited for monitoring rapid changes in polymerization rate.

For studying time resolved conversion and conversion rate, thermal analysis methods, such as differential scanning calorimetry (DSC), have often been used [39][65] [71]. With this method the exothermic heat output during the reaction is continuously measured, and based on the known heat of reaction for polymerization, the rate of bond formation can be calculated and used to deduce conversion rate. DSC is generally capable of higher sampling rates than IR spectroscopy, however some machines suffer from a long response time, limiting the temporal resolution that can be achieved. Also DSC is greatly limited by stringent experimental conditions, based on the need for the sample to be placed in a thermally isolated chamber during the reaction, while also allowing for a port of entry for the curing light. In addition, sample size is typically limited to the milligram range, making it difficult to compare the results from this method to samples of clinically relevant dimension.

Another common method for monitoring the reaction kinetics has been through measurements of the rate of sample shrinkage, or strain rate. This can be accomplished through a number of experimental techniques including dilatometry [72] and the bonded-disk method [73], among others. While several studies have shown final shrinkage and DC to be proportional [20][69] others have suggested that when considering the time resolved reaction, there may be a lag between the development of conversion and shrinkage [49][74].

Dynamic light scattering (DLS) is a well-established optical technique used to study dynamic processes of liquids and solids [1]. When a scattering medium is in motion, the light that it scatters will fluctuate with time. In DLS the intensity of this scattered light is measured and its temporal fluctuations are quantified to characterize the underlying motion. For the case in which each photon is scattered no more than once (the single scattering regime), the electric field at a point detector at a given time t can be described by

$$E(t) = \sum_{m=1}^{N} a(\mathbf{r}_m(t)) e^{i\mathbf{q}\Box\mathbf{r}_m(t)} \qquad (4.1)$$

where m is the number of scattering sites, r_m is the position of the mth scattering site, a is the complex amplitude of the scattered light, and q is the scattering vector defined as

$$\mathbf{q} = \mathbf{k}_i - \mathbf{k}_f . \qquad (4.2)$$

Here k_i and k_f are the wave vectors of the incident and detected light, respectively. The intensity, which is the parameter that is actually measured by the detector, is related to the electric field by

$$I(t) = \left\langle E(t)E^*(t) \right\rangle, \qquad (4.3)$$

where the asterisk represents the complex conjugate and the angle brackets indicate an

ensemble average. In a typical DLS experiment, the intensity autocorrelation function,

$G_2(\tau)$, is calculated as a measure of the average timescale of the fluctuations:

$$G_2(\tau) = \langle I(t)I(t+\tau) \rangle \qquad (4.4)$$

where τ is time delay. The shape of this autocorrelation function and its corresponding

1/e decay time can be used to assess the kinetic behavior of the system, especially for

diffusion or ordered motion of the scattering particles. As an alternative to using a point

detector, a multi-detector array such as a CCD camera may be used, allowing the spatial

distribution of the scattered light to be observed along with temporal fluctuations. In

this case, at any given time, the spatial variations in intensity will appear granular in

structure, a phenomenon known as laser speckle (Fig. 4.1) [75]
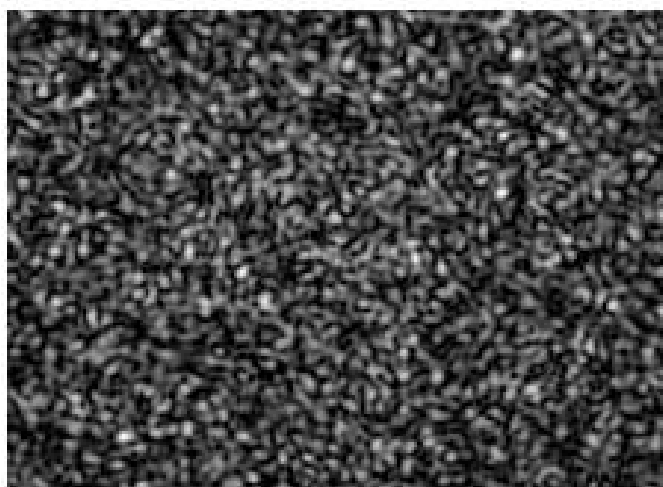
Fig. 4.1. An example of a laser speckle pattern. The granular structure is a result the random interference of coherent scattered light.

In this report we present a new method for monitoring the polymerization reaction of dental composite based on DLS. It relies on calculating the correlation between sequential pairs of dynamic speckle patterns, rather than using the autocorrelation function, as a means of assessing internal motion within the composite. It has the advantages of being simple in design and setup, non-destructive, non-contact, and has a high temporal resolution enabling it to detect rapid changes in reaction rate on the order of milliseconds. It has the added benefit of being able to measure a wide range of sample sizes cured under a variety of experimental protocols. We demonstrate the use of the new method by monitoring the polymerization kinetics of composite samples cured at three different irradiances, while specifically examining the hypothesis that motion within the composite begins immediately upon exposure to the curing light.

4.2 Materials and Methods

4.2.1. Sample preparation

The experimental composite used in this study consisted of 82% (by weight) fused quartz silica hybrid filler particles (0.1-3 μm diameter) and 18% resin matrix, which was composed of 50:50 w/w ratio mixture of BisGMA (2,2-bis[4-(2-hydroxy-3-methacryloxypropoxy)phenyl]-propane) and TEGDMA (triethylene glycol dimethacrylate), 0.8 % CQ (camphorquinone) photoinitiator, 0.4% EDMAB (ethyl-4-

dimethylaminobenzoate) amine coinitiator and 0.05 % BHT (butylated hydroxytoluene) inhibitor. To construct the samples, plastic rings were glued to glass slide backings and then filled with the uncured composite paste. The dimensions of the disk-shaped samples were 1.9 cm in diameter and 1.7 mm in thickness. Sample preparation occurred under low ambient light to prevent premature light activation.

4.2.2. Experimental configuration
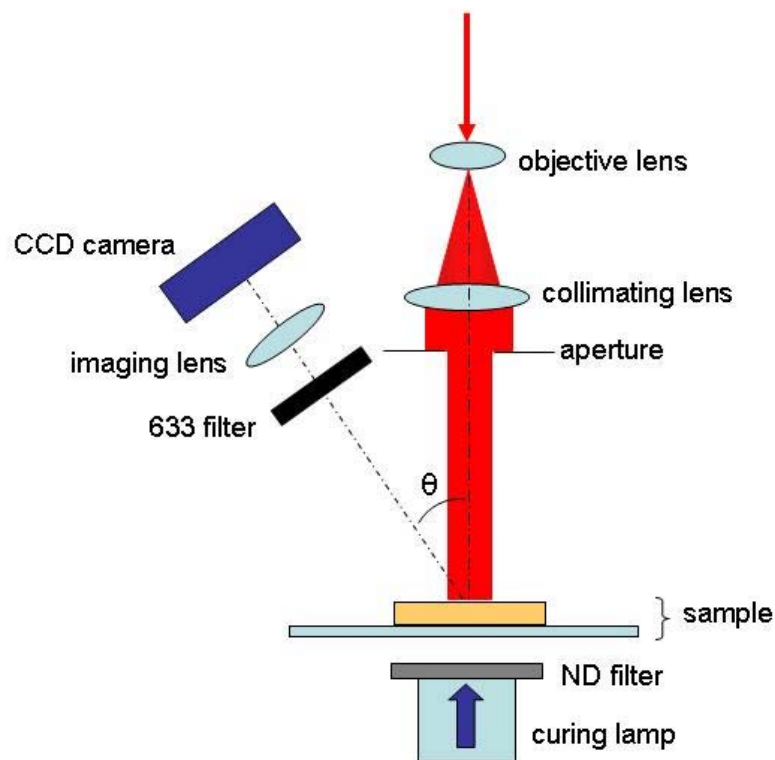
Fig. 4.2. Experimental configuration used to monitor composite curing reaction.
$\theta = 15°$.

The experimental DLS configuration used to monitor the curing reaction is shown in Fig. 4.2. It was necessary to be able to expose the sample to the light from the curing lamp and the interrogating laser beam simultaneously so that measurements could be made during the reaction. To accomplish this we cured the sample from the bottom surface through the glass backing, while illuminating with the laser beam from the top surface. Samples were placed on an open-backed stage 3.5 mm above the light guide of the halogen curing lamp (Demetron Optilux, VCL 401, Demetron Research Corporation, Danbury, CT), which had a diameter of 11mm. The top surface was probed by a 5 mm diameter collimated beam of nearly uniform intensity from a 633 nm HeNe laser. The 3.5 mm between the curing lamp and the bottom surface of the sample allowed room for the placement of neutral density (ND) attenuation filters for the purpose of varying the curing irradiance.

The laser speckle pattern back-scattered from the sample was imaged onto a CCD camera (Dragonfly Express, Point Grey, Richmond, BC, Canada) with a magnification of $M = 0.2$ and the imaging aperture adjusted to achieve a minimum speckle size of two pixels. The light from the probing beam was able to propagate into the sample and scatter multiple times before being detected by the camera, and was therefore indicative of motion within a volume of the composite, not only that at the surface. To avoid imaging the light from the curing lamp, which was much brighter than the speckle pattern of interest, a bandpass filter with a bandwidth of 10 nm

centered at 633 nm was placed before the camera, blocking nearly all light from the lamp.

4.2.3. Data acquisition

Three trials were performed corresponding to three curing lamp intensities, with three composite samples tested in each trial. Neutral density (ND) filters (Melles Griot, Carlsbad, CA) were placed between the light guide and the bottom of the sample for two of the trials to alter the irradiance. The ND filters only attenuated the irradiance, and had no effect on the spectrum of the curing light. The optical densities of the filters used for the three trials were 0 (no filter), 0.3, and 0.5, corresponding to curing lamp irradiances on the bottom surface of the sample of 320, 160, and 100 mW/cm^2, respectively. Irradiance was measured with a radiometer (Nova II, Ophir, Logan, UT) prior to the trials. The CCD camera sampled at a rate of 32 frames per second, for a total of two minutes, or 3,820 total frames. The curing lamp was turned on 5 seconds after the start of CCD image acquisition and was automatically shut off after 30 seconds of illumination. The recorded frames were saved as an .avi movie file for post processing. A fourth trial was conducted at an irradiance of 160 mW/cm^2 in which the curing lamp was blocked with a black card for 10 seconds prior to sample exposure in order to allow the lamp to warm up and reach a steady irradiance, after which the card was suddenly removed. The samples were then irradiated for 30 seconds as in the other trials. This allowed the effect of the curing lamp rise time to be determined. A final trial was conducted in which an infrared (IR) bandpass filter was placed between the curing

lamp and the sample, which only allowed transmission of light within the wavelength

range of 630-1100 nm. This effectively blocked all light within the absorption band of

CQ, thereby preventing polymerization. The purpose of this was to determine how

much motion could be attributed to thermal expansion caused by IR absorption, as

opposed to motion caused directly by the polymerization process.

2.4.4 Data processing

Each frame from the original .avi files were subsequently cropped to a region of

interest (ROI) of 64 by 64 pixels, corresponding to an area of 2.5 by 2.5 mm in the

center of the sample, thereby forming a "speckle cube" of dimensions 64 pixels by 64

pixels by 3820 frames. The ROI was selected to ensure that measurements were made

in a region over which the probing beam had uniform intensity profile. To quantify the

fluctuation of the speckle pattern, the following correlation calculation was performed:

$$C(t)_{\Delta t} = \left\langle \frac{I(t)I(t + \Delta t)}{I(t)^2} \right\rangle, \tag{4.5}$$

where I is the intensity at a single pixel, t is the current time, $\varDelta t$ is the time delay

between successive frames (the inverse of the recording rate, in this case 31ms), and the

brackets indicate an ensemble average over all pixels in the ROI. This calculation is

referred to as sequential speckle correlation (SSC) because it represents a comparison of

only two back-to-back, sequential frames at any given time. It is not the same as the

autocorrelation function. To present the results in a manner that is more intuitive for

describing motion, the sequential correlation was inverted, yielding decorrelation. In addition the results were normalized by the sampling time to remove the effect of recording rate. The resulting normalized decorrelation rate is given by:

$$r_{decorr}(t) = \frac{\left(1 - C(t)_{\Delta t}\right)}{\Delta t} \, .$$

(4.6)

4.3 Results
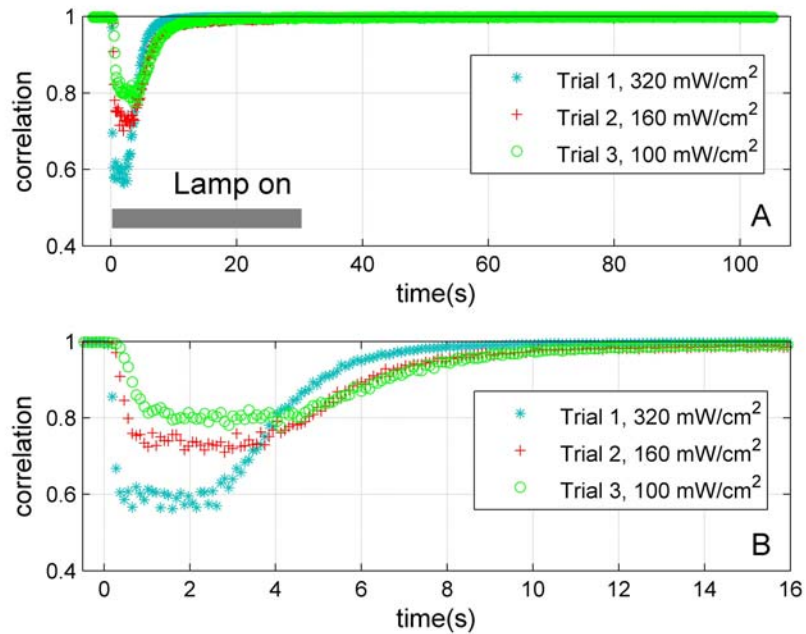
Fig. 4.3. Sequential correlation of the fluctuating backscattered speckle pattern during composite curing for Δt=0.0313 s. Each trial represents the mean of three samples. A. Entire correlation results B. First 20 seconds only.

The sequential correlation results for the first three curing trials, as calculated via Eq. 5, are shown in Fig 4.3. Each curve is the average of the three samples in that trial. Here the correlation coefficient is a measure of the similarity between speckle pattern images at two subsequent time points, such that a value of unity indicates complete correlation (the two speckle patterns are exactly the same), while a value of zero indicates no correlation between the two patterns. The results for each sample were aligned so that time $t = 0$ corresponds to the onset of curing lamp illumination. Prior to illumination with the curing lamp, the correlation for each trial was nearly unity, indicating little to no internal motion within the composite. Once the lamp was turned on there was a brief induction period during which the correlation slowly decreased, the duration of which was approximately inversely related to irradiance (see Table 1). This was followed by a sharper, nearly linear decrease, which then led to several seconds during which the correlation coefficient remained at a relatively constant low value. Afterward the correlation gradually increased back towards unity. Though the shapes of the correlation curves were similar for the three trials, the relative magnitudes were dependent on the irradiance of the curing light.
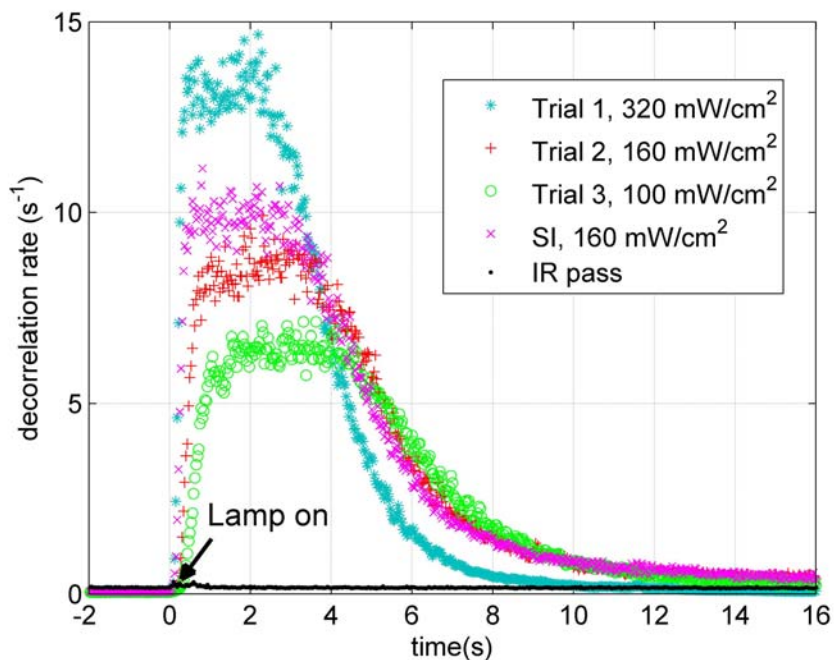
Fig. 4.4. Decorrelation rate obtained by inverting the sequential correlation and normalizing by the sampling interval. SI stands for sudden illumination. IR pass result using 630-1100 nm bandpass filter can be seen near the noise floor.

The results for the normalized decorrelation rate (Eq. 6) are shown in Fig. 4.4. Representing the data in this way is useful for characterizing the polymerization reaction because the magnitude of the decorrelation is expected to be directly related to the rate of motion, whereas the correlation is inversely related. The acceleration in decorrelation rate, excluding the brief initial induction period, was fit to a straight line, the slope of which is given in Table 1. The maximum decorrelation rate was determined from the average decorrelation rate over a one second window centered around the peak of the curve, based on visual inspection. The fall-off of the rate peak was least-squares fit to a negative exponential curve to quantify the deceleration. The decay constant is defined as the time it takes for the decorrelation rate reach a value of $1/e$ times the value at the start of the rate decline, as determined by the fitting. The

kinetic parameters describing the decorrelation rate during polymerization are given in

Table 1. The initial acceleration and the maximum rate of reaction increased with

increasing curing irradiance, while the decay constant decreased. For the trial using the

IR filter aimed at quantifying the effects of heat absorption, the motion was small

enough as to be below the noise floor of this technique. Correlation values were greater

than 0.99, with corresponding decorrelation rate of less than 0.2 s^{-1}.

	Irradiance (mW/cm2)	Induction period (ms)	Acceleration (s^{-2})	Max rate (s^{-1})	Decay constant (s)
Trial 1	320	146 (18)	58.8 (6.9)	13.3 (0.7)	1.50 (0.08)
Trial 2	160	271 (18)	19.5 (2.5)	8.5 (0.3)	2.11 (0.10)
Trial 3	100	396 (36)	10.0 (0.6)	6.4 (0.2)	2.38 (0.09)
SI	160	146 (18)	40.55 (3.4)	9.9 (0.1)	1.79 (0.09)

Table 4.1. Decorrelation rate parameters. SI stands for sudden illumination
All parameters are means over the trial (I=3). Standard deviation is in parentheses.
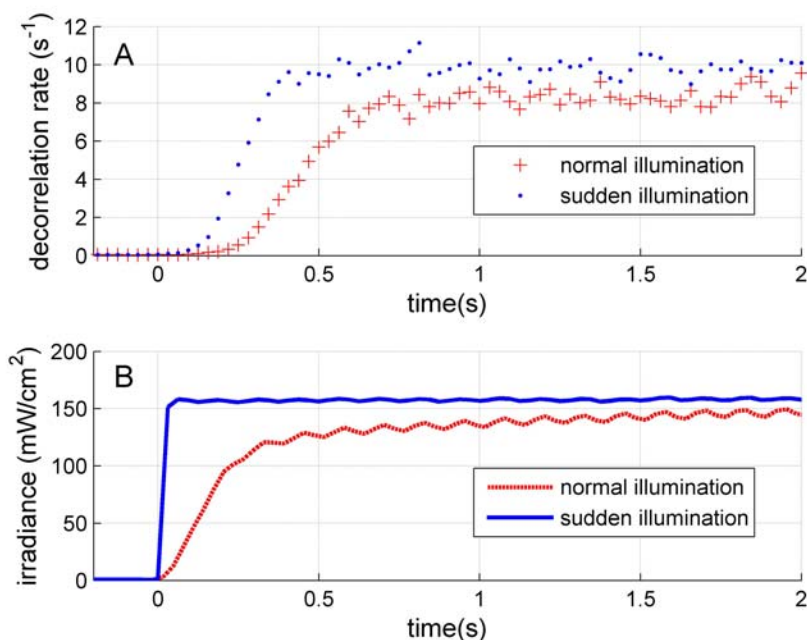
Fig. 4.5. Effect of curing lamp rise time on initial reaction acceleration. A. Decorrelation rate for normal curing illumination and for sudden illumination, achieved by blocking the curing lamp with a black card and then removing it once irradiance reached a steady value (160 mW/cm^2). B. The corresponding curing irradiance profiles.

The first 2 seconds of the reaction for Trial 2 is shown in Fig. 4.5A, along with the results of Trial 4, for which the curing lamp was blocked until the output irradiance reached a steady value (referred to as sudden illumination, or SI). Figure 4.5B shows the corresponding curing lamp irradiance at the sample as a function of time for these 2 trials. For normal curing illumination, it took 300 ms for the lamp to reach 75% of the final irradiance (120 mW/cm^2), although it took another ~ 6-8 seconds to reach the final value of 160 mW/cm^2. By blocking the lamp for 10 seconds prior to exposing the sample, an irradiance of 160 mW/cm^2 was achieved in less than 31 ms. As can be seen in Fig.4.5A the acceleration in decorrelation was considerably steeper for sudden illumination as compared to normal illumination, 40.6 s^{-2} vs 19.5 s^{-2} respectively.

Fig. 4.6 shows the cumulative decorrelation obtained by integrating over the normalized decorrelation rate curve for the first 60 seconds of the reaction. For Trials 1-3, which were cured under normal illumination, cumulative decorrelation at 60 seconds increased with curing irradiance. Sudden illumination at 160 mW/cm^2 achieved a higher cumulative decorrelation than normal illumination at both 160 mW/cm^2, and 320 mW/cm^2.
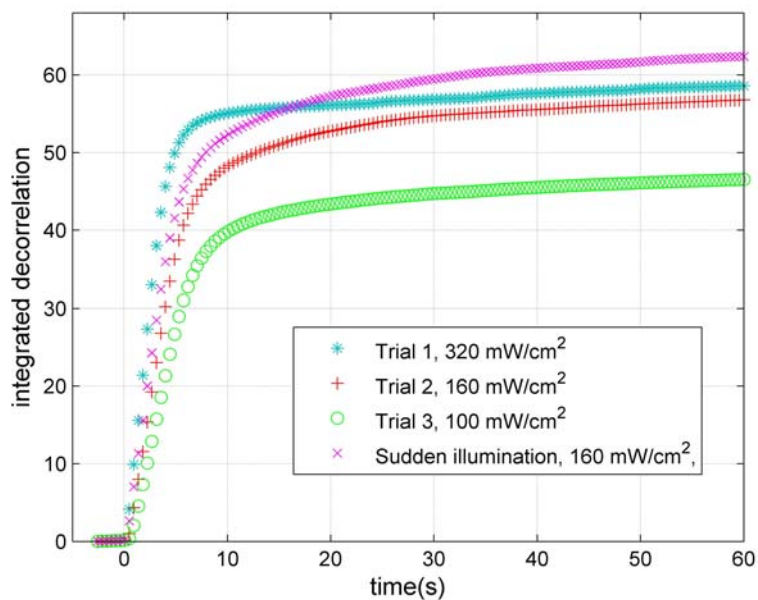
Fig. 4.6. Integrated decorrelation rate for the first 60 seconds of the reaction.

4.4 Discussion

We have implemented a novel technique for monitoring polymerization kinetics, which utilizes dynamic light scattering as a means of assessing motion within composite resin samples. The decorrelation rate results we present show a great deal of similarity to results from previous polymerization kinetics studies, when taken as an indicator of reaction rate.

Time resolved rate of conversion curves obtained by DSC [58][71] and measurements of shrinkage strain rate [22][66] have demonstrated similar peaks for the polymerization of dimethacrylate resins and composites. The peak in decorrelation rate that we observed has a steep rise, lasts for several seconds, and then falls off with a comparatively less steep exponential decay. While the general shape of this peak is similar to those found in the literature, our results appear to contain greater discernable detail due to the higher sampling rate of this technique. For example, we are able to observe a ~270 ms induction period (for normal illumination at 160 mW/cm^2, see Fig.4.5A) at the start of the reaction in which the composite gradually transitions from being completely stationary to being in a state of sharp, nearly linear acceleration. Also, at the top of the peak the rate appears to plateau for several seconds, a detail which we have not observed in results from other studies. We found that the maximum decorrelation rate for each of the 3 normal illumination trials varied with curing irradiance raised to the 0.6 power, mirroring the findings of Lovell *et al.* [67] obtained

with 50:50 BisGMA/TEGDMA resin. The similarity of the results presented herein with those in the literature obtained via other techniques suggests that dynamic light scattering methods may provide a simple and effective means of monitoring the rate and extent of cure of dental composites.

The cumulative decorrelation (Fig. 4.6), which is obtained by integrating the decorrelation rate, demonstrates the same general inverted negative exponential shape as has been seen in numerous reports on time resolved DC, obtained both directly via IR spectroscopy [57][76] and indirectly through shrinkage measurements [24][25][69]. It is interesting to note the dependence on irradiance of the cumulative decorrelation obtained at 60 seconds. Although Trial 2 was conducted at half the irradiance as Trial 1, it achieved nearly the same cumulative decorrelation at 60 seconds, yet Trial 3, which was conducted at a third of the irradiance, achieved 20% less. It is also interesting that the sudden illumination trial that was conducted at 160 mW/cm^2 surpassed the cumulative decorrelation of Trial 1 (320 mW/cm^2) 15 seconds into the reaction, despite having been exposed to only 54% of the radiant exposure as Trial 1.

To gain a better understanding of this method and how it can best be utilized, it is necessary to take a detailed look at what exactly is being measured. As mentioned, the decorrelation rate is related to the level of motion within the composite, however it can be influenced by several other factors as well. Specifically, decorrelation rate is a measure of how fast photon migration pathlengths change with time. Because the path a photon travels is determined by the position of scattering particles as well as the optical

properties of the composite, either the movement of scatterers or a change in optical

properties may give rise to decorrelation in the dynamic speckle pattern. It should be

pointed out that because the scattering is predominantly caused by filler particles, this

method is not suited to looking at unfilled resins. We have previously looked at curing

of 50:50 BisGMA/TEGDMA resin and found there to be negligible scattering.

The optical properties that govern photon transport include absorption,

scattering and index of refraction. We did not measure the optical properties of the

composite for this study, however Chen *et al.* [77] measured the pre and post-cure

absorption and reduced scattering coefficients of a commercial BisGMA/TEGDMA

composite of comparable filler size (Z100). They found the absorption coefficient at

633 nm to be around 0.3 cm^{-1} before curing and 0.2 cm^{-1} afterward, while the reduced

scattering coefficient increased from about 8 cm^{-1} to 8.5 cm^{-1}. For the case of

absorption, because both the overall absorption coefficient as well as the change in

absorption are small, it is reasonable to assume it contributes little to the measured

decorrelation. The increase in scattering on the other hand, though relatively small, may

be problematic when considering the entire reaction as a whole, because an increase in

the average number of scattering events per detected photon would make the

decorrelation rate more sensitive to composite motion, thereby introducing a bias.

Tomlins *et al.* [78], using a BIS-GMA, BIS-EMA, UDMA composite (Filtek),

measured the change in refractive index over the course of the curing, and found it to be

~0.005, which may have an effect on decorrelation rate. Changes in scattering and

refractive index may have an appreciable effect on decorrelation rate over the course of

the reaction, however it is expected to be dominated by decorrelation due to motion. This is because the change in these optical properties over the time of a single sampling interval (31 ms) would be quite small, and therefore contribute only a small amount to the observed decorrelation rate, particularly for high reaction rates. Although the effect of changes in optical properties on the dynamic speckle pattern are expected to be small compared to the overall decorrelation rate, it's important to keep these issues in mind when interpreting the results

After accounting for the changes in optical properties, it can be assumed that the remaining speckle decorrelation arises from, and is proportional to, the rate of motion within the composite. There are several potential sources of motion during curing. The first is motion caused by the polymerization reaction itself, which is predominantly a result of chemical bond formation within the resin, but some motion may also result from the exothermic heat generation of the reaction. Bond formation is largely comprised of polymerization primary chain growth, though cross linking and cyclization also occur to a smaller extent [51][79]. We had considered another potential source of motion to be thermal expansion caused by heating from the curing lamp. However, we found the decorrelation rate due to IR band absorption of the curing light to be less than 0.2 s^{-1}, which is approximately the noise floor at the given sampling rate. We therefore conclude that thermal effects from the curing light are negligible compared to motion caused by the reaction itself.

Another issue that should be considered when using this method is the effect of depth dependent light attenuation on the measured decorrelation rate, both by the curing light and the laser beam. Due to absorption and scattering, the number of photons reaching a certain depth within a material is less than that at the surface. For the case of the curing light, samples were illuminated at the bottom surface, which was the location at which the reported irradiances were measured. Because of attenuation however, the irradiance reaching the opposite (top) surface of the sample, where the camera views the sample, is less. The practical outcome of this is that curing rate and extent of cure are depth dependent, a result that has been well documented in a number of other studies [77][80][81]. Similarly, the laser beam probes the upper layers of the composite to a greater extent because the light is attenuated as it penetrates into the sample. In this case it's only the backscattered light that is of interest, which must exit the sample via the top surface in order to be observed by the camera. For each photon that reaches the camera, every scattering event undergone contributes equally to the measured decorrelation. However, because the light is attenuated by absorption and scattering, fewer photons reach deeper into the sample, and of those that do, fewer make it back to the camera compared to photons that only reach shallower depths. Adding to this effect, any photon that does reach the bottom layers of the sample and then makes it all the way back to the top sample and to the camera will have undergone more scattering events in the upper portions of the samples because the photon must travel the shallower layers twice in order to exit the sample from the top surface. Calculating the precise pathlength distribution of photons is beyond the scope of this paper, but it suffices to say that the photons which reach the camera probe all depths of the sample, but the vast

majority of the scattering events occur in the upper layers of the sample. Therefore it is this region being predominantly measured. A clinical implication of this is that the decorrelation results presented herein represent a situation similar to measuring the motion due to polymerization which occurs at the bottom of a 1.7 mm thick composite restoration.

As mentioned, this method is dependent on the extent to which the laser beam probes the sample, which is governed by the scattering properties of the composite. The scattering is caused by photons interacting with filler particles, and therefore composites with different filler content and size might be probed differently. Generally, larger particles scatter photons in a more forward direction, while smaller particles scatter more isotropically[82]. Therefore filler particles affect the decorrelation rate by influencing the photon migration paths of the probing beam, which determines the depth to which the reaction is measured. If the optical properties of the composite are known, modeling approaches such as Monte Carlo can be used to determine the precise probing region within the sample [77].

Having discussed the technical details of our measurement technique we can now consider how it may best be utilized. Because of its high temporal resolution, this method is well-suited toward monitoring the early behavior of the polymerization reaction during which the rate changes rapidly with time, the details of which may be missed by methods such as IR spectroscopy that have a lower sampling rate. A straightforward use of this method may be as a simple means of identifying the time at

which maximum reaction rate occurs. Even with a potential bias due to a change in optical properties over the course of the reaction, the time at which the decorrelation rate reaches its peak is readily identifiable and should correspond to the time of maximum polymerization rate. This technique could also be easily incorporated into other testing apparatus to allow for simultaneous measurement of reaction kinetics. For example, it could be used concurrently with stress or strain testing in order to directly correlate the development of composite mechanical properties with the rate of curing. In this situation all that is necessary is for one surface of the composite sample to be accessible to interrogation by a laser beam. Experimental setup and data analysis are straightforward. For future application of this method it would be advantageous to be able to assume a semi-linear relationship between decorrelation rate and conversion, or to be able to directly relate the two via calibration. Work is currently underway to correlate the kinetic curves of this technique to time resolved conversion curves obtained via DSC for this purpose.

As a simple modification to our method, a polarizer could be added prior to the CCD camera, oriented linearly to the polarization of the incident laser beam. Because singly scattered light retains its polarization while multiply scattered light does not, this would effectively make the camera measure surface scatter (singly scattered photons) nearly exclusively. This would be advantageous because the photons being detected would not have propagated into the sample and therefore changes in optical properties would not influence the decorrelation rate. It would not, however, be representative of bulk motion within the sample.

The method presented in this work is not the first to use laser methods to investigate dental composite polymerization. Fogleman *et al*. [83] used an apparatus based on a Michelson interferometer to measure linear shrinkage during curing for optically thin samples. Demoli *et al*. [84] used a similar interferometric technique to report on thickness variation during the reaction. In both cases dimensional changes were determined based on the interferometric signal generated by the displacement of a mirror that had been attached to the sample which moved with the composite as it contracted. Another study attempted to combine laser speckle contrast analysis (LASCA) and speckle interferometry to measure dimensional changes [85]. Li *et al*. [86] used an optical technique based not on laser illumination, but rather white light illumination, which used a spatial correlation technique to track deformation on the composite. Unlike these previous studies, the method presented here, based on the theory of DLS, provides a measure of the motion within the sample that is indicative of reaction kinetics, rather than composite shrinkage. There are no system compliance issues to account for, such as displacement of a mirror, and because it is a laser-based technique, the wavelength of the light provides intrinsic calibration.

To our knowledge DLS has not before been utilized to study the reaction kinetics of dental composite and it is a technique that has a number of potential uses in the field of restorative dentistry. As an example, diffusing wave spectroscopy (DWS) [87], an extension of DLS in which the scattering of photons is treated as a diffusive process, has been used as a rheological method for measuring the viscoelasticity of

liquids and soft solids [88][89]. Applying DWS to study composite curing may provide insight into how the viscoelastic properties of the composite change with time.

Finally, our results confirm our hypothesis that composite motion begins immediately upon exposure to the curing light. After a brief induction period of 100-400 ms (depending on irradiance), during which decorrelation rate ramped up, the acceleration in the reaction kinetics was shown to be quick, reaching a maximum rate of motion within 500 ms of curing lamp illumination for samples irradiated at 320 mW/cm^2. This is significant because it indicates that there would be little opportunity for viscous flow within the composite and therefore limited opportunity for relief of accumulating shrinkage stress.

4.5 Conclusions

A measurement technique based on dynamic light scattering has been described which can be used to monitor the polymerization reaction of light activated dental composites. It measures the decorrelation between successive imaged speckle patterns to assess the motion occurring within the composite as it cures. Our results for thin disk-shaped samples appear similar to reaction kinetics data found in the literature. We showed that the polymerization reaction begins immediately upon curing light exposure, offering limited opportunity for viscous flow. This technique, which is being further developed, is not limited by sample configuration so long as illumination with

the curing lamp and probing laser beam can occur simultaneously. It has the added

advantages of being non-contact, non-destructive, does not require calibration and has

high temporal resolution. We believe this method provides a straightforward means of

monitoring composite curing kinetics and may be useful in the development and

evaluation of new composite materials and curing protocols.

Chapter 5

Technical considerations for the application of laser speckle contrast analysis (LSCA) to resin composite polymerization

5.1 Introduction

Laser speckle contrast analysis (LSCA) is an optical technique for studying dynamic processes that uses the spatial statistics of backscattered laser light to assess motion within a scattering medium. Unlike the other DLS methods, which typically rely on temporal fluctuations, LSCA utilizes the spatial statistics (specifically contrast) of a *time integrated* signal to arrive at a description of the motion. This method has been used primarily for studying changes in blood flow velocity, with few other documented applications in the biological or medical fields. The aims of this chapter are to present a theoretical description of LSCA, and to explore its technical details relating to dental composite polymerization.

5.1.1 History of LSCA

In the field of biomedical research, laser speckle contrast analysis (LSCA) has seen a great deal of development and application over the last 30 years, particularly related to the aim of measuring blood flow [3][90-92]. From the standpoint of the scattering process, LSCA is in many ways analogous to other DLS techniques. However it has two key distinguishing features. One is that is uses spatial statistics to assess the motion of the scattering process. The other is that the scattered intensity is temporally averaged—either at the time of acquisition or during post processing—prior to analysis.

The LSCA techniques stemmed from earlier studies of DLS, especially those on quasi-elastic light scattering (QLS), which developed in the 1960 and 70s [3]. Because QLS is a point measurement, LSCA was developed from the desire to extend the capabilities of QLS to measure dynamics over a field of view. In 1980 Fercher and Briers [90] used time-integrated speckle images, obtained from single-exposure photography with a known camera exposure time, to the visualize flow velocity of a scattering medium. The basis of their technique was to use the degree of blurring in the speckle image to characterize the flow velocity. Considerable work in this area continued in subsequent years with the primary aim of monitoring blood flow, based on the premise that an increase in flow velocity causes a decrease in the speckle contrast [93].

The usefulness of single-exposure speckle photography was limited, however, by the need to develop and process the photographs, and the difficulty associated with obtaining measurements as a function of time. This was resolved with the introduction

of a digital version of the method [94] which utilized a multi-detector array (a CCD camera) to record the time-varying speckle pattern.

Much of the recent research on LSCA has focused on determining how, and in what circumstances, quantitative assessments may be made from the measured contrast [95]. Many have shown [91][96], theoretically and experimentally, the *qualitative* relationship between contrast and flow, but truly quantitative results, in vivo, have yet to be presented. Even though quantitative measurements might not be attainable, qualitative results are often sufficient for monitoring *changes* in dynamic behavior.

5.1.2 Speckle contrast and composite curing

Experimental studies using the LSCA method that are not focused on characterizing blood flow are relatively few. It has found use in monitoring paint drying [97], studying seed germination [98], as well as for describing the motion of bacteria [12]. However few other industrial or biological uses have been reported. LSCA seems to be a promising method for characterizing the polymerization reaction of dental composite; it is inherently non-destructive, requires no calibration, and has no mechanical compliance issues. In addition LSCA is capable of high temporal resolution while simultaneously providing a spatial map of dynamics, something that is difficult, if not impossible with other common testing methods.

5.2 Theoretical description of LSCA

5.2.1 Speckle statistics

Laser speckle contrast analysis uses the contrast of the intensity distribution of a speckle pattern to assess motion within a scattering medium. Contrast in this case is defined as the intensity standard deviation divided by the mean intensity,

$$C = \frac{\sigma_I}{\mu_I} \qquad (5.1)$$

typically over some well-defined region of interest (ROI). Depending on the intensity probability distribution within the ROI, a range of contrast values are feasible but generally they fall between zero and unity.

A fully-formed, or "ideal" speckle pattern, formed by non-moving scatterers, exhibits a negative exponential intensity distribution given by [52]

$$p(I)_I = \frac{1}{\langle I \rangle} e^{-I/\langle I \rangle} \qquad (5.2)$$

This equation is valid under the assumptions previously mentioned in Chapter 3 for fully-formed speckle. In this case the expected contrast is unity. Conversely, contrast

other that unity indicates an intensity distribution that deviates from that of Eq (5.2). A commonly encountered example is that of un-polarized speckle which has an intensity distribution given by [56]

$$p_I(I) = \begin{cases} \left(\dfrac{2}{\langle I \rangle}\right)^2 I e^{-2I/\langle I \rangle}, & I \geq 0 \\ 0 & \text{otherwise} \end{cases},$$ (5.3)

yielding an expected contrast of $1/\sqrt{2}$.

5.2.2 Effect of scatterer motion

The previous intensity distributions are valid only for the case of single scattering. They also assume that the scattering particles are not moving or, alternatively, that the speckle pattern is recorded with detector integration time T much shorter than the intensity decorrelation time τ_{dc}. When these are true, the distributions in Eqs (5.2) and (5.3), and their corresponding contrasts, are expected to hold.

If the scattering particles are non-moving, then regardless of detector integration time T, polarized speckle contrast is expected to be unity. However when the scattering particles *are* in motion, the scattered intensity signal and the associated speckle pattern will change with time. In this case, if T is on the order of, or longer than τ_{dc}, high frequency details in the scattered signal will be lost in the integration, resulting in a

reduction of contrast. Neither T nor τ_{dc} alone can be used to predict the reduction in

contrast; instead it is useful to consider their ratio, T/τ_{dc} .

5.2.3 Quantitative assessment

Quantitative assessment of dynamic processes using LSCA requires relating

change in contrast to the motion of the scatterers. Unfortunately there is currently no

accurate mean of relating these two quantities that is generally accepted [95]. The

motion of the scatterers tends to be complicated since motion is not always in a well

defined direction, and there may be a combination of ordered and ordered flow. The

general approach [53][94] is to assume a shape for the temporal intensity

autocorrelation function that can be used to relate the measured contrast to the relative

integration time T/τ_c (or alternatively τ_c/T) .

The measured, time-integrated intensity $\overline{I}$ is related to the instantaneous

intensity I by

$$\overline{I}(t) = \frac{1}{T}\int_t^{t+T} I(t')dt' \quad .$$

(5.4)

For an instantaneous intensity signal with auto-covariance $\mathrm{Cov}_I(\tau)$, the variance may

be represented by [53]

$$\sigma_I^2(t) = \frac{1}{T} \int_t^{t+T} \mathrm{Cov}_I(\tau) \big[2(1 - \tau/T) \big] d\tau, \qquad (5.5)$$

where $\mathrm{Cov}_I(\tau)$ is related to the intensity autocorrelation function $G_2(\tau)$ by

$$\mathrm{Cov}_I(\tau) = G_2(\tau) - \langle I \rangle^2. \qquad (5.6)$$

Based on Eq (5.5), if the shape of the autocovariance (or autocorrelation) function is known or assumed, the contrast can be directly related to τ_c/T.

5.2.4 Sampling considerations

The size of the ROI used to calculate contrast affects the signal to noise and spatial resolution of the results. Because the ROI contains few independent speckles, a degree of variation is expected in the contrast. The more speckles in the ROI, the smaller this variation. In the limit of a large number of speckles, the variation about the expected contrast goes to zero, assuming a dynamically homogeneous medium. However to monitor the dynamics over different regions, the ROI is kept as small as practical to improve spatial resolution.

The contrast calculated from a single ROI is referred to as the *local contrast*. Each speckle may be considered a statistically independent sample. For the case of N_s speckles in the ROI, the local mean is

$$\bar{\mu} = \frac{1}{N_s} \sum_{i=1}^{N_s} I_i ,$$
(5.7)

and the local variance is

$$\bar{\sigma}^2 = \frac{1}{N_s - 1} \sum_{i=1}^{N_s} \left(I_i - \bar{\mu} \right)^2 ,$$
(5.8)

where I_i is the intensity value at the ith pixel.

The local contrast is accordingly

$$\bar{C} = \frac{\bar{\mu}}{\bar{\sigma}} ,$$
(5.9)

and as $N_s \rightarrow \infty$, $\bar{C} \rightarrow C$.

A kernel of dimension k x k pixels is defined (where k is odd) that calculates local contrast. This kernel is convolved with the speckle image and the result is a contrast map in which the value at any pixel corresponds to the contrast calculated from

a kernel centered at that location in the original speckle image. The choice of k is a

trade-off between balancing accuracy of the local contrast with spatial resolution. For a

fully-formed speckle pattern with a minimum speckle dimension of two pixels (thus

meeting the spatial Nyquist criterion), a kernel dimension of seven pixels achieves a

good balance between producing reliable estimates of contrast and achieving high

spatial resolution [99].

5.3 Experimental Methods

5.3.1 Experimental configuration

Figure 5.1 shows the optical configuration used acquire dynamic speckle data

for LSCA and is the same optical system described in Chapter 4. The laser speckle

pattern back-scattered from the composite sample was imaged onto a CCD camera

(Dragonfly Express, Point Grey, Richmond, BC, Canada) with a magnification of $M =$

0.2 and the imaging aperture adjusted to achieve a minimum speckle size of two pixels.

To avoid imaging the light from the curing lamp, which was much brighter than the

speckle pattern of interest, a 633 nm bandpass filter (bandwidth = 10 nm) was placed

before the camera, blocking nearly all light from the lamp. Polarizers were used to

control the polarization states of the incident and detected light. Curing irradiance was

160 mW/cm^2 at the bottom surface of the sample, with an illumination diameter of ~ 3

cm.
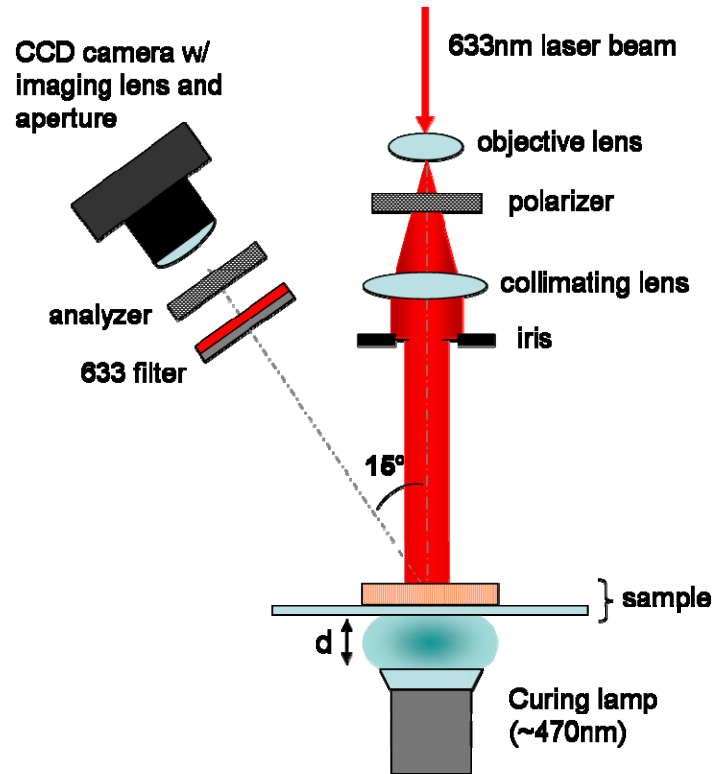
Fig. 5.1. Experimental configuration used to acquire dynamic speckle data

5.3.2 Sample preparation

The experimental composite used in this study consisted of 82% (by weight)
fused quartz silica hybrid filler particles (0.1-3 μm diameter) and 18% resin matrix,
which was composed of 50:50 w/w ratio mixture of BisGMA (2,2-bis[4-(2-hydroxy-3-

methacryloxypropoxy)phenyl]-propane or bisphenol A diglycidyl methacrylate) and TEGDMA (triethylene glycol dimethacrylate), 0.8 % CQ (camphorquinone) photoinitiator, 0.4% EDMAB (ethyl-4-dimethylaminobenzoate) amine coinitiator and 0.05 % BHT (butylated hydroxytoluene) inhibitor. To construct the samples, plastic rings were glued to glass slide backings and then filled with the uncured composite paste. The disk-shaped samples were 19 mm in diameter and 1.7 mm in thickness. Sample preparation occurred under low ambient light to prevent premature curing.

5.3.3 Data acquisition

Dynamic speckle data were initially recorded with the Point Gray software in .avi format. Movies were subsequently extracted into individual 8 bit .bmp frames (using Irfan View), and stored in a subdirectory for post-processing. A matlab script was used to read this data and format it into a so-called 'speckle cube', which could be saved and used as a quick and convenient starting point for contrast analysis.

5.3.4. Contrast analysis

Two contrast algorithms were implemented for the work described in this chapter. The first method determined a single contrast value for each frame in the recorded data sequence. This basic approach was useful when it was expected *a priori* that the sample dynamics were uniform over the field of view. It was advantageous because it provided a statistically reliable (large N_s) contrast value that could be

assumed to represent the expected (i.e. population) contrast. It was useful for comparing

the result of different curing methods or processing techniques, without the uncertainty

associated with a small sample size (small N_s). The second algorithm determines local

contrast, and was adapted from Duncan *et al.* [99]. It was used to produce a map of the

contrast, showing spatial variation in dynamic behavior.

5.4 Technical Considerations

Previous research on LSCA has focused primarily on optimizing the method for

measuring blood flow velocity. When LSCA is used to study composite polymerization

kinetics, technical issues arise due to differences in these two dynamic processes.

5.4.1 Integration time

The intensity integration (i.e. exposure) time T must be chosen carefully because

it affects the degree of blurring and therefore the contrast. If T is too short there may be

little reduction in contrast during the course of the reaction; if T is too long the contrast

may always stay near zero.

To examine the effect of integration time, two samples were tested with

identical curing protocols. For the first sample, the CCD camera exposure time was set

to 31 ms; for the second it was set to 500 ms. Contrast was determined over a 64 x 64

pixel region in the center of the sample, corresponding to an area ~2 x 2 mm.

The results are shown in Fig. 5.2 and clearly illustrate the basic principle of the LSCA technique: as the ratio of intensity decorrelation time to integration time decreases, the speckle contrast decreases. Or in other words, an increase in motion or an increase in exposure time will lead to reduction in contrast. From the results for the short integration time (31 ms) shown in blue, it can be concluded that the intensity decorrelation time τ_{dc} at the peak of the reaction is longer than 31 ms because there is no reduction in contrast. In addition, τ_{dc} is *not* longer than 500 ms because the contrast *is* considerably reduced for this integration time.
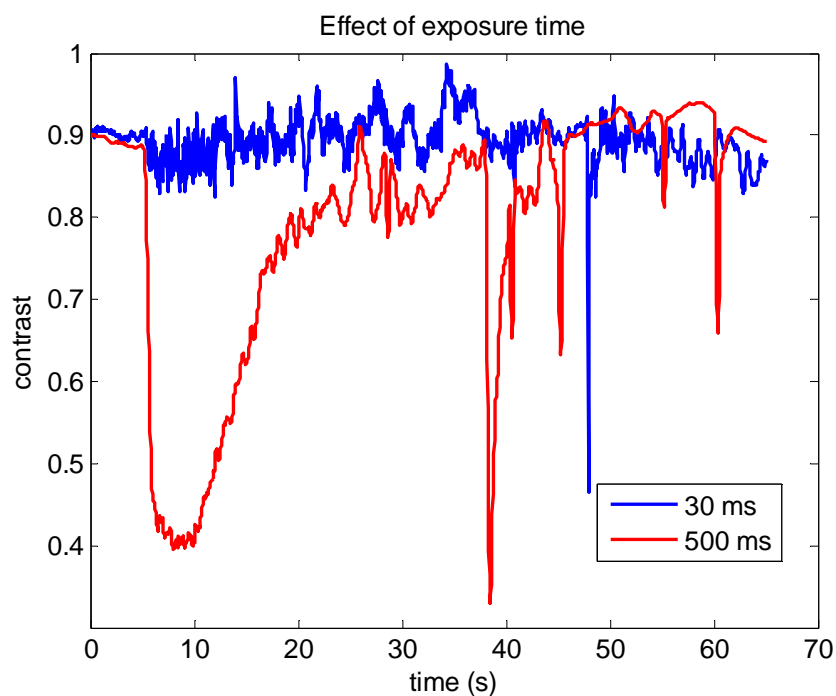
Fig. 5.2. Contrast as a function of time for 2 camera exposure times. The blue line T=31.3 ms; red line T=500ms. Contrast was calculated over a 64 x 64 pixel (2 mm x 2 mm) window. Lamp on at 5 s. The spikes in contrast occurring later in the reaction are due to rigid body motion which occurs as the composite debonds from the glass backing.

Since there was no reduction in speckle contrast observed for an exposure time of 31 ms, each speckle pattern recorded at this exposure time can be considered equivalent to an instantaneous realization. Therefore, using the speckle data recorded with $T = 31$ ms, we performed a simulation in which running averages were taken over n sequential speckle frames. This effectively simulates the results that would be expected had the camera exposure time been set to $T = 31 \cdot n$ ms. The contrast results for these simulations are shown in Fig. 5.3 for several simulated values of T.
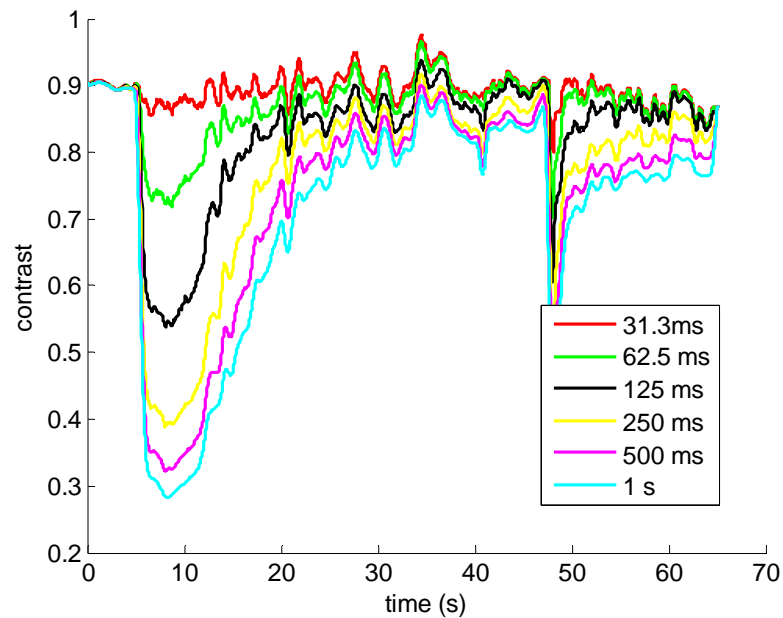
Fig. 5.3. Contrast as a function of time for various simulated integration times. Contrast calculated over 64x64 pixels window. Lamp on at 5 s.

The contrast values at the peak of the reaction were plotted as a function of T, as shown in Fig 5.4. Over the range of 31-250 ms the contrast experiences significant reductions, but afterward tapers off. These results suggest that for the composite samples cured at the given irradiance (160 mW/cm^2), $T = 250$ ms is a good choice because it offers nearly the full dynamic range in contrast.
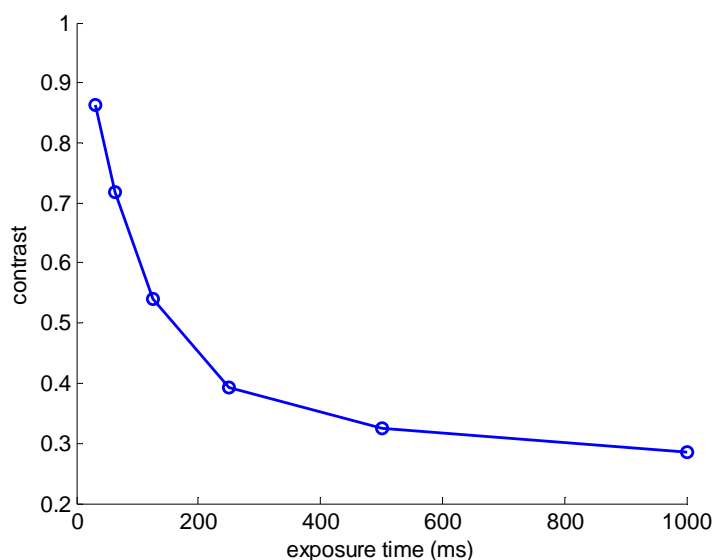
Fig. 5.4. Peak contrast values for the integration times shown in Fig. 5.3

5.4.2 Polarization

The state of polarization of the back-scattered light is known to affect the intensity distribution and contrast of a speckle pattern [52]. Based on the polarization of the incident beam, and the polarization orientation of the analyzer (with respect to the incident beam), a number of different polarization scenarios may arise. As previously

discussed, to achieve a fully-formed speckle pattern with unity contrast, only a single polarization state should be observed. In the case of unpolarized (or partially-polarized) speckle, the orthogonal polarization states produce independent speckle realizations that add together at the detector to reduce the speckle contrast.

To examine the effect of polarization three conditions were tested: 1) analyzer pass-axis aligned parallel to the linear incident polarization 2) analyzer pass-axis aligned perpendicular to the indecent polarization and 3) no analyzer. Two composite samples were tested under each condition with a curing irradiance of 160 mW/cm^2 and $T = 500\,\text{ms}$. The mean results for each polarization scenario are shown in Fig. 5.5.
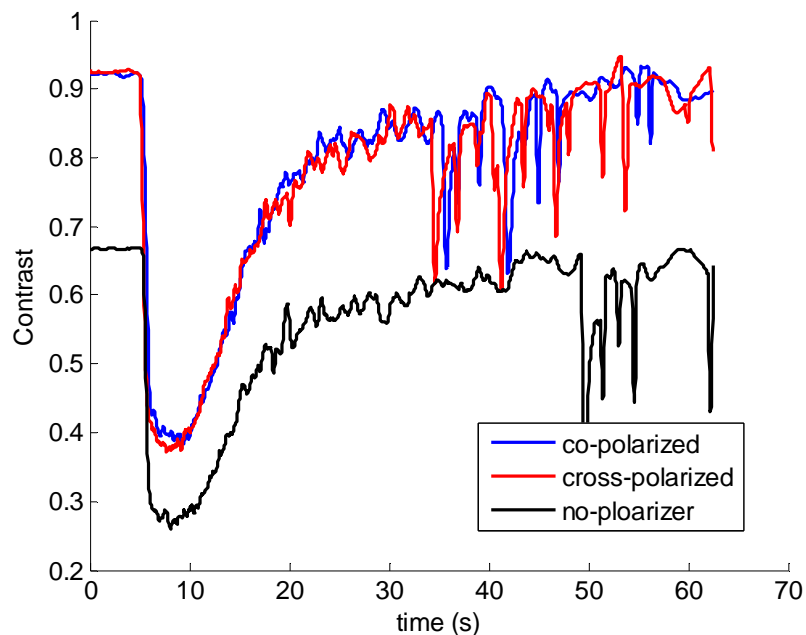
Fig. 5.5. Contrast as a function of time for 3 polarization detection schemes. Blue: analyzer parallel to incident polarization; red: analyzer perpendicular to incident polarization; black: no analyzer. Contrast calculated over a 64 x 64 pixel window. T=500ms.

Co- and cross-polarized trials yielded nearly identical results, which is indicative of multiple scattering. Unpolarized detection had considerably lower contrast than the polarized trials. For all trials the initial (and final) contrast values were slightly lower than theoretically predicted: 0.93 instead of 1.0 for polarized detection, and 0.67 instead of 0.71 for unpolarized detection. Looking at the speckle intensity PDF prior to the start of the reaction (see Fig 5.6 for an example) revealed that fewer than expected pixels had intensity values near zero, which explains the lower than expected contrasts (this was observed for each sample).
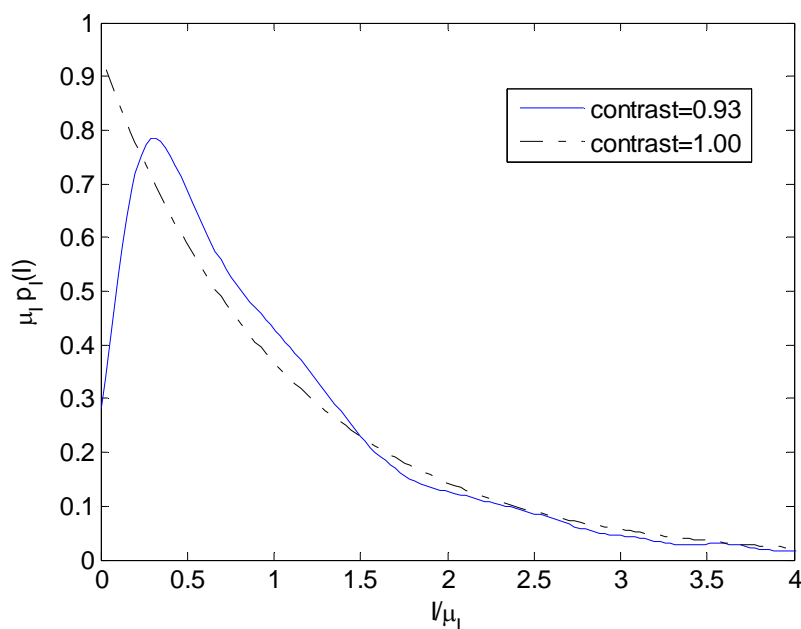
Fig. 5. 6. Intensity PDF for a co-polarized sample prior to start of the reaction. Lower than expected intensity values near zero resulted in lower than expected contrast values. Dashed line is the corresponding exponential PDF that yields contrast=1.

5.5 Spatial map of dynamic behavior

One advantage LSCA offers compared to other DLS techniques is the ability to image spatial dynamic behavior. Since traditional methods for studying the polymerization kinetics of dental composites provide either bulk or single point measurements, in this section spatial kinetics are examined using LSCA.

5.5.1 Normal curing illumination

Figure 5.7 shows the contrast results for one sample calculated over a 64 x 64 pixel ROI, with T=500ms (obtained by a 16 frame running average), and co-polarized detection. With this same set of data, but using the entire image field of view, we explored the local contrast at various time points in the polymerization reaction (which are denoted by the red circles). Figure 5.8 illustrates the results at the given time points for kernel size $k = 9$ pixels. Because the diameter of the curing illumination was broad (~3 cm diameter) and relatively smooth over the area of the sample, sharp transitions in contrast were not expected. Therefore we could afford the slight reduction in spatial resolution that comes with $k = 9$ as opposed to $k = 5$ or 7 pixels.

Figure 5.9 focuses on the first second of the reaction. This is a significant period for the polymerization due to the sharp acceleration in reaction rate. The results show that contrast is relatively uniform across the sample by 0.7 seconds. At the onset of the

reaction there is a contrast gradient indicating greater motion in the center of the

sample. The samples appear elliptical in these images due to off axis (~15 degrees)

camera orientation.
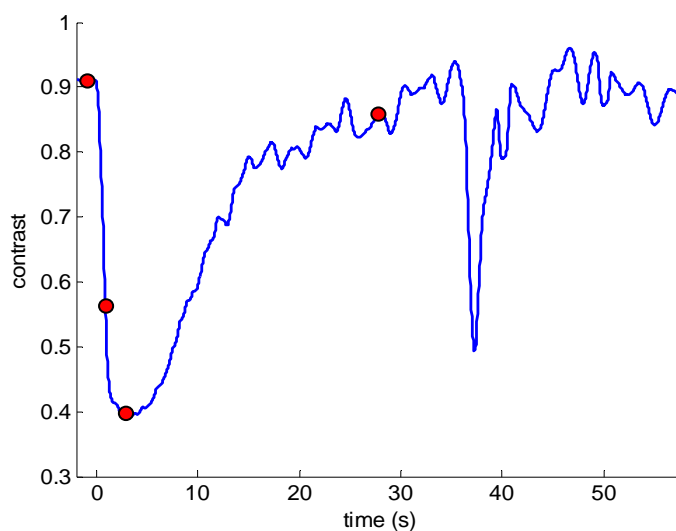
Fig. 5.7. Contrast as a function of time for composite sample cured with broad illumination beam. Contrast was determined over a 64 x 64 pixel (~2 x 2 mm) region in the center of sample with a T=500 ms. Red dots denote time point shown in the contrast maps below (Fig. 5.8).
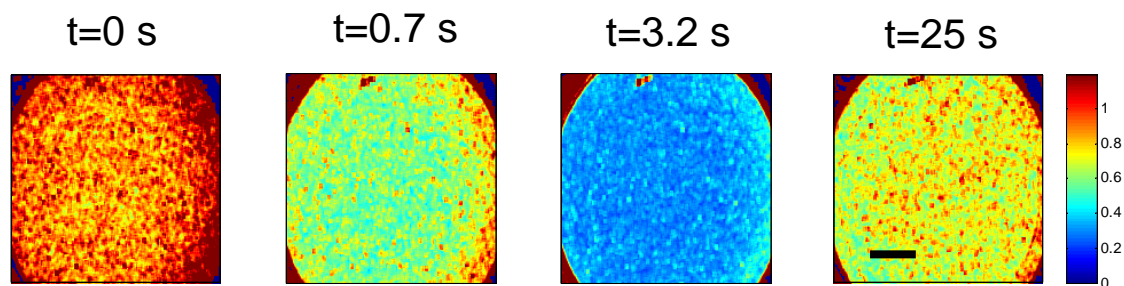
Fig. 5.8. Contrast map of the sample surface at several points of the reaction. Time points are shown in Fig. 5.7. Local contrast calculated over a 9 x 9 pixel window. Scalebar =5 mm.
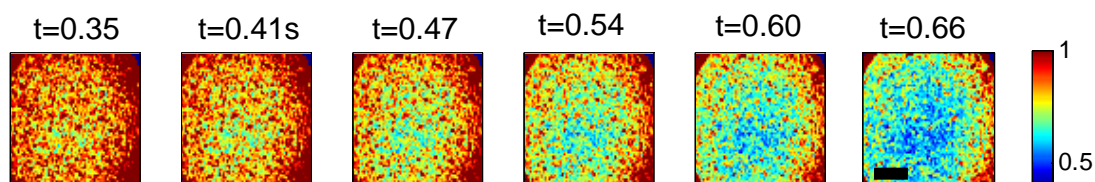
Fig. 5.9. Start of the curing reaction for broad curing illumination. Scalebar =5mm.

5.5.2 Restricted illumination

A further trial was performed in which the curing illumination was altered to allow only a small diameter beam of light to hit the sample. This was accomplished by placing a small iris (diameter = ~0.5 mm) between the lamp and the sample. At the opposite (top) surface of the sample, the curing beam had reached a diameter of ~ 2.8 mm (due to scattering). Because the radiant energy reaching the sample was considerably reduced (although irradiance was the same) compared to the previous experiment, the curing kinetics were much slower. An integration time of $T = 1\,\text{s}$ was used to determine contrast, therefore care must be taken if comparing the magnitude of the contrast in these two experiments.

Figure 5.10 shows the contrast map at the peak of the reaction. A circle representing the 2.8 mm diameter of the curing beam is shown for perspective. In Fig. 5.11 the progression of the reaction over the first 8 seconds is shown. As observed for

the previous experiment, the reaction here initially begins in the center of illumination ($t = 1\text{s}$), and then progresses outward. It would appear that at the peak of the reaction, polymerization is limited to a region that extends ~3mm beyond that of the diameter of the curing beam.
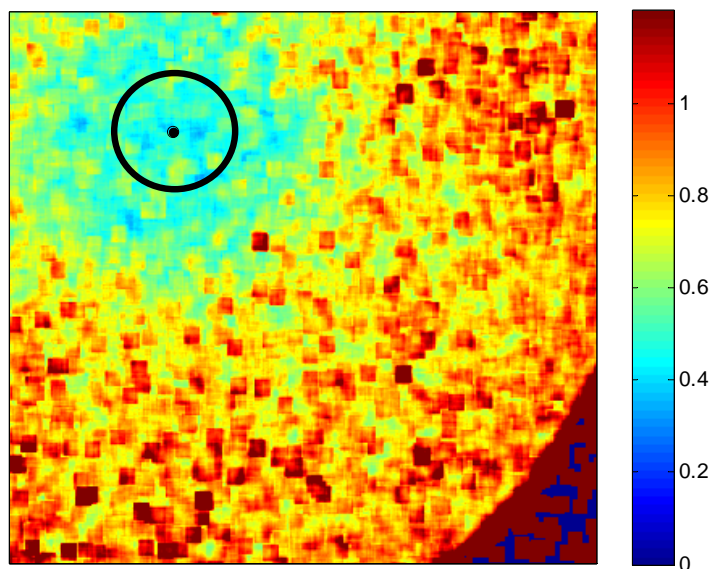
Fig. 5.10. Contrast map at the peak of reaction for small diameter curing beam. Circle represents the diameter of the curing beam at the surface of the sample,~2.8mm. Color scale is from 0 to 1.2.
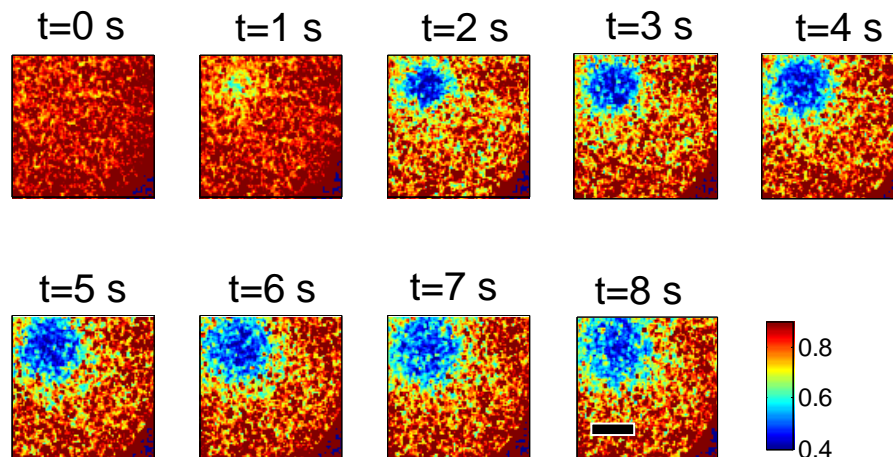
Fig. 5.11. Contrast map for the initial 8 seconds of the curing reaction for small diameter curing beam. Contrast color scale is from 0.4 to 1.0. Scalebar is 3mm.

5.6 Conclusions

We have presented an overview of the dynamic light scattering technique known as laser speckle contrast analysis (LSCA). This method was explored through simple experiments on dental resin composite during the polymerization reaction. Because LSCA has not before been used for this application we investigated several technical aspects (polarization and integration time) that are specific to this material and the dynamics of the reaction. We demonstrated how LSCA can be used to monitor the profile of the reaction, as well as explore spatial variations in polymerization behavior.

Ultimately, when studying dynamic processes, the rate of scatterer motion is of interest and not the contrast per se. We briefly mentioned in this chapter how the

contrast can be related to the underlying dynamics, but for the most part we did not attempt to do so here. The next chapter takes a more detailed look into the kinetics of the composite polymerization reaction by using the LSCA technique to study thin composite samples cured as a function of irradiance.

Chapter 6

A laser speckle contrast analysis (LSCA) study of the effect of curing irradiance on composite polymerization kinetics

6.1. Introduction

6.1.1 Background and significance

The polymerization kinetics of dental resin composites are known to play an important role in the development of many properties of the final restoration, such as storage modulus, hardness, and resistance to wear [32][27][100]. It is widely believed that the rate of monomer conversion influences the extent to which the composite experiences primary chain growth, cross-linking, and cyclization [36][79], which affect the development of mechanical properties. Several authors have suggested that polymerization rate may also significantly impact the shrinkage experienced by the composite and the detrimental stress that ensues [64][29][101]. Therefore gaining a better understanding of the kinetic behavior of composite polymerization, as well as ways to manipulate the reaction, may lead to the development of better composites and curing protocols that minimize shrinkage stresses while maintaining adequate material properties of the restoration [32].

The polymerization of photo-cured resin composite is known to be influenced by the resin and filler composition, as well as by the curing protocol [64]. In particular, the rate of polymerization is dependent on the irradiance of the curing light I (which in the dental literature is typically referred to as the curing intensity). For dimethacrylate resins, monomer conversion rate has been shown theoretically to vary with the square root of curing irradiance [36][102], while experimental investigations have found results that vary from $I^{0.3}$ to $I^{0.9}$ [74][103].

This study investigates the relationship between curing light irradiance and polymerization kinetics, using a laser method that has not before been used to study this reaction. Laser speckle contrast analysis (LSCA) is a dynamic light scattering (DLS) technique that offers high temporal resolution, has no mechanical compliance issues, and is inherently non-destructive. Here LSCA is used to monitor the polymerization reaction in thin composite samples. The effect of thickness is explored and accounted for, prior to examining the effect of curing irradiance. Implications of the kinetic results are discussed, as well as technical issues relating to the application of this method.

6.1.2 Overview of the LSCA

When coherent light (i.e. laser light) is scattered by an object that is rough on the scale of the wavelength, the observed intensity (the squared modulus of the electric field) exhibits a granular pattern of bright and dark regions. This is the optical

phenomenon known as laser speckle. When light is scattered by an object consisting of *moving* scattering particles, the observed speckle pattern will fluctuate with time. With the LSCA method this dynamic speckle pattern is imaged onto a CCD camera. Either during recording or during post processing, the intensity at each pixel is averaged over a time period T, which is referred to as the integration or exposure time. This has the effect of 'blurring' the temporal variations in the intensity signal, causing a reduction in the contrast of the speckle pattern. Speckle contrast is defined as the standard deviation divided by the mean of the integrated intensity:

$$C(t) = \frac{\sigma_{\bar{I}}(t)}{\mu_{\bar{I}}(t)}. \qquad (6.1)$$

The greater the motion of the scatterers—or the longer the integration time T—the lower the contrast.

The aim of LSCA is to relate the measured speckle contrast to the motion of the scatterers. This is done by assuming a shape for the intensity temporal autocorrelation function, $g_2(\tau)$, which may be characterized by its $1/e$ decorrelation time τ_{dc}, or its decorrelation rate:

$$r_{dc} = 1/\tau_{dc}. \qquad (6.2)$$

Analytic expressions have been derived [53][90][104] for Gaussian and negative exponential (Lorentzian) autocorrelation functions that relate the measured contrast C to the ratio τ_{dc}/T :

$$C_{Lorentzian} = \left\{ \frac{\tau_{dc}}{2T} \left[2 - \frac{\tau_{dc}}{T} \left(1 - e^{-2T/\tau_{dc}} \right) \right] \right\}^{1/2} \tag{6.3}$$

and

$$C_{Gaussian} = \left\{ \frac{\tau_{dc}}{2T} \left[\sqrt{2\pi}\,\mathrm{erf}\left(\frac{\sqrt{2}T}{\tau_{dc}} \right) - \frac{\tau_c}{T} \left(1 - e^{-2(T/\tau_{dc})^2} \right) \right] \right\}^{1/2} . \tag{6.4}$$

Figure 6.1 shows the relationship between contrast and relative integration time for these two models.
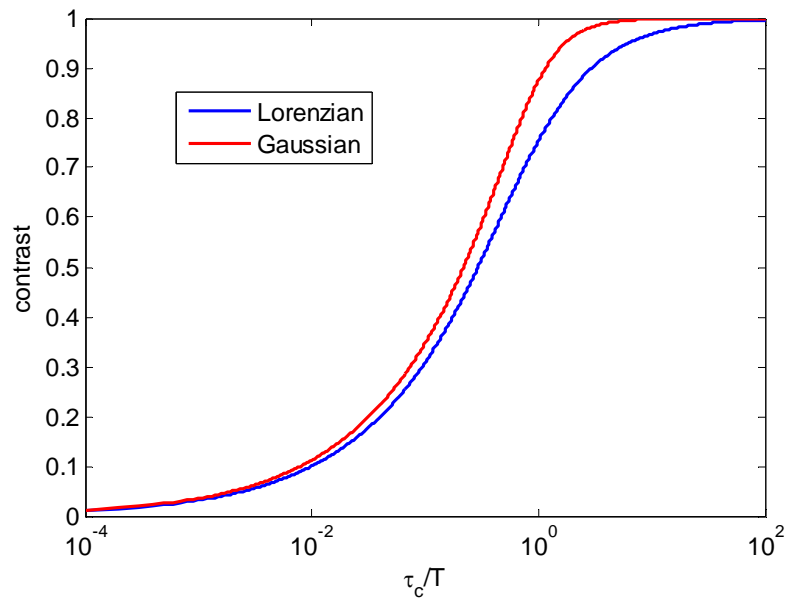
Fig. 6.1. Contrast as a function of relative decay time for Lorentzian and Gaussian models

.

6.1.3 Decorrelation rate as a measure of polymerization rate

The aim of this study is to use the intensity decorrelation rate r_{dc}, obtained from LSCA and using Eqs (6-2)-(6.4), to characterize dental composite polymerization rate r_{poly} as a function of curing light irradiance I. For this purpose it is assumed that the rate of motion $M\left[\text{cm}^2\text{s}^{-1}\right]$ of the filler particles (which act as scatterers) is proportional to the rate of polymerization r_{poly}. Based on quasi-elastic light scattering (QLS) [1][40], in the case of single scattering (number of scattering events $N=1$), intensity decorrelation rate r_{dc} is expected to be directly proportional to particle motion M:

$$r_{dc}\left(N=1\right) \sim M \ \Box \ r_{poly}. \tag{6.5}$$

However, the light backscattered from composite samples is *multiply* scattered light, and r_{dc} is known to increase with the square root of the number of scattering events $\sqrt{N}$ [105]. Because N increases with sample thickness (up to a point), r_{dc} will also increase. This effect must be considered when using LSCA to compare the polymerization kinetics for samples of differing thickness.

A model is adopted to describe decorrelation rate r_{dc} as a function of both irradiance I and sample thickness h, the two variables examined in this study. It is assumed that the effects of I and h are independent from each other, and that their effects can be determined separately:

$$r_{dc}\left(I,h\right)\Box \ f_1(I)f_2(h) \tag{6.6}$$

This is supported by noting that the increase in r_{dc} with thickness h occurs due to the increase in scattering events N of the *probing* beam, which is governed by the optical properties of the composite at the probing wavelength. The absorptions and reduced scattering coefficient at 633 nm (the probing wavelength for this study) have been shown to undergo little change during polymerization [77], and therefore curing irradiance I is not expected to influence $f_2(h)$.

As described in the literature, the effect of I on r_{poly} is expected to follow a power law relationship. Therefore from Eq. (6.5)

$$r_{dc}(I)\big|_{N=1} \square \, I^{\mathcal{E}} \tag{6.7}$$

and, because $N=1$ in the limit of $h \to 0$,

$$r_{dc}(I, h=0) \square \, I^{\mathcal{E}}. \tag{6.8}$$

This implies that

$$f_1(I) = I^{\mathcal{E}} \tag{6.9}$$

and

$$f_2(0) = 1. \tag{6.10}$$

The effect of h on r_{dc} is not entirely clear. A recent study on backscattering of γ photons, using Monte Carlo simulations, found that the number of scattering events as a function of sample thickness followed a sigmoidal curve, increasing exponentially for small thicknesses and then tapering off when a maximum probing depth was reached [106]. Other studies [107][108] have found an approximately linear relationship between reflectance and thickness for thin scattering samples. This indicates that, for

thin enough samples, each added layer of thickness results in an equivalent number of photons being backscattered. However photons that propagate deeper will undergo a disproportionately greater number of scattering events due to multiple scattering. Based on this limited evidence, in this study an exponential model is adopted to describe the effect of thickness:

$$f_2(I) = e^{b \cdot h}.$$

<div align="right">(6.11)</div>

Such a model is also convenient because it satisfies Eq. (6.10), but it will only be valid for samples up to a certain thickness, after which a maximum probing depth is reached. The final model for decorrelation rate as a function of I and h is

$$r_{dc}(I, h) = c\, I^{\varepsilon}\, e^{b \cdot h}$$

<div align="right">(6.12)</div>

where ε and b are the parameters of interest, and c is a proportionality constant.

6.2. Materials and Methods

6.2.1 Sample preparation

The experimental composite used in this study consisted of 82% (by weight) fused quartz silica hybrid filler particles (0.1-3 μm diameter) and 18% resin matrix, which was composed of 50:50 w/w ratio mixture of BisGMA (2,2-bis[4-(2-hydroxy-3-methacryloxypropoxy)phenyl]-propane) and TEGDMA (triethylene glycol dimethacrylate), 0.8 % CQ (camphorquinone) photoinitiator, 0.4% EDMAB (ethyl-4-dimethylaminobenzoate) amine coinitiator and 0.05 % BHT (butylated hydroxytoluene) inhibitor.

Thin composite samples were made with thickness ranging from 0.1-1.3 mm, and diameter of ~15 mm. Uncured composite was placed on glass backing and pressed into a thin film, under low ambient light conditions. Thickness of the samples were measured with digital calipers post-cure. The reported values are the mean thickness obtained from multiple measurements near the center of the sample.

6.2.2 Optical configuration
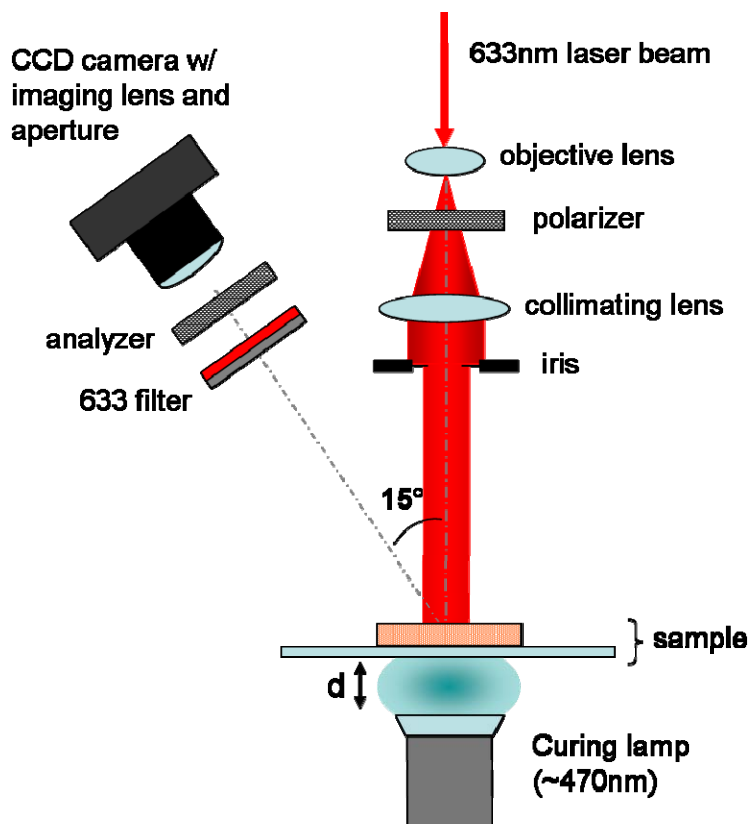
Fig. 6.2. Experimental configuration used to acquire dynamic speckle.

The experimental configuration used to cure the samples and obtain dynamic speckle data is shown in Fig. 6.2. Details of the system are described in Chapter 4. To change the curing irradiance, the distance d between the lamp and sample was varied by raising or lowering the stage on which the samples were placed (between 5 and 15 cm). At any vertical position of the stage, several irradiances could be tested by use of neutral density attenuation filters (Melles-Griot). We employed filters that had optical densities of 0.3, 0.5, and 1.0.

The output of the lamp was measured at several distances via a power meter (Nova II, Ophir). These results are shown in Fig. 6.3 plotted on a semi-log scale. Irradiance is seen to decrease exponentially with distance from the light guide. The results of an exponential fit are also shown.

$$I = 596\ e^{-0.07*d}$$
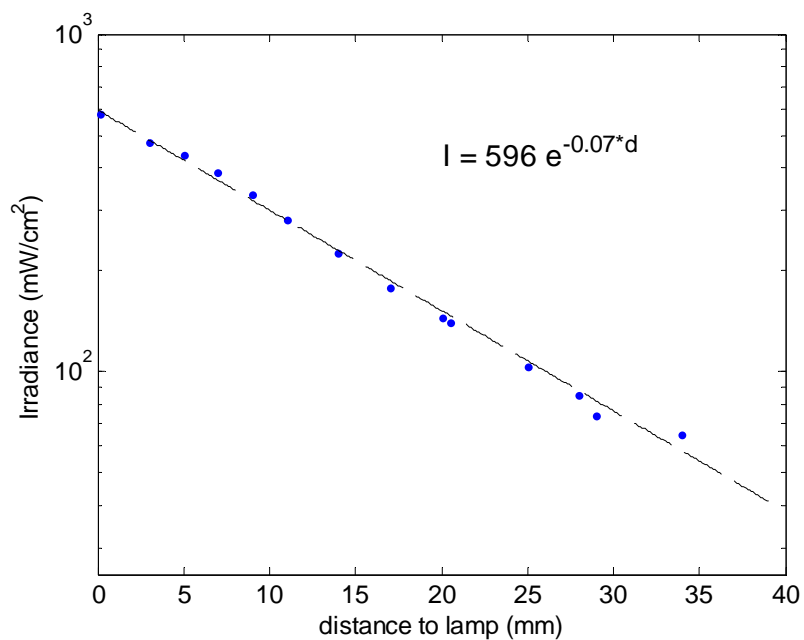
Fig. 6.3. Lamp output as a function of distance to the light guide. Dashed line is the fit to an exponential curve. (Semi-log plot)

Each time the distance d was adjusted, the telecentric imaging lens was re-focused onto the surface of the sample and the aperture was adjusted to achieve a minimum speckle dimension of just over two pixels. Also the gain was adjusted to

avoid pixel saturation while utilizing most of the dynamic range, which was done by observing the histogram of pixel intensity in the Point Grey interface.

6.2.3 Curing protocol and data acquisition

A first group of samples of thickness h ranging from 0.1-1.3 mm was curing with irradiance $I = 160\text{mW/cm}^2$ to determine the effect of thickness. A second group of samples was cured at a range of irradiances, from 10-210 mW/cm^2, and variable thickness. Dynamic speckle images were recorded at 32 frames per second with a camera exposure time $T = 31\text{ms}$ for a total of 35 seconds. The images were saved as .avi files for post processing. The curing lamp was turned on manually at 5 s, and remained on for the duration of the reaction.

6.2.4 Data Processing

Speckle integration

The 31 ms camera integration time was short enough that minimal speckle blurring occurred in the raw speckle data (see Chapter 5). Exposure integration was performed during post-processing. An effective integration time of $T = 1\text{s}$ was achieved by performing a sequential averaging over 32 frames, for each pixel in the data set.

Calculating contrast

Contrast analysis was performed on a 64 x 64 pixel (2 x 2 mm) region of interest (ROI) in the center of the sample, which coincided with the center of the probing and curing beams. The contrast for each frame was calculated as the intensity standard deviation divided by the mean (Eq. 6.1), as described in Chapter 5. Due to the large diameter of the sample (compared to thickness), and the broad curing and probing beams (>1 cm and 1 cm respectively), the curing behavior of the composite within this ROI was expected to be homogeneous.

Reaction kinetics

The intensity decorrelation time τ_{dc} was found using the Lorentzian and Gaussian models in Eqs (6.3) and (6.4), and Eq (6.2) was used to obtain decorrelation rate r_{dc}. The data for the samples cured at 160 mW/cm^2 were least-squares fit to the exponential model

$$r_{dc} = a\,e^{b\cdot h} \tag{6.13}$$

to determine the effect of sample thickness h. The parameter b was then used to normalize the r_{dc} results for all samples by $e^{b\cdot h}$ to remove the dependence on thickness. This effectively yields the decorrelation rate expected in the limit of single scattering which has been assumed to be proportional filler motion within the composite and the

rate of polymerization (Eq 6.5). From the normalized results, the effect of curing

irradiance was then examined and least-squares fit to

$$r_{dc} = I^{\varepsilon} \tag{6.14}$$

6.3. Results

The peak contrast for all samples cured at 160 mW/cm^2 is shown in Fig. 6.4A.

The corresponding intensity decorrelation rates r_{dc}, calculated from the Lorentzian and

Gaussian models, are shown in Fig 6.4B. The decorrelation rate increases from 0.1 to

approximately 0.8 mm then levels off. The data for samples < 0.8 mm were fit to the

exponential model in Eq. (6.13), the results of which are included in Fig. 6.4B. The

parameter b describing the effect of thickness was 2.30 mm^{-1} (± 0.28) for the Lorentzian

model and 2.22 mm^{-1} (± 0.26) for the Gaussian model.
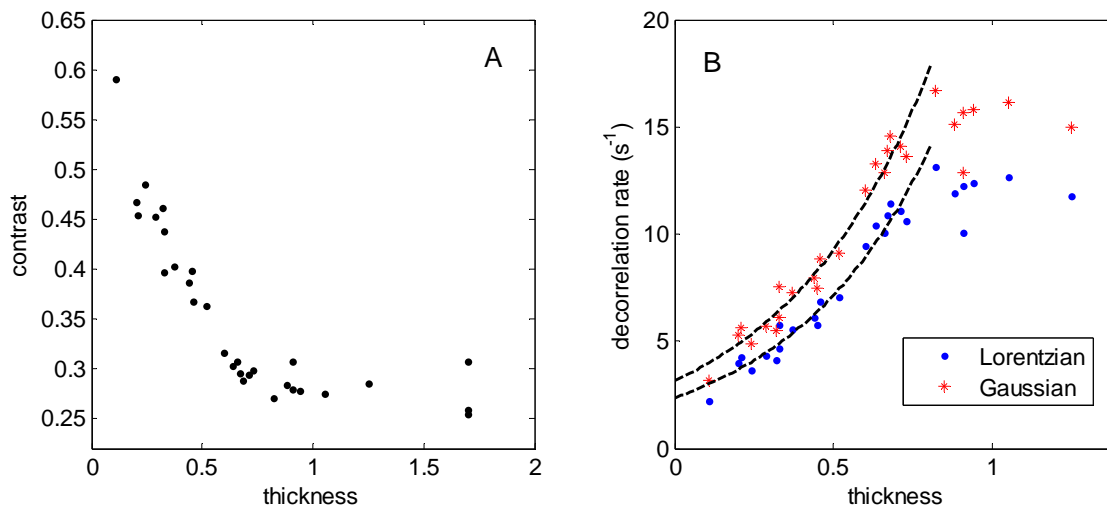
Fig. 6.4. Effect of thickness for samples cured at 160 mW/cm^2. A. Peak contrast for all samples using an integration time T=1 s. B. Corresponding intensity decorrelation rates obtained from Lorentzian and Gaussian models.

Decorrelation rate results for all samples were normalized by $e^{2.30 \cdot h}$ for Lorentzian results and $e^{2.22 \cdot h}$ for Gaussian results, to account for thickness. Figure 6.5 shows the decorrelation rate results before and after correcting for thickness. Included in this figure are the power law (Eq. (6.14)) fits of the data. The ε parameters for the corrected Gaussian and Lorentzian data were 0.51 ($\pm$ 0.09) and 0.46 ($\pm$ 0.08) respectively.
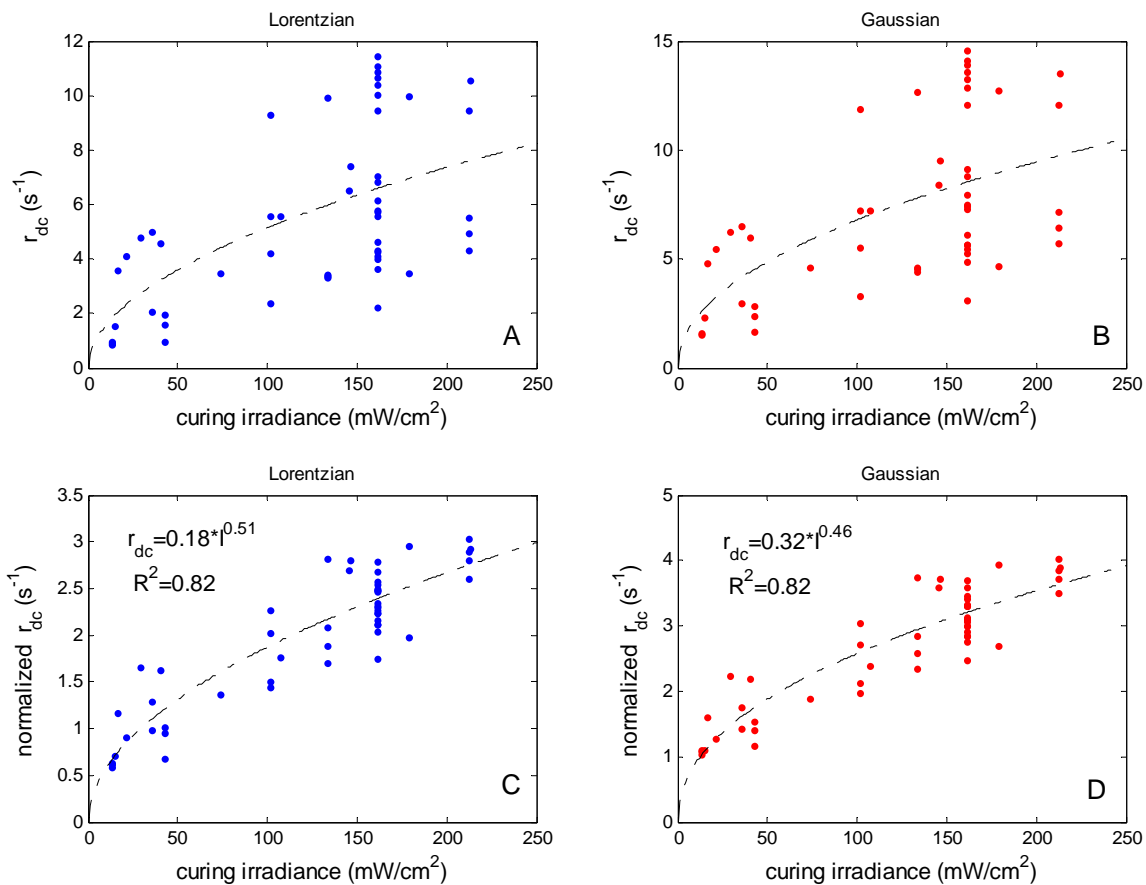
Fig. 6.5. Decorrelation rate result as a function of curing irradiance. A and B. Raw results for Lorentzian and Gaussian models. C and D Results normalized by the exponential thickness correction factor. Dashed lines indicate least-squares power law fits.

6.4 Discussion

In this study laser speckle contrast analysis (LSCA) was used to characterize the polymerization kinetics of dental composite. The primary objective was to evaluate the effect of curing irradiance on the polymerization rate, in order to provide a validation of the method. The results indicate that motion within the composite at the peak of the reaction—as determined by the thickness-normalized intensity decorrelation rate r_{dc}— scales approximately with the square root of curing irradiance. When the temporal intensity fluctuations are assumed to have a Lorentzian spectral shape this relationship was shown to be $r_{dc} \square I^{0.51}$; for the case of a Gaussian model the result was $r_{dc} \square I^{0.46}$. Theoretical models predict that dimethacrylate polymerization rate varies with $I^{0.5}$ [36][102]. Anseth *et al* [74] found a rate dependence of $I^{0.34}$ using differential scanning calorimetry (DSC), and Lovell and colleagues [103] found a $\square I^{0.6}$ dependence using near-IR spectroscopy. The results from this study using LSCA are in reasonable agreement with these previous experimental studies, as well as the theoretical polymerization model.

This method uses decorrelation rate r_{dc} as a measure of polymerization rate r_{poly} based on the premise that the fluctuations in scattered intensity (which give rise to the decrease in contrast that LSCA measures) are a result of motion of the scattering filler

particles (Eq. (6.1)). The intensity fluctuations are caused by changes in phase ϕ of the

scattered photons:

$$\phi = \frac{2\pi n d}{\lambda} \qquad (6.15)$$

where n is the medium index of refraction, λ is the wavelength, and d is the propagation

pathlength of the photon. Motion of scattering particles results in a change in

pathlength Δd, causing a change in phase and intensity of the scattered light. Many

photons contribute to the measured intensity signal at each camera pixel, and the

combined phase change of all the individual contributions results in the observed

intensity fluctuations.

However the phase is also influenced by the index of refraction n of the resin,

which is known to change during polymerization [78]. Therefore a change in either n or

d may give rise to fluctuations in scattered light. Using a commercial resin, Tomlins et

al [78] found n to increase from 1.524 to 1.529 (Δn=0.005) over the course of

polymerization. At the peak of the reaction, which lasted ~ 4 s, the change in index was

$\Delta n = 0.001$. The change in phase $\Delta\phi$ resulting from an index change of this magnitude

depends on the pathlength d. For an example pathlength $d = 1$ mm (which is a feasible

pathlength for a sample thickness of ~0.5 mm), the phase change rate would be on the

order of $\Delta\phi/dt \approx 2.5\,\mathrm{rad}\cdot\mathrm{s}^{-1}$ (for $\lambda = 633\,\mathrm{nm}$ and constant d). By comparison, a change

in pathlength of $\Delta d/dt \approx 170$ nm$\cdot$s^{-1} produces the same phase change rate (for

constant $n = 1.525$). Polymerization shrinkage strain rates in composites have been shown to be ~0.2-0.3 s^{-1} [66][78][101], which is equivalent to ~1 μ m s^{-1} across a 0.5 mm sample. Considering that this is ~6 times larger than the estimated phase change from index of refraction, it is likely that the effect of Δd is dominant over the effect of Δn in contributing to phase change $\Delta \phi$, and the resulting intensity fluctuations.

The assertion that the rate of motion M within the composite is indicative of polymerization rate has yet to be verified. Several authors have used strain rate as a measure of polymerization rate [31][66], and filler motion is likely associated, to some degree, with shrinkage strain. However, there may be additional non-strain related contributions to the particle motion, but the extent of this is unclear at this time.

Multiple scattering and the effect of thickness complicate the interpretation of LSCA results [109]. In this study the effect of h on r_{dc} was determined in order to provide a normalization that allows the results for different sample thicknesses to be compared. Data were normalized by a factor e^{bh} to remove the effect of thickness, where b was determined by fitting to the data at 160 mW/cm^2 only. The assumption was made that, because the optical properties μ_a and $\mu_s^{'}$ undergo little change at the probing wavelength [77], the exponential constant b should be independent of I. Only $I = 160$ mW / cm^2 was used for the full range of thickness (0.1-1.3 mm), however the results at other irradiances can be used to explore the validity of this assumption.

For five different irradiance values, six or mores samples were tested (some irradiances are not included due to too few samples). The r_{dc} results for each of these irradiance sub-subsets were fit to the exponential model in Eq. (6.13) and the resulting b parameters are shown in Fig 6.6 for the Lorentzian model. The results are inconclusive due to the small sample sizes (average n=7, except for 160 mW/cm^2), however it appears that b may decrease slightly with increasing I. Therefore a more appropriate model may be of the form

$$r_{dc}(I,h) = c\,I^{\varepsilon}\,e^{(b-\alpha I)h}, \qquad\qquad (6.16)$$

but further experiments are needed to explore this.
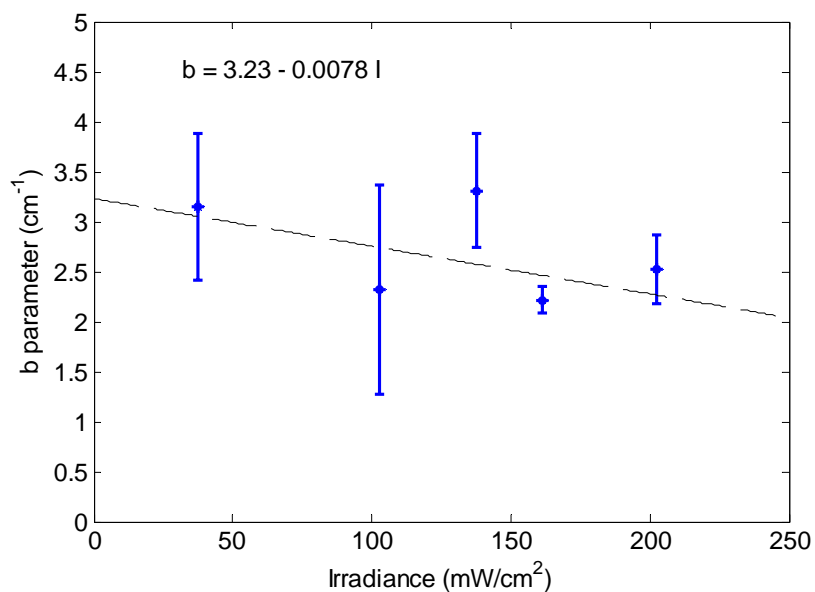
Fig. 6.6. Lorentzian model b parameters obtained from exponential fits of decorrelation data for samples grouped by curing irradiance. Dashed line is a linear fit to the data (R^2=0.32).

It should be pointed out that the r_{dc} results for samples cured at 160 mW/cm^2 (Fig 6.4B) were also well fit by a linear relationship with h (R^2=0.95, compared to R^2=0.96 for the exponential model). However the linear model predicted that the decorrelation rate approaches zero as sample thickness approaches zero, for the I =160 mW/cm^2 data. And for I = 40 mW/cm^2 and 137 mW/cm^2, the linear model predicted negative decorrelation rates as thickness approached zero. As mentioned in the introduction, several studies [106-108] have suggested a possible exponential relationship between number of scattering events and thickness, for thin samples. Monte Carlo simulations would be valuable for investigating how the mean number of scattering events (or the mean optical pathlength) is affected by sample thickness, and could be applied to composites with varying optical properties.

For this work the depth dependence of polymerization rate has been ignored. With the experimental system, samples were cured from the bottom surface while probing beam irradiance occurred from the top. Because the curing light attenuates with depth, the layers near the bottom (closest to the curing lamp) are expected to experience a higher polymerization rate than those near the top surface. However, for simplicity, the polymerization rate was treated as uniform over all depths.

A major limitation to this study was the large amount of variability in decorrelation rate results, even after correcting for sample thickness. This lends a degree

of uncertainty to the interpretation of the results from this method. A large part of this variability may be attributed to the difficulty in making samples of uniform thickness, due construction of samples in the dark and the high viscosity of the composite. Improvements in sample construction methodology that produce more uniform samples would likely lead to reduced variability and easier interpretation of the results.

6.5 Conclusions

Laser speckle contrast analysis (LSCA) was used to quantitatively characterize the polymerization kinetics of thin composite samples as a function of curing irradiance. After correcting for sample thickness, our results indicate that polymerization rate scales approximately with the square root of curing irradiance, which is in agreement with theory and previous experimental studies. The LSCA method is a relatively simple, non-contact, high resolution technique that is well-suited to the study of dental composite polymerization kinetics.

Chapter 7

Conclusions: Comparison of DLS Methods and Future Work

7.1 Overview

In this dissertation a number of approaches for studying dynamically scattered light (DLS) were presented. The rationale for much of this research was to develop advanced methodologies for studying dynamic processes. Although the scope the experimental work was limited primarily to the specific case of composite polymerization, the ideas presented in this dissertation are relevant to a wide array of dynamic applications.

Two different experimental DSL configurations were implemented for this work. The first was a point-detection-based quasi-elastic light scattering (QLS) apparatus. QLS is a powerful method for studying stationary processes, as demonstrated by the microsphere experiments presented in Chapter 2. However, due to the long sampling duration required for accurate dynamic measurements, QLS it is not suitable for monitoring some certain reactions.

The study of QLS led to the implementation of a second experimental system, which utilized a CCD camera to measure the scattered intensity. This had the added benefit of ensemble averaging over many pixels, which allowed faster characterization of dynamic behavior. This CCD-based system was used for the bulk of the experimental work presented here (Chapters 4-6). With this system, speckle patterns were recorded and used to characterize dental composite polymerization using two ensemble-average based algorithms. The first, referred to as sequential speckle correlation (SSC), was developed as part of this research. The second was the DLS technique laser speckle contrast analysis (LSCA), which is an established method for studing blood flow. The research presented here marks its first successful application to the characterization of composite polymerization.

7.2 Studying dynamic processes with DLS

7.2.1 General overview

The DLS measurement techniques described here comprise two parts: 1) the method of detection, which is an optical design problem, and 2) the method of analysis. In this dissertation, the focus was primarily on the second element. However, there are aspects of detection that are influential for the analysis of the signal. These include detection polarization state, dimension of the imaging aperture, and spatial and temporal detector integration.

7.2.2 Correlation analysis

A common theme that connects the different methods presented in this work is the use of second order statistics (i.e. correlations) to describe dynamically scattered light. This was first introduced in Chapter 2, pertaining to QLS, where the autocorrelation function was shown to be directly related to the diffusive motion and the physical properties of the scattering medium.

With the sequential speckle correlation (SSC) method, dynamic behavior is described via the correlation of speckle patterns separated by a fixed temporal delay τ. The method does not provide a measure of the autocorrelation *function*, as with QLS. The measure of correlation used for SCC is the commonly used Pearson's correlation coefficient ρ, which is the covariance of the two speckle patterns normalized by the product of their standard deviations [46]. If it is assumed that the integration time of the CCD camera is short enough that the speckle is fully-formed, and that the intensity standard deviation σ is the same for the two patterns, then the following relationships hold:

$$\rho_\tau \equiv \frac{\text{Cov}\big(I(t), I(t+\tau)\big)}{\sigma_t \sigma_{t+\tau}} \qquad (7.1)$$

$$\rho_\tau(t) = \frac{\left\langle \left(I(t) - \mu_I\right)\left(I(t + \tau) - \mu_I\right)\right\rangle}{\sigma_I{}^2}$$

(7.2)

$$= \frac{\left\langle I(t)I(t + \tau)\right\rangle - \mu_I{}^2}{\sigma_I{}^2} = \frac{G_2(\tau) - \mu_I{}^2}{\sigma_I{}^2}.$$

(7.3)

Assuming fully-formed statistics leads to $\sigma_I{}^2 = \mu_I{}^2$ and thus

$$\rho_\tau(t) = \frac{G_2(\tau)}{\mu_I{}^2} - 1 = g_2(\tau) - 1$$

(7.4)

If the minimum speckle size is larger than the pixel dimension and only a single

polarization state is detected, then the zero time delay value is equal to unity and the

coherence factor $\beta = 1$ (see Chapter 2). In the work presented here, the speckle always

satisfied this condition, since the spatial Nyquist sampling criterion was always met and

polarizers were used. In this manner, it is clearly demonstrated that the correlation

coefficient used for SSC analysis is directly related to the normalized intensity

autocorrelation function.

For LSCA, the connection to autocorrelation is not immediately clear. However,

recalling Eq. (5.6),

$$\sigma_I^2(t) = \frac{1}{T}\int_t^{t+T}\text{Cov}_I(\tau)\left[2(1 - \tau/T)\right]d\tau,$$

it is evident that the contrast (the standard deviation divided by the mean) of the time

integrated speckle pattern is directly related to the covariance of the underlying

instantaneous intensity. In this equation the instantaneous intensity is denoted as I and

time-averaged intensity as $\overline{I}$.

In neither the SSC method nor LSCA is the autocorrelation function actually

measured. This is not done for two reasons. First, a transitioning dynamic process often

changes faster than it can be measured. Second, the sampling rates of current CCD

cameras are often too slow to resolve the autocorrelation function of many scattering

processes.

7.2.3 Sampling issues

Quasi-elastic light scattering, because it is a single detector method, is not able

to measure changes in dynamic behavior that occur faster than a certain rate. It takes a

duration of approximately 1000 decorrelation times to get a statistically reliable

measure of dynamic behavior, based on the data and statistical analysis presented in

Chapter 3. Therefore reactions that change faster that $\sim 1000\,\tau_{dc}$ cannot be monitored

with a high level of confidence using QLS. For the example of composite

polymerization in Chapter 4, at the height of the reaction the intensity decorrelation rate

$r_{dc} \approx 10\ \text{s}^{-1}$ and $\tau_{dc} = 100\,\text{ms}$. To accurately measure an equivalent fluctuation rate

using a point detection scheme would require > 100 s. However, the reaction

acceleration occurs on the order of 1 s, which is clearly too fast to be resolved with

QLS.

Both CCD- based methods presented here used ensemble averaging over

multiple speckles to achieve faster dynamic characterization. For the SCC study of

composite polymerization, a 64 x 64 pixel region, containing more ~1000 independent

speckles, was used. The time required to obtain a reliable measurement is therefore less

than one second. From empirical analysis, the temporal resolution appeared on the order

of 100 ms. One issue with this method, however, is that the material should be

statistically homogenous over the ROI. This was a reasonable assumption for the

composite experiments in Chapter 4 based on the sample and curing geometries, but

may not be the case for other applications.

The LSCA method similarly benefited from ensemble averaging. However, it

had a lower temporal resolution due to the smaller windows over which local contrast

was determined. This is not necessarily a disadvantage though, because LSCA may be

used explore the spatial variation in dynamic behavior, which is not possible with most

other DLS methods.

7.2.4 Limitations and future work

A major limitation of the dynamic speckle methods described in this dissertation

is their inability to provide quantitative measurement of actual scatter motion. In this

work, the results were presented in terms of intensity decorrelation rate, or decorrelation time. The assumption, discussed in Chapter 6, is that the rate of intensity fluctuation is directly related to the underlying rate of motion of the scattering particles. However, changes in optical properties, particularly index of refraction, will also contribute to the fluctuations. For this work, the index of refraction n was not measured, nor was the photon pathlength d distribution determined. Based on results in the literature for change in index of refraction Δn [78], as well as studies of shrinkage strain rate [66], it was speculated that motion of the scattering particles is the dominant factor. However future work is needed to verify this assertion and to determine the relative contributions of both effects on the observed intensity fluctuation.

The QLS technique *is* able to determine the actual diffusion coefficient of a scattering suspension, because the scattering process is well-controlled and well-described theoretically. Additionally, the method has a high enough sampling rate to fully resolve the autocorrelation function. For the dynamic speckle methods, SSC and LSCA, an autocorrelation profile must be *assumed* in order to convert intensity rate to scatterer motion. If the general scattering behavior is known *a priori*, a reasonable assumption can perhaps be made. However, the problem is further complicated by the presence of multiple scattering. Even when a less that perfect autocorrelation model may be acceptable, if the number of scattering events is not known, it is not possible to get a quantitative measure of motion.

As CCD cameras with higher sampling rates and sensitivities become available, it may be possible to resolve the full autocorrelation function, so that models for the intensity statistics will not be required. For some processes this is already within reach [110]. Future work is needed to interpret the physical scattering process from a theoretical point of view that includes multiple scattering, and to relate this to the statistical behavior of the scattered light. This may involve ways of dealing with sub-diffusive multiple scattering, correlated scattering events, or directionality and organization of scatterer motion.

7.3 Composite polymerization kinetics

7.1 Summary of results

Using DLS techniques the polymerization of dental resin composite was characterized using the intensity fluctuations in scattered light. This approach differs from other commonly used techniques, which instead measure monomer conversion rate or strain rate.

The SSC and LSCA methods produced reaction rate curves that appeared qualitatively similar to results found in the literature using methods such as IR spectroscopy, calorimetry, and strain measurement. More detail was discernable in the results from DLS, however, likely due to the higher temporal resolution of these DLS

methods. The polymerization reaction was characterized in detail over the first seconds of the reaction, for composite cured at clinically relevant irradiances. It was observed that the polymerization rate, as indicated by intensity decorrelation rate, began a sharp increase within less than 500 ms of the onset curing illumination. This finding is significant because it indicates that there is relatively little time for viscous flow and the dissipation of curing stress.

In the study on thin samples using LSCA, results were in good agreement with the often cited theoretical relationship that polymerization rate varies with the square root of curing irradiance. This study suggests that DLS methods such as LSCA can provide valuable insight into composite polymerization when appropriately applied.

7.3.3 Future DLS applications for studying composite

A capability of LSCA that was briefly touched upon, but not thoroughly explored, is the spatial mapping of dynamic behavior via contrast imaging. In Chapter 5 contrast images of disk-shaped composite samples were shown that enable visualization of spatial changes in dynamics during the progression of the reaction. While the few results shown in Chapter 5 were useful in demonstrating this important aspect of LSCA, the full potential of such a tool was not explored. LSCA could be used to explore spatial variations in curing kinetics under a variety of test conditions. For example it could be used to explore the dynamic response to uneven or off axis curing illumination, or it could be used to look at curing behavior near restoration boundaries. Using LSCA with

low-coherence light (for example with optical coherence tomography), may also be a useful direction for future research. The extent of sub-surface curing is of great clinical importance [111-113], and this approach would allow monitoring of polymerization at different depths within the composite[99][114].

There are likely many other ways in which DLS techniques, and specifically those implemented in this work, could be applied to study composite polymerization. It is feasible that DLS could be used in combination with other testing apparati, so long as one face of the composite sample is available for laser interrogation. With such an approach, DLS results could complement the results of stress or strain measurements. DLS methods are relatively simple to implement, are non-contact, and offer high sampling rates.

7.4 Conclusions

In summary, DLS methods for studying reactions that exhibit high rates of dynamic change were designed and implemented. The measurement of such processes, which is difficult with traditional point-detector DLS techniques, was made possible through use of CCD camera detection and dynamic speckle pattern ensemble averaging. The use of these methods was demonstrated with experimental studies on the polymerization of dental resin composites, in which kinetic detail could be discerned

with high temporal resolution. Dynamic light scatting techniques that utilize multi-pixel

ensemble averaging offer many advantages for the study of dynamic processes

References

[1]   B. J. Berne and R. Pecora, *Dynamic Light Scattering: with Applications to Chemistry, Biology, and Physics*. Courier Dover Publications, 2000.

[2]   Y. Georgalis et al., "Huntingtin aggregation monitored by dynamic light scattering," *Proceedings of the National Academy of Sciences of the United States of America*, vol. 95, no. 11, pp. 6118 -6121, May. 1998.

[3]   D. A. Boas and A. K. Dunn, "Laser speckle contrast imaging in biomedical optics," *Journal of Biomedical Optics*, vol. 15, no. 1, pp. 011109-12, Jan. 2010.

[4]   D. G. Dalgleish and F. R. Hallett, "Dynamic light scattering: applications to food systems," *Food Research International*, vol. 28, no. 3, pp. 181-193, 1995.

[5]   R. Tishler and F. Carlson, "A study of the dynamic properties of the human red blood cell membrane using quasi-elastic light-scattering spectroscopy," *Biophysical Journal*, vol. 65, no. 6, pp. 2586-2600, Dec. 1993.

[6]   N. A. Mazer and M. C. Carey, "Quasi-elastic light-scattering studies of aqueous biliary lipid systems. Cholesterol solubilization and precipitation in model bile solutions," *Biochemistry*, vol. 22, no. 2, pp. 426-442, Jan. 1983.

[7]   F. R. Hallett, J. Watton, and P. Krygsman, "Vesicle sizing:: Number distributions by dynamic light scattering," *Biophysical journal*, vol. 59, no. 2, pp. 357–362, 1991.

[8]   J. Pencer, G. F. White, and F. R. Hallett, "Osmotically induced shape changes of large unilamellar vesicles measured by dynamic light scattering," *Biophysical*

Journal, vol. 81, no. 5, pp. 2716-2728, Nov. 2001.

[9] R. Bonner and R. Nossal, "Model for laser Doppler measurements of blood flow in tissue," *Applied Optics*, vol. 20, no. 12, pp. 2097-2107, Jun. 1981.

[10] T. Tanaka and G. Benedek, "Observation of protein diffusivity in intact human and bovine lenses with application to cataract," *Invest. Ophthalmol. Vis. Sci.*, vol. 14, no. 6, pp. 449-456, Jun. 1975.

[11] B. Ware and W. Flygare, "The simultaneous measurement of the electrophoretic mobility and diffusion coefficient in bovine serum albumin solutions by light scattering," *Chemical Physics Letters*, vol. 12, no. 1, pp. 81-85, Dec. 1971.

[12] H. Sendra, S. Murialdo, and L. Passoni, "Dynamic laser speckle to detect motile bacterial response of Pseudomonas aeruginosa," *Journal of Physics Conference Series*, vol. 90, p. 2064, Nov. 2007.

[13] S. Chen, M. Holz, and P. Tartaglia, "Quasi-elastic light scattering from structured particles," *Applied Optics*, vol. 16, no. 1, pp. 187-194, Jan. 1977.

[14] T. Maeda and S. Fujime, "Dynamic light-scattering study of suspensions of fd virus. Application of a theory of light-scattering spectrum of weakly bending filaments," *Macromolecules*, vol. 18, no. 12, pp. 2430-2437, Dec. 1985.

[15] H. Z. Cummins, N. Knable, and Y. Yeh, "Observation of diffusion broadening of rayleigh scattered light," *Physical Review Letters*, vol. 12, no. 6, p. 150, Feb. 1964.

[16] E. Pike, "Photon statistics," *Rivista del Nuovo Cimento*, vol. 1, pp. 277-314, 1969.

[17] T. G. Mason, "Estimating the viscoelastic moduli of complex fluids using the

generalized Stokes-Einstein equation," *Rheologica Acta*, vol. 39, no. 4, pp. 371-378, 2000.

[18] K. Schätzel, M. Drewel, and S. Stimac, "Photon correlation measurements at large lag times: improving statistical accuracy," *Journal of Modern Optics*, vol. 35, no. 4, p. 711, 1988.

[19] D. J. Pine, D. A. Weitz, P. M. Chaikin, and E. Herbolzheimer, "Diffusing wave spectroscopy," *Physical Review Letters*, vol. 60, no. 12, p. 1134, Mar. 1988.

[20] J. D. Briers, "Laser speckle contrast analysis (LASCA): a nonscanning, full-field technique for monitoring capillary blood flow," *Journal of Biomedical Optics*, vol. 1, no. 2, p. 174, 1996.

[21] J. Aksiyote-Benbasat, V. A. Bloomfield, and D. I. Stimpson, "Kinetics of head-tail joining in bacteriophage T4D studied by quasi-electric light scattering: effects of temperature, pH, and ionic strength. Calculation of the steric factors affecting the head-tail joining reaction," *Biochemistry*, vol. 20, no. 17, pp. 5018-5025, 1981.

[22] H. P. Feng, D. S. Scherl, and J. Widom, "Lifetime of the histone octamer studied by continuous-flow quasielastic light scattering: Test of a model for nucleosome transcription," *Biochemistry*, vol. 32, no. 30, pp. 7824-7831, 1993.

[23] L. Cipelletti and D. A. Weitz, "Ultralow-angle dynamic light scattering with a charge coupled device camera based multispeckle, multitau correlator," *Review of Scientific Instruments*, vol. 70, no. 8, pp. 3214-3221, 1999.

[24] K. J. Anusavice, *Phillips' Science of Dental Materials*. Philadelphia: Saunders, 2003.

[25] J. W. Simecek, K. E. Diefenderfer, and M. E. Cohen, "An evaluation of replacement rates for posterior resin-based composite and amalgam restorations in U.S. Navy and Marine Corps recruits," *J Am Dent Assoc*, vol. 140, no. 2, pp. 200-209, Feb. 2009.

[26] T. Beazoglou, S. Eklund, D. Heffley, J. Meiers, L. J. Brown, and H. Bailit, "Economic Impact of Regulating the Use of Amalgam Restorations," *Public Health Reports*, vol. 122, no. 5, pp. 657-663, 2007.

[27] J. Stansbury, M. Trujillolemon, H. Lu, X. Ding, Y. Lin, and J. Ge, "Conversion-dependent shrinkage stress and strain in dental resins and composites," *Dental Materials*, vol. 21, no. 1, pp. 56-67, 2005.

[28] J. L. Ferracane, "Developing a more complete understanding of stresses produced in dental composites during polymerization," *Dental Materials*, vol. 21, no. 1, pp. 36-42, Jan. 2005.

[29] R. Braga and J. Ferracane, "Contraction stress related to degree of conversion and reaction kinetics," *Journal of Dental Research*, vol. 81, no. 2, pp. 114-118, Feb. 2002.

[30] R. Sakaguchi, W. Douglas, and M. Peters, "Curing light performance and polymerization of composite restorative materials," *Journal of Dentistry*, vol. 20, no. 3, pp. 183-188, Jun. 1992.

[31] B. A. M. Venhoven, A. J. de Gee, and C. L. Davidson, "Light initiation of dental resins: dynamics of the polymerization," *Biomaterials*, vol. 17, no. 24, pp. 2313-2318, 1996.

[32] L. G. Lovell, H. Lu, J. E. Elliott, J. W. Stansbury, and C. N. Bowman, "The

effect of cure rate on the mechanical properties of dental resins," *Dental Materials*, vol. 17, no. 6, pp. 504-511, Nov. 2001.

[33] A. Feilzer and B. Dauvillier, "Effect of TEGDMA/BisGMA ratio on stress development and viscoelastic properties of experimental two-paste composites," *Journal of Dental Research*, pp. 824 -828, Oct. 2003.

[34] D. C. Watts, A. S. Marouf, and A. M. Al-Hindi, "Photo-polymerization shrinkage-stress kinetics in resin-composites: methods development," *Dental Materials*, vol. 19, no. 1, pp. 1-11, Jan. 2003.

[35] C. L. Davidson and A. J. Feilzer, "Polymerization shrinkage and polymerization shrinkage stress in polymer-based restoratives," *Journal of Dentistry*, vol. 25, no. 6, pp. 435-440, Nov. 1997.

[36] E. Andrzejewska, "Photopolymerization kinetics of multifunctional monomers," *Progress in Polymer Science*, vol. 26, no. 4, pp. 605-665, May. 2001.

[37] Venhoven B.A.M., de Gee A.J.[1], and Davidson C.L., "Light initiation of dental resins: dynamics of the polymerization," *Biomaterials*, vol. 17, pp. 2313-2318, Dec. 1996.

[38] W. F. Schroeder and C. I. Vallo, "Effect of different photoinitiator systems on conversion profiles of a model unfilled light-cured resin," *Dental Materials*, vol. 23, no. 10, pp. 1313-1321, Oct. 2007.

[39] Y. Tanimoto, T. Hayakawa, and K. Nemoto, "Analysis of photopolymerization behavior of UDMA/TEGDMA resin mixture and its composite by differential scanning calorimetry," *Journal of Biomedical Materials Research Part B: Applied Biomaterials*, vol. 72, no. 2, pp. 310-315, 2005.

[40] K. Schätzel, "Correlation techniques in dynamic light scattering," *Applied Physics B Photophysics and Laser Chemistry*, vol. 42, no. 4, pp. 193-213, 1987.

[41] A. T. Forrester, R. A. Gudmundsen, and P. O. Johnson, "Photoelectric mixing of incoherent light," *Physical Review*, vol. 99, no. 6, p. 1691, 1955.

[42] R. H. Brown and R. Q. Twiss, "Correlation between photons in two coherent beams of light," *Nature*, vol. 177, no. 4497, pp. 27-29, 1956.

[43] P. N. Pusey and W. van Megen, "Observation of a glass transition in suspensions of spherical colloidal particles," *Physical Review Letters*, vol. 59, no. 18, p. 2083, Nov. 1987.

[44] A. Akcasu, M. Benmouna, and C. C. Han, "Interpretation of dynamic scattering from polymer solutions," *Polymer*, vol. 21, no. 8, pp. 866-890, Aug. 1980.

[45] S. C. Lin, W. I. Lee, and J. M. Schurr, "Brownian motion of highly charged poly (L-lysine). Effects of salt and polyion concentration," *Biopolymers*, vol. 17, no. 4, pp. 1041–1064, 1978.

[46] J. L. Rodgers and W. A. Nicewander, "Thirteen ways to look at the correlation coefficient," *The American Statistician*, vol. 42, no. 1, pp. 59-66, Feb. 1988.

[47] J. Xue, D. J. Pine, S. T. Milner, X. Wu, and P. M. Chaikin, "Nonergodicity and light scattering from polymer gels," *Physical Review A*, vol. 46, no. 10, p. 6550, Nov. 1992.

[48] P. Pusey and W. Van Megen, "Dynamic light scattering by non-ergodic media," *Physica A: Statistical Mechanics and its Applications*, vol. 157, no. 2, pp. 705-741, Jun. 1989.

[49] F. Scheffold, S. E. Skipetrov, S. Romer, and P. Schurtenberger, "Diffusing-wave

spectroscopy of nonergodic media," *Physical Review E*, vol. 63, no. 6, p. 061404, May. 2001.

[50] R. S. Stock and W. H. Ray, "Interpretation of photon correlation spectroscopy data: A comparison of analysis methods," *Journal of Polymer Science: Polymer Physics Edition*, vol. 23, no. 7, pp. 1393-1447, 1985.

[51] P. Lemieux and D. J. Durian, "Investigating non-Gaussian scattering processes by using nth-order intensity correlation functions," *Journal of the Optical Society of America A*, vol. 16, no. 7, pp. 1651-1664, Jul. 1999.

[52] J. Goodman, "Statistical properties of laser speckle patterns," in *Laser Speckle and Related Phenomena*, Berlin: Springer-Verlag, 1975, pp. 9-75.

[53] R. Bandyopadhyay, A. S. Gittings, S. S. Suh, P. K. Dixon, and D. J. Durian, "Speckle-visibility spectroscopy: A tool to study time-varying dynamics," *Review of Scientific Instruments*, vol. 76, no. 9, pp. 093110-11, 2005.

[54] S. J. Orfanidis, *Optimum signal processing: An introduction*. New York: Macmillan, 1985.

[55] P. Vaitkus and R. Cobbold, "A comparative study and assessment of doppler ultrasound spectral estimation techniques part I: Estimation methods," *Ultrasound in Medicine & Biology*, vol. 14, no. 8, pp. 661-672, 1988.

[56] J. Goodman, *Statistical Optics*. New York: Wiley, 1985.

[57] D. Duncan, Note: Derivation of expected value of exponential GRV, 2010.

[58] Papoulis A, Pillai AU, *Probability, Random Variables And Stochastic Processes*. McGraw-Hill Higher Education, 2002.

[59] S. Prahl, "http://omlc.ogi.edu/calc/mie_calc.html," 2007.

[60] J. A. Rice, *Mathematical statistics and data analysis*. Belmont, Ca: Duxbury, 2007.

[61] J. W. Goodman, *Introduction to Fourier Optics*. Boston: McGraw Hill, 2005.

[62] E. M. Wells-Gray, S. J. Kirkpatrick, and R. L. Sakaguchi, "A dynamic light scattering approach for monitoring dental composite curing kinetics," *Dental Materials*, vol. 26, no. 7, pp. 634-642, Jul. 2010.

[63] R. Sakaguchi, B. Wiltbank, and C. Murchison, "Cure induced stresses and damage in particulate reinforced polymer matrix composites: a review of the scientific literature," *Dental Materials*, vol. 21, no. 1, pp. 43-46, 2005.

[64] R. Braga, R. Ballester, and J. Ferracane, "Factors involved in the development of polymerization shrinkage stress in resin-composites: A systematic review," *Dental Materials*, vol. 21, no. 10, pp. 962-970, 2005.

[65] K. S. Anseth, C. M. Wang, and C. N. Bowman, "Kinetic evidence of reaction diffusion during the polymerization of multi(meth)acrylate monomers," *Macromolecules*, vol. 27, no. 3, pp. 650-655, Jan. 1994.

[66] M. Atai, D. C. Watts, and Z. Atai, "Shrinkage strain-rates of dental resin-monomer and composite systems," *Biomaterials*, vol. 26, no. 24, pp. 5015-5020, Aug. 2005.

[67] L. G. Lovell, S. M. Newman, M. M. Donaldson, and C. N. Bowman, "The effect of light intensity on double bond conversion and flexural strength of a model, unfilled dental resin," *Dental Materials*, vol. 19, no. 6, pp. 458-465, Sep. 2003.

[68] J. Ferracane and E. Greener, "Fourier transform infrared analysis of degree of polymerization in unfilled resins—Methods comparison," *Journal of Dental*

Research, pp. 1093 -1095, 1984.

[69] N. Silikas, G. Eliades, and D. C. Watts, "Light intensity effects on resin-composite degree of conversion and shrinkage strain," *Dental Materials*, vol. 16, no. 4, pp. 292-296, Jul. 2000.

[70] J. W. Stansbury and S. H. Dickens, "Determination of double bond conversion in dental resins by near infrared spectroscopy," *Dental Materials*, vol. 17, no. 1, pp. 71-79, Jan. 2001.

[71] M. Cadenaro et al., "Degree of conversion and permeability of dental adhesives," *European Journal of Oral Sciences*, vol. 113, no. 6, pp. 525-530, 2005.

[72] A. de Gee, C. Davidson, and A. Smith, "A modified dilatometer for continuous recording of volumetric polymerization shrinkage of composite restorative materials," *Journal of Dentistry*, vol. 9, no. 1, pp. 36-42, Mar. 1981.

[73] D. Watts and A. Cash, "Determination of polymerization shrinkage kinetics in visible-light-cured materials: methods development," *Dental Materials*, vol. 7, no. 4, pp. 281-287, Oct. 1991.

[74] K. S. Anseth, L. M. Kline, T. A. Walker, K. J. Anderson, and C. N. Bowman, "Reaction kinetics and volume relaxation during polymerizations of multiethylene glycol dimethacrylates," *Macromolecules*, vol. 28, no. 7, pp. 2491-2499, Mar. 1995.

[75] J. W. Goodman, *Statistical optics*. New York: Wiley, 2000.

[76] M. Trujillo, S. M. Newman, and J. W. Stansbury, "Use of near-IR to monitor the influence of external heating on dental composite photopolymerization," *Dental Materials*, vol. 20, no. 8, pp. 766-777, Oct. 2004.

[77] Y. Chen, J. L. Ferracane, and S. A. Prahl, "A pilot study of a simple photon migration model for predicting depth of cure in dental composite," *Dental Materials*, vol. 21, no. 11, pp. 1075-1086, Nov. 2005.

[78] P. H. Tomlins, W. M. Palin, A. C. Shortall, and R. K. Wang, "Time-resolved simultaneous measurement of group index and physical thickness during photopolymerization of resin-based dental composite," *Journal of Biomedical Optics*, vol. 12, no. 1, pp. 014020-7, Jan. 2007.

[79] J. E. Elliott, L. G. Lovell, and C. N. Bowman, "Primary cyclization in the polymerization of bis-GMA and TEGDMA: a modeling approach to understanding the cure of dental resins," *Dental Materials*, vol. 17, no. 3, pp. 221-229, May. 2001.

[80] W. D. Cook, "Factors affecting the depth of cure of UV-polymerized composites," *Journal of Dental Research*, pp. 800 -808, May. 1980.

[81] K. Jandt, R. Mills, G. Blackwell, and S. Ashworth, "Depth of cure and compressive strength of dental composites cured with blue light emitting diodes (LEDs)," *Dental Materials*, vol. 16, no. 1, pp. 41-47, Jan. 2000.

[82] H. C. van de Hulst, *Light Scattering by Small Particles*. New York: Wiley, 1957.

[83] E. A. Fogleman, M. T. Kelly, and W. T. Grubbs, "Laser interferometric method for measuring linear polymerization shrinkage in light cured dental restoratives," *Dental Materials*, vol. 18, no. 4, pp. 324-330, Jun. 2002.

[84] N. Demoli, A. Knezevic, Z. Tarle, A. Meniga, J. Sutalo, and G. Pichler, "Digital interferometry for measuring of the resin composite thickness variation during blue light polymerization," *Optics Communications*, vol. 231, no. 1, pp. 45-51,

Feb. 2004.

[85] T. Sato, M. Miyazaki, and A. Rikuta, "Real-time dimensional change in light-cured composites at various depths using laser speckle contrast analysis," *European Journal of Oral Sciences*, vol. 112, no. 6, pp. 538-544, 2004.

[86] J. Li, A. S. Fok, J. Satterthwaite, and D. C. Watts, "Measurement of the full-field polymerization shrinkage and depth of cure of dental composites using digital image correlation," *Dental Materials*, vol. 25, no. 5, pp. 582-588, May. 2009.

[87] D. Weitz and D. Pine, "Diffusing-wave spectroscopy," in *Dynamic Light Scattering*, Clarendon Press, 1993, pp. 720, 652.

[88] T. G. Mason and D. A. Weitz, "Optical measurements of frequency-dependent linear viscoelastic moduli of complex fluids," *Physical Review Letters*, vol. 74, no. 7, p. 1250, Feb. 1995.

[89] H. M. Wyss, S. Romer, F. Scheffold, P. Schurtenberger, and L. J. Gauckler, "Diffusing-wave spectroscopy of concentrated alumina suspensions during gelation," *Journal of Colloid and Interface Science*, vol. 241, no. 1, pp. 89-97, Sep. 2001.

[90] A. F. Fercher and J. D. Briers, "Flow visualization by means of single-exposure speckle photography," *Optics Communications*, vol. 37, no. 5, pp. 326-330, Jun. 1981.

[91] A. K. Dunn, H. Bolay, M. A. Moskowitz, and D. A. Boas, "Dynamic imaging of cerebral blood flow using laser speckle," *J Cereb Blood Flow Metab*, vol. 21, no. 3, pp. 195-201, Mar. 2001.

[92] Y. Aizu and T. Asakura, "Bio-speckle phenomena and their application to the

evaluation of blood flow," *Optics & Laser Technology*, vol. 23, no. 4, pp. 205-219, Aug. 1991.

[93] J. M. Huntley, "An image processing system for the analysis of speckle photographs," *Journal of Physics E Scientific Instruments*, vol. 19, pp. 43–48, 1986.

[94] J. D. Briers and S. Webster, "Quasi real-time digital version of single-exposure speckle photography for full-field monitoring of velocity or flow fields," *Optics Communications*, vol. 116, no. 1, pp. 36-42, Apr. 1995.

[95] D. D. Duncan and S. J. Kirkpatrick, "Can laser speckle flowmetry be made a quantitative tool?," *Journal of the Optical Society of America A*, vol. 25, no. 8, pp. 2088-2094, 2008.

[96] Y. Aizu and T. Asakura, "Coherent optical techniques for diagnostics of retinal blood flow," *Journal of Biomedical Optics*, vol. 4, no. 1, pp. 61-75, Jan. 1999.

[97] H. Rabal et al., "Speckle activity images based on the spatial variance of the phase," *Applied Optics*, vol. 45, no. 34, pp. 8733-8738, Dec. 2006.

[98] G. H. Sendra, R. Arizaga, H. Rabal, and M. Trivi, "Decomposition of biospeckle images in temporary spectral bands," *Optics Letters*, vol. 30, no. 13, pp. 1641-1643, Jul. 2005.

[99] D. D. Duncan, S. J. Kirkpatrick, and R. K. Wang, "Statistics of local speckle contrast," *Journal of the Optical Society of America A*, vol. 25, no. 1, pp. 9-15, Jan. 2008.

[100] D. Watts, "Reaction kinetics and mechanics in photo-polymerised networks," *Dental Materials*, vol. 21, no. 1, pp. 27-35, 2005.

[101] M. Atai and D. C. Watts, "A new kinetic model for the photopolymerization shrinkage-strain of dental composites and resin-monomers," *Dental Materials*, vol. 22, no. 8, pp. 785-791, Aug. 2006.

[102] G. G. Odian, *Principles of Polymerization*. John Wiley and Sons, 2004.

[103] L. G. Lovell, S. M. Newman, and C. N. Bowman, "The effects of light intensity, temperature, and comonomer composition on the polymerization behavior of dimethacrylate dental resins," *Journal of Dental Research*, vol. 78, no. 8, pp. 1469-1476, Aug. 1999.

[104] S. J. Kirkpatrick, D. D. Duncan, R. K. Wang, and M. T. Hinds, "Quantitative temporal speckle contrast imaging for tissue mechanics," *Journal of the Optical Society of America A*, vol. 24, no. 12, pp. 3728–3734, 2007.

[105] G. Popescu and A. Dogariu, "Dynamic light scattering in subdiffusive regimes," *Applied Optics*, vol. 40, no. 24, pp. 4215–4221, 2001.

[106] M. Singh, B. Singh, and B. S. Sandhu, "Investigations of multiple scattering of 320 keV γ rays: a new technique for assigning effective atomic number to composite material," *Physica Scripta*, vol. 79, no. 3, p. 035101, 2009.

[107] M. R. Jerath, C. M. Gardner, H. Rylander III, and A. J. Welch, "Dynamic optical property changes: Implications for reflectance feedback control of photocoagulation," *Journal of Photochemistry and Photobiology B: Biology*, vol. 16, no. 2, pp. 113-126, Oct. 1992.

[108] A. H. Gandjbakhche, P. Mills, and P. Snabre, "Light-scattering technique for the study of orientation and deformation of red blood cells in a concentrated suspension," *Applied Optics*, vol. 33, no. 6, pp. 1070-1078, Feb. 1994.

[109] J. D. Briers, G. Richards, and X. W. He, "Capillary Blood Flow Monitoring Using Laser Speckle Contrast Analysis (LASCA)," *Journal of Biomedical Optics*, vol. 4, no. 1, pp. 164-175, Jan. 1999.

[110] O. B. Thompson and M. K. Andrews, "Tissue perfusion measurements: multiple-exposure laser speckle analysis generates laser Doppler--like spectra," *Journal of Biomedical Optics*, vol. 15, no. 2, pp. 027015-7, Mar. 2010.

[111] P. C. L. Tsai, I. A. Meyers, and L. J. Walsh, "Depth of cure and surface microhardness of composite resin cured with blue LED curing lights," *Dental Materials*, vol. 20, no. 4, pp. 364-369, May. 2004.

[112] C. A. Munoz, P. R. Bond, J. Sy-Munoz, D. Tan, and J. Peterson, "Effect of pre-heating on depth of cure and surface hardness of light-polymerized resin composites," *Am J Dent*, vol. 21, no. 4, pp. 215–22, 2008.

[113] A. Lindberg, A. Peutzfeldt, and J. W. V. Dijken, "Effect of power density of curing unit, exposure duration, and light guide distance on composite depth of cure," *Clinical Oral Investigations*, vol. 9, no. 2, pp. 71-76, 2005.

[114] Z. Luo, Z. Yuan, M. Tully, Y. Pan, and C. Du, "Quantification of cocaine-induced cortical blood flow changes using laser speckle contrast imaging and Doppler optical coherence tomography," *Applied Optics*, vol. 48, no. 10, pp. D247-D255, Apr. 2009.

APPENDIX

A1. Quasielastic light scattering Matlab code

```
close all
clear all


%%%%%%%%%%%%%%%%%%%%%%%%%%%%%%%%%%%%%%%%%%%%%%%%%%%%%%%%%%%%%%%%%%%%

% FILE NAME
p=load('c:\july21G2.lvm');


Rad=.1E-6;   %% radius of spherical scatterers, in meters
r=3000;      %% SMAMPLING RATE, Hz
angle=12;    %% ANGLE degrees, measured from goniometer
T=20.2;      %% TEMPERATURE, degrees C. no more tha 1 decimal place
lamda=660E-9; %% WAVELEGTH in meters
n=1.33       %% refractive index of media


kb=1.38065E-23; % BOLTZMANNS constant[m^2 kg s^-2 K^-1]



Filt='on'    %% used 60Hz line filter; 'on' or 'of'


%%%%%%%%%%%%%%%%%%%%%%%%%%%%%%%%%%%%%%%%%%%%%%%%%%%%%%%%%%%%%%%%%%%
%%%%%%%%%%%%%%%%%%%%%%%%%%%%%%%%%%%%%%%%%%%%%%%%%%%%%%%%%%%%%%%%%%

% Correct for index of refraction mismatch

    theta=angle*(pi/180);        %radians
    theta=asin(sin(theta)/1.33) % radians, 1.33 is n of water
    angle_corrected=theta*(180/pi); %angles in degrees

% Correct for temperature
% Viscosity (as a function of TEMP)

    %[C] only one decimal place
    %T=293.95; %[K]
    %nu=0.001028; % at 19 deg C
    %nu=0.001003; % at 20 deg C
    %nu=0.000979; % at 21 deg C
    %nu=0.000955; % at 22 deg C
    %nu=0.000933; % at 23D deg C
    nu=[.001028 .001003 .000979 .000955 .000933]'
    temp=[19 20 21 22 23]'
    tempi=[19:.1:23]';
    ind=find(tempi==T);
    nui=interp1q(temp, nu, tempi);
```

```matlab
    clear nu
    % Viscosity at the specified temperature
    nu=nui(ind)

% Scattering wave vector
k=4*n*pi*sin(theta/2)/lamda;

T=T+273.15;
D=(kb*T/(6*pi*nu*Rad)); % diffusion constant of the scatterers
tau_0=1/(k^2*D);      % field decorrelation time
tau_1=1/(2*(k^2)*D);    % intensity decorrelation time
HWHM=D*(k^2);

%%%%%%%%%%%%%%%%%%%%%%%%%%%%%%%%%%%%%%%%%%%%%%%%%%%%%%%%%%%%%
%%%%%%%%%%%%%%%%%%%%%%%%%%%%%%%%%%%%%%%%%%%%%%%%%%%%%%%%%%%%%

% BASIC SIGNAL STATISTICS
% p is the intensity signal
R=length(p);
mean_p=mean(p)
std_p=std(p)
min_p=min(p)

t=(1:R)*(1/r);  % time signal
t=t';           % even better...

%%%%%%%%%
figure(1);%%%%%%%%%%%%%%%%%%%%%
%%%%%%%%%
    %plot(t,p)
    plot(p)

    xlabel('sample number')
    %xlabel('time [s]')
    ylabel('intensity [au]')
    title('choose points to exclude, must be left to right')
    %xlim([2 2.15])
    hold on

%%%%%%%%%%%%%%%%%%%%%%%%%%%%%%%%%%%%%%%%%%%%%%%%%%%%%%%%%%%%%
%%%%%%%%%%%%%%%%%%%%%%%%%%%%%%%%%%%%%%%%%%%%%%%%%%%%%%%%%%%%%
% Intensity autocorrelation function

G2=find_G_2(p,r,Filt);

% normalize
g2=G2./mean_p^2;%mean(p)^2;
t2=(0:length(g2)-1)/r;

fit_lim=.5

%%%%%%%%%
figure(5) %%%%%%%%%%%%%%%%%%%
%%%%%%%%%
```

```matlab
    plot(t2,G2)
    xlim1=tau_1*8;
    xlim([0 xlim1])


%%%%%%%
figure(6) %%%%%%%%%%%%%%%%
%%%%%%%

    clf;axes('FontSize',12);hold on
    plot(t2*1000,g2,'.r')
    xlim2=tau_1*5;
    xlim([0 xlim2*1000])
    %ylim([.95 1.3])

    ylabel('g_2')
    xlabel('\tau (ms)')

% Coherence factor, beta
B=g2(1)-1;


%%%%%%%%%%%%%%%%%%%%%%%%%%%%%%%%%%%%%%%%%%%%%%%%%%%%%%%%%%%%%%%%%

% Fit a negative exponential to g2

f_exp=@(a,x)(a(3)*exp(-x.*a(1))+a(2));

% determines how much data to fit over
val=find((g2-1)./(g2(1)-1)<=.4,1,'first');

a_start=[r/val mean(g2) .2];
[g2_fit,resnorm,residual]=lsqcurvefit(f_exp,a_start,t2(1:5*val),g2(1:5*val)');

%%%%%%%%%
figure(6)%%%%%%%%%%%%%%%%%%%%%%%%%%%%%
%%%%%%%%%
    plot(t2*1000,f_exp(g2_fit,t2),'k--')
    tau_fit=1/g2_fit(1);

    text(tau_1*1000,g2(5),sprintf...
        ('g_2=%3.2f e^{-%6.1f \\tau} +%3.2f\n\n\\tau_{fit} = %2.1f
ms\n\\tau_{theory}=%2.1f ms',...
    g2_fit(3),g2_fit(1),g2_fit(2),1/g2_fit(1)*1000,tau_1*1000),'FontSize',12)
```

```matlab
%%%%%%%%%%%%%%%%%%%%%%%%%%%%%%%%%%%%%%%%%%%%%%%%%%%%%%%%%%%%%%%%%
% find_G_2
% Caluclates the unbiased intensity autocorrelation function
% Does not perfome nomalization
%%%%%%%%%%%%%%%%%%%%%%%%%%%%%%%%%%%%%%%%%%%%%%%%%%%%%%%%%%%%%

function f=find_G_2(p,r,Filt)

% p is the intensity signal
% r is the sampling rate
% Filt is either 'on' or 'off', decides whether to use line filter

R=length(p);
t=(0:R-1)*(1/r);
t=t';

N = R*2;% number of points in FFT
DC = N/2+1;
dt = t(2)-t(1);
freq = [-DC+1:DC-2]/(N*dt);

F=fftshift(fft(p,N));
PSD=F.*conj(F);

if Filt=='on'

    width=10;
    % remove 60Hz
    %%%%%%%%%%%%%%%%%%%%%%%%%%%%%%%%%%%%%%%%%%%%%%%%%
    PSD(round((60-width/2)*dt*N)+DC:round((60+width/2)*dt*N)+DC)=0;
    PSD(DC-round((60+width/2)*dt*N):DC-round((60-width/2)*dt*N))=0;
    %%%%%%%%%%%%%%%%%%%%%%%%%%%%%%%%%%%%%%%%%%%%%%%%%
    % remove 120Hz
    %%%%%%%%%%%%%%%%%%%%%%%%%%%%%%%%%%%%%%%%%%%%%%%%%
    PSD(round((120-width/2)*dt*N)+DC:round((120+width/2)*dt*N)+DC)=0;
    PSD(DC-round((120+width/2)*dt*N):DC-round((120-width/2)*dt*N))=0;

end

G2full=real(ifft(fftshift(PSD)));
G2_bias=G2full(1:R);
w=[R:-1:1]; %biased weighting
G2=(G2_bias./w');

f=G2;
% return
```